

Wang Xindan (Orcid ID: 0000-0001-6458-180X)

Winkler Malcolm E. (Orcid ID: 0000-0002-1482-2588)

## Accepted Article

# Roles of RodZ and Class A PBP1b in the Assembly and Regulation of the Peripheral Peptidoglycan Elongasome in Ovoid-Shaped Cells of *Streptococcus pneumoniae* D39

Melissa M. Lamanna<sup>1</sup>, Irfan Manzoor<sup>1</sup>, Merrin Joseph<sup>1</sup>, Ziyun A. Ye<sup>1</sup>, Mattia Benedet<sup>2</sup>, Alessia Zanardi<sup>2</sup>, Zhongqing Ren<sup>1</sup>, Xindan Wang<sup>1</sup>, Orietta Massidda<sup>2</sup>, Ho-Ching T. Tsui<sup>1\*</sup>, and Malcolm E. Winkler<sup>1\*</sup>

<sup>1</sup>Department of Biology, Indiana University Bloomington, Bloomington, IN 47405 USA

<sup>2</sup>Department of Cellular, Computational and Integrative Biology (CIBIO), University of Trento, Italy

Running title: RodZ(*Spn*) Regulates Elongasome and aPBP1b Function

Keywords: peptidoglycan synthesis; elongasome assembly; Class A PBP function and regulation; synthetic-viable genetic relationships

\*Co-corresponding authors:

Malcolm E. Winkler

Phone: 812-856-1318

E-mail: [winklerm@indiana.edu](mailto:winklerm@indiana.edu)

Ho-Ching T. Tsui

Phone: 812-856-1781

E-mail: [ttsui@indiana.edu](mailto:ttsui@indiana.edu)

This article has been accepted for publication and undergone full peer review but has not been through the copyediting, typesetting, pagination and proofreading process which may lead to differences between this version and the [Version of Record](#). Please cite this article as doi: [10.1111/mmi.14969](https://doi.org/10.1111/mmi.14969)

This article is protected by copyright. All rights reserved.

## SUMMARY

RodZ of rod-shaped bacteria functions to link MreB filaments to the Rod peptidoglycan (PG) synthase complex that moves circumferentially perpendicular to the long cell axis, creating hoop-like sidewall PG. Ovoid-shaped bacteria, such as *Streptococcus pneumoniae* (pneumococcus; *Spn*) that lack MreB, use a different modality for peripheral PG elongation that emanates from the midcell of dividing cells. Yet, *S. pneumoniae* encodes a RodZ homolog similar to RodZ in rod-shaped bacteria. We show here that the helix-turn-helix and transmembrane domains of RodZ(*Spn*) are essential for growth at 37°C.  $\Delta$ rodZ mutations are suppressed by  $\Delta$ pbp1a, mpgA(Y488D), and  $\Delta$ khpA mutations that suppress  $\Delta$ mreC, but not  $\Delta$ cozE. Consistent with a role in PG elongation, RodZ(*Spn*) co-localizes with MreC and aPBP1a throughout the cell cycle and forms complexes and interacts with PG elongasome proteins and regulators. Depletion of RodZ(*Spn*) results in aberrantly shaped, non-growing cells and mislocalization of elongasome proteins MreC, PBP2b, and RodA. Moreover, Tn-seq reveals that RodZ(*Spn*), but not MreCD(*Spn*), displays a specific synthetic-viable genetic relationship with aPBP1b, whose function is unknown. We conclude that RodZ(*Spn*) acts as a scaffolding protein required for elongasome assembly and function and that aPBP1b, like aPBP1a, plays a role in elongasome regulation and possibly peripheral PG synthesis.

## 1 | INTRODUCTION

The peptidoglycan (PG) mesh, which consists of peptide-crosslinked glycan chains, determines the shape of eubacteria, contributing to their colonization and survival in

different environmental niches (Daitch & Goley, 2020, Egan *et al.*, 2020, Kumar *et al.*, 2022, Rohs & Bernhardt, 2021, Young, 2006). PG also protects bacteria from turgor pressure and serves as a scaffold for the attachment of extracellular proteins and exopolysaccharide capsules and wall-teichoic acids of Gram-positive bacteria, which lack an outer membrane (Rajagopal & Walker, 2017, Vollmer *et al.*, 2019). PG synthesis has been a major target for many classes of antibiotics, starting with the  $\beta$ -lactam penicillin (Bush & Bradford, 2016); however, resistance to cell-wall targeted antibiotics is now a serious, widespread health problem (CDC, 2019, Hakenbeck, 2014, Hakenbeck *et al.*, 2012). Because of its extracellular location, absence in eukaryotic hosts, and many vulnerable enzymatic and regulatory steps, PG synthesis remains a leading target for the discovery and development of new classes of antibiotics (CDC, 2019, den Blaauwen *et al.*, 2014, Lewis, 2020, Ling *et al.*, 2015, Sham *et al.*, 2012).

Formation of ovoid-shaped (ovococcal) bacteria (Zapun *et al.*, 2008), such as the major respiratory pathogen *Streptococcus pneumoniae* (pneumococcus; *Spn*) (Weiser *et al.*, 2018), requires two modes of PG synthesis (reviewed in (Briggs *et al.*, 2021, Massidda *et al.*, 2013, Perez *et al.*, 2021a, Vollmer *et al.*, 2019)). Septal PG (sPG) synthesis separates dividing pneumococcal cells at midcell into two daughter cells, whereas peripheral PG (pPG) synthesis is a form of sidewall PG synthesis that also emanates from the midcell division ring of dividing pneumococcal cells. All protein components for both modes of PG synthesis are initially organized by FtsZ, FtsA, and EzrA into a single ring at the equators of predivisional pneumococcal cells (Perez *et al.*, 2019). In the course of division, the sPG synthesis machine moves with the constricting FtsZ ring at the leading edge of the closing septal annulus, separate from the pPG synthesis machine that

Accepted Article

remains at the outer edge of the septal disk (Briggs *et al.*, 2021). This dual pattern of PG synthesis was recently visualized as two concentric midcell rings by high-resolution structured-illumination microscopy (3D-SIM) (Perez *et al.*, 2021a) and direct stochastic optical reconstruction microscopy (dSTORM) (Trouve *et al.*, 2021) microscopy of vertically oriented pneumococcal cells. At the start of division, pPG synthesis likely begins slightly before sPG synthesis, but throughout most of the cell cycle, sPG and pPG synthesis and PG remodeling at midcell are concurrent and highly coordinated (Briggs *et al.*, 2021, Perez *et al.*, 2021a, Trouve *et al.*, 2021, Tsui *et al.*, 2014, Wheeler *et al.*, 2011).

Midcell localization of sPG and pPG synthesis in ovococci is fundamentally different in many ways from the patterns of sPG and sidewall PG synthesis used by rod-shaped bacteria (Rohs & Bernhardt, 2021). In *Bacillus subtilis*, which like *S. pneumoniae* is a low-GC Gram-positive bacterium, a wall of sPG is synthesized during septal closure without surface constriction between daughter cells that are later separated by PG hydrolases (Errington & Wu, 2017, Straume *et al.*, 2021). Gram-positive coccoid bacteria, such as *Staphylococcus aureus*, also synthesize a septal cell wall between daughter cells, which are later separated by a rapid PG hydrolytic popping mechanism (Lund *et al.*, 2018, Saraiva *et al.*, 2020, Straume *et al.*, 2021). In Gram-negative *Escherichia coli*, septal closure and cell separation are largely concurrent (Rohs & Bernhardt, 2021), similar to what is observed for *S. pneumoniae*. However, in *E. coli*, the regulation of sPG synthesis occurs by a different mechanism than in *S. pneumoniae*, which lacks FtsN-mediated activation of essential Class B PBP3 (FtsI) transpeptidase activity required for septal closure in *E. coli* (Briggs *et al.*, 2021, Pichoff *et al.*, 2019, Rohs & Bernhardt, 2021).

Early in cell division of rod-shaped bacteria, preseptal PG synthesis pushes sidewall PG outward from the Z-ring (Aaron *et al.*, 2007, Pazos *et al.*, 2018, van Teeseling, 2021), resembling the pPG synthesis that occurs throughout the pneumococcal cell cycle (Briggs *et al.*, 2021). However, following preseptal PG synthesis, the Rod-complex elongasome, containing conditionally essential MreB and the sidewall PG synthase complex, assembles along the curved cylindrical body of rod-shaped cells (Bratton *et al.*, 2018, Hussain *et al.*, 2018, Morgenstein *et al.*, 2015, Rohs & Bernhardt, 2021). MreB is an actin-like homolog that polymerizes into multiple, short, curved filaments along the cell membrane, perpendicular to the cell long axis, which is the direction of maximum negative Gaussian curvature (Bratton *et al.*, 2018, Hussain *et al.*, 2018, Morgenstein *et al.*, 2015, Rohs & Bernhardt, 2021). MreB filaments are linked to the sidewall PG synthase complex by RodZ, whose cytoplasmic helix-turn-helix (HTH) interacts with MreB inside the cell (Ago & Shiomi, 2019, Bendezu *et al.*, 2009, Morgenstein *et al.*, 2015, van den Ent *et al.*, 2010). Bitopic RodZ (see Fig. 1 and S1) also forms a complex with the bitopic and polytopic PG synthesis proteins in the elongasome, including MreC and MreD (positive regulators) (Rohs & Bernhardt, 2021, Rohs *et al.*, 2018, Rohs *et al.*, 2021), RodA (SEDS glycosyl transferase) (Meeske *et al.*, 2016, Sjodt *et al.*, 2018, Sjodt *et al.*, 2020), and an essential Class B penicillin-binding protein (bPBP2 transpeptidase in *E. coli*) (Rohs & Bernhardt, 2021, Sjodt *et al.*, 2020). The interaction between RodZ and MreB can modulate the density and length of MreB filaments (Bratton *et al.*, 2018, Colavin *et al.*, 2018, Hussain *et al.*, 2018). In *E. coli*, a limiting amount of bPBP2 seems to bind to PG and recruit the rest of the Rod elongasome (Ozbaykal *et al.*, 2020). Movement of the assembled Rod elongasome is driven by sidewall PG synthesis itself, rather than by

ATPase-dependent treadmilling of MreB (Rohs & Bernhardt, 2021), with the MreB filaments serving as curvature-sensing rudders (Hussain *et al.*, 2018). Finally, in contrast to the parallel PG synthesis by the Rod elongasome, synthesis of sidewall PG by Class A PBPs appears to be largely non-ordered, possibly filling in or reinforcing gaps left by the Rod system (Cho *et al.*, 2016, Dion *et al.*, 2019, Lamanna & Maurelli, 2022, Rohs & Bernhardt, 2021).

In contrast to rod-shaped bacteria, the pPG elongasome of *S. pneumoniae* is zonal and confined to the midcell of dividing pneumococcal cells. As division proceeds, the pPG elongasome locates to an outer ring of PG synthesis at the edge of the septal annulus (Briggs *et al.*, 2021, Perez *et al.*, 2021a, Trouve *et al.*, 2021). Homologs of MreC, MreD, an essential Class B PBP (bPBP2b), and RodA have been associated with the pneumococcal pPG elongasome by genetic, physiological, and bacterial two-hybrid (B2H) experiments (Berg *et al.*, 2013, Land & Winkler, 2011, Massidda *et al.*, 2013, Philippe *et al.*, 2014, Stamsas *et al.*, 2017, Straume *et al.*, 2017, Tsui *et al.*, 2014, Zheng *et al.*, 2017). In addition, Class A aPBP1a and CozE have been linked to pneumococcal pPG elongasome function through a synthetic-viable genetic relationship, in that  $\Delta pbp1a$  or *cozE* depletion suppresses  $\Delta mreCD$  (Fenton *et al.*, 2016, Land & Winkler, 2011, Tsui *et al.*, 2016). Complexes containing aPBP1a and pPG elongasome proteins have also been detected by co-immunoprecipitation (co-IP) and bacterial two-hybrid (B2H) assays (Fenton *et al.*, 2016, Stamsas *et al.*, 2017)}. Similarly, aPBP1a is synthetically viable with muramidase MpgA (formerly MltG(*Spn*)), in that  $\Delta pbp1a$  suppresses  $\Delta mpgA$  (Taguchi *et al.*, 2021, Tsui *et al.*, 2016). Each of these proteins localizes to the midcell of dividing

pneumococcal cells, consistent with the zonal mechanism of pPG elongation (Briggs *et al.*, 2021, Land *et al.*, 2013, Tsui *et al.*, 2016, Tsui *et al.*, 2014).

*S. pneumoniae*, like most non-rod-shaped bacteria, encodes a RodZ homolog (Fig. 1 and S1), despite the absence of an MreB homolog. The secondary structure of RodZ(*Spn*) is remarkably similar to RodZ homologs in rod-shaped bacteria (Fig. 1 and S1) (Ago & Shiomi, 2019, Alyahya *et al.*, 2009, Bendezu *et al.*, 2009, Shiomi *et al.*, 2008). RodZ(*Spn*) contains a cytoplasmic N-terminal HTH domain of the XRE family, which contains five helices that often mediate protein interactions (Aravind *et al.*, 2005). The HTH domain is connected to a TM domain by a disordered “juxtamembrane” domain, which is positively charged in RodZ(*Spn*) and RodZ(*Eco*) (Fig. 1D and S1) (Bendezu *et al.*, 2009). Non-conserved Ser85 in this linker region of RodZ(*Bsu*) (Fig. 1 and S1B) has been reported to be phosphorylated in a preliminary report (Sun & Garner, 2020)}. The non-conserved extracellular linker of RodZ(*Spn*) contains a large number of repeated Ser residues and connects the TM domain to a domain of unknown function (DUF#4115) that is predicted by AlphaFold2 to fold into a beta-strand structure (Fig. 1C), similar to DUF determined for RodZ(*Bsu*) (Ago & Shiomi, 2019). *rodZ* is essential or conditionally essential in *E. coli*, *B. subtilis*, and *Caulobacter crescentus* (Alyahya *et al.*, 2009, Bendezu *et al.*, 2009, Muchova *et al.*, 2013). Structure-function mutagenesis shows that the cytoplasmic HTH and TM domains of RodZ are essential for its function in *E. coli* and *C. crescentus*, whereas extracellular domains can be deleted without severe cell growth and morphology phenotypes (Alyahya *et al.*, 2009, Bendezu *et al.*, 2009, Morgenstein *et al.*, 2015). In this regard, RodZ of *Rickettsia* and *Chlamydia* species lack an extracellular domain (Kemege *et al.*, 2015). These obligate intracellular pathogens lack FtsZ and use

a modified Rod complex consisting of homologs of MreB, RodZ, MreC, a bPBP, and RodA to synthesize midcell PG (Liechti *et al.*, 2016, Ouellette *et al.*, 2020, Ranjit *et al.*, 2020).

In this paper, we demonstrate by Tn-seq, transformation assays, and protein depletion that RodZ(*Spn*) is conditionally essential in serotype-2 D39 strains of *S. pneumoniae* at 37°C. Tn-seq and structure-function analyses show that this essentiality requires the HTH and TM domains of RodZ(*Spn*), but not the extracellular linker or DUF domains. Suppression patterns of  $\Delta rodZ$  and  $\Delta mreC$ , but not  $\Delta cozE$ , mutants phenocopy each other, linking RodZ(*Spn*) to the pPG elongasome. The conclusion that RodZ(*Spn*) is a member of the pPG elongasome is supported by interaction studies using co-IP and B2H assays and by microscopic co-localization of RodZ(*Spn*) and MreC(*Spn*) or aPBP1a(*Spn*) throughout the pneumococcal cell cycle. Depletion of RodZ(*Spn*) stops growth and results in viable, rounded, heterogeneous cells with a qualitatively different appearance from cells depleted for MreC or bPBP2b (Berg *et al.*, 2013, Land & Winkler, 2011, Tsui *et al.*, 2014). Depletion of RodZ(*Spn*) or MreC(*Spn*) further reveals a hierarchy for pPG elongasome assembly. Finally, Tn-seq experiments show the unexpected result that Class A aPBP1b, whose function is not known, is in a synthetic-viable genetic relationship with RodZ, but not MreCD, whereas Class A aPBP1a is in a synthetic-viable genetic relationship with MreC, MreD, and RodZ. Together, these results show that RodZ(*Spn*) still acts as an essential scaffold protein through its HTH and TM domains for pneumococcal pPG elongasome assembly and function, despite the absence of MreB. This study also shows that diverse cell morphology and genetic phenotypes result when different members of the pPG elongasome are absent or depleted. Last, this work shows that aPBP1b and aPBP1a play different roles in modulating the function of the *S.*

*pneumoniae* pPG elongasome and possibly participate in pPG synthesis. These results are discussed in terms of a model in which failsafe mechanisms can bypass or regulate the function of the pneumococcal core RodZ-MreCD-bPBP2b-RodA elongasome to ensure viability.

## 2 | RESULTS

### 2.1 | RodZ is conditionally essential in *Streptococcus pneumoniae* D39 at 37°C

RodZ(*Spn*) is annotated as “probably not essential” in serotype 2 D39 strains based on recent genomics approaches (see PneumoBrowse site) (Slager *et al.*, 2018). Likewise, a Tn-seq screen of serotype 4 TIGR4 strains recovered insertions in *rodZ* that seemed to grow in laboratory media (van Opijken & Camilli, 2012).  $\Delta rodZ$  mutants were reported in unencapsulated ( $\Delta cps$ ) R6 laboratory strains (Martin-Galiano *et al.*, 2014, Stamsas *et al.*, 2017, Straume *et al.*, 2017), whose progenitor is strain D39 (Lanie *et al.*, 2007). However, we previously reported that we could not obtain  $\Delta rodZ$  mutants in an unencapsulated ( $\Delta cps$ ) derivative constructed in progenitor strain D39 (Tsui *et al.*, 2016).

We performed a series of experiments to reconcile these conflicting previous results, leading to the conclusion that *rodZ* is essential for growth at 37°C in unencapsulated and encapsulated D39 strains, although poor growth occurs at 32°C (Fig. S2). Tn-seq analysis showed that insertions occur in the non-essential carboxyl-terminal DUF-domain half of *rodZ*(*Spn*), but are not recovered in the essential transmembrane and amino-terminal domains (Fig. 1D and 2A (WT)). This pattern of insertions relative to RodZ(*Spn*) domain functions is taken up further below and underlies why a substantial number of non-essential *rodZ* insertions were detected in previous Tn-seq experiments. In addition, the

Tn-seq profile here (Fig 2A) confirms previous Tn-seq (Fenton *et al.*, 2016) and complementation results (see below; (Rued *et al.*, 2017)) showing that *mreC* is essential in *S. pneumoniae* D39, contrary to a conclusion in (Straume *et al.*, 2017).

Transformation assays confirmed that  $\Delta rodZ$  was not viable in unencapsulated WT D39 strains at 37°C, unless it was complemented in a merodiploid strain by an ectopic copy of *rodZ*<sup>+</sup> that was under control of a zinc-inducible promoter (Table 1, rows 1-4). At the lower temperature of 32°C, we did observe small colonies of  $\Delta rodZ$  mutants in merodiploid strains lacking the -Zn inducer for *rodZ*<sup>+</sup> expression (Fig. S2A) or in transformation assays (Fig. S2C, line 3). However, we found that slow growth at 32°C is a phenotype of mutants lacking other components of the pneumococcal pPG elongasome, including MreC, bPBP2b, or RodA (Fig. S2B; Fig. S2C, lines 4-6). In contrast to the unencapsulated D39 background,  $\Delta rodZ$  transformed into the R6 laboratory strain (Table 1, line 17), as reported previously (Stamsas *et al.*, 2017, Straume *et al.*, 2017); however, R6 derivatives contain mutations in *pbp1a* that suppress mutations in genes encoding the peripheral PG (pPG) synthesis elongasome machine (Land & Winkler, 2011, Tsui *et al.*, 2016), including  $\Delta mreC$  (Table 1, line 17). Finally, comparable experiments at 37°C showed that  $\Delta rodZ$  could not be transformed into encapsulated D39 progenitor strains (Table 1, lines 18 and 19). Numerous mutations suppress  $\Delta rodZ$  in *S. pneumoniae* (see next section) and likely account for the small number of colonies that arose in the D39 strains transformed with  $\Delta rodZ$  amplicons. The essentiality of *rodZ* in the encapsulated D39 strains was corroborated in merodiploid strains, where hundreds of colonies were obtained only in the complementation strain (+Zn), but not in the depleted  $\Delta rodZ$  strain (-Zn; Table 1, lines 20 and 21). We conclude that *rodZ* is essential for growth

of unencapsulated or encapsulated D39 strains of *S. pneumoniae* at the optimal culture temperature of 37°C. Because capsule partially masks primary phenotypes of PG synthesis mutants in *S. pneumoniae* and complicates microscopy due to cell chaining (Barendt *et al.*, 2009), the rest of these studies of *rodZ* physiology and function were performed in the D39 unencapsulated genetic background.

## 2.2 | $\Delta rodZ$ has a similar suppression pattern as $\Delta mreC$ , but not to $\Delta cozE$ , in transformation assays at 37°C

Mutations in essential genes of the pneumococcal PG elongasome complex, including *mreC*, *pbp2b*, and *rodA*, are suppressed by several kinds of mutations (Land & Winkler, 2011, Stamsas *et al.*, 2017, Tsui *et al.*, 2016, Zheng *et al.*, 2017). For example,  $\Delta mreC$  is suppressed by  $\Delta pbp1a$  (Class A aPBP1a), *mpgA*(Y488D) (reduced activity of MpgA (formerly MltG(*Spn*)) muramidase,  $\Delta khpA$  (RNA binding regulator), and overexpression of FtsA (division actin-homolog) (Table 1, lines 9-14) (Land & Winkler, 2011, Stamsas *et al.*, 2017, Taguchi *et al.*, 2021, Tsui *et al.*, 2016, Zheng *et al.*, 2017). To link RodZ to MreC and pPG synthesis, we showed that  $\Delta rodZ$  has the same suppression pattern as  $\Delta mreC$ .  $\Delta rodZ$  or  $\Delta mreC$  is complemented in merodiploid strains by ectopic expression (+Zn) of *rodZ*<sup>+</sup> or *mreC*<sup>+</sup>, respectively (Table 1, lines 4 and 6). Like  $\Delta mreC$ ,  $\Delta rodZ$  is suppressed by  $\Delta pbp1a$ , *mpgA*(Y488D),  $\Delta khpA$ , and overexpression of FtsA (Table 1, lines 9-14). This identical suppression pattern provides strong evidence that RodZ functions in the pPG synthesis elongasome, along with MreC, bPBP2b, and RodA. In addition, overexpression of MreC or FtsZ in merodiploid strains did not bypass the requirement for RodZ (Table 1, lines 6 and 16). Likewise, the requirement for MreC was not bypassed by overexpression of RodZ or FtsZ (Table 1, lines 4 and 16).

We used transformation assays to study two other aspects of RodZ function. CozE was discovered in a Tn-seq of essential genes that become dispensable in a mutant lacking aPBP1a (Fenton *et al.*, 2016). Localization and interaction studies indicated that CozE is a member of the MreCD complex in the pneumococcal elongasome. Therefore, we fully expected  $\Delta cozE$  mutants to show the same suppression patterns as  $\Delta mreC$  and  $\Delta rodZ$  mutants. Unexpectedly, we found that  $\Delta cozE$  significantly reduced, but did not abolish, colony growth, indicating that *cozE* is dispensable under the conditions used here (Table 1, line 1 and 2). This non-essentiality was recapitulated in Tn-seq experiments showing that insertion in *cozE* are recovered in the WT strain propagated in BHI broth (see below; data not shown). The colony growth defect of a  $\Delta cozE$  mutant was fully complemented by ectopic expression of *cozE<sup>+</sup>* in a merodiploid strain (Table 1; line 8). However, the  $\Delta cozE$  colony growth was not ostensibly improved by any of the mutations that suppressed both  $\Delta mreC$  and  $\Delta rodZ$ , including  $\Delta pbp1a$  (Table 1, lines 9-16). Thus, loss of CozE is not equivalent to loss of MreC or RodZ under some growth conditions, suggesting different functions in the elongasome and/or cell growth. This difference was not studied further here.

Last, *rodZ* is immediately upstream of essential *pgsA*, which encodes phosphatidylglycerol phosphate synthase, required for phospholipid synthesis (Fig 1A). In *B. subtilis*, insertion mutations in *rodZ* can have polar effects on *pgsA* expression (van Beilen *et al.*, 2016). In this study of *S. pneumoniae*, *rodZ* mutant growth and cell morphology phenotypes are complemented by expression of an ectopic copy of *rodZ<sup>+</sup>* and markerless  $\Delta rodZ$  mutations are used for most experiments (Table 1, lines 4, 20, and 21; Fig. 3 and 4). Conversely, ectopic expression of *pgsA<sup>+</sup>* (+Zn) complemented  $\Delta pgsA$

for growth in a  $\Delta pgsA//P_{Zn}-pgsA^+$  merodiploid (Table S5, line 11), but overexpression of PgsA in a  $pgsA^+//P_{Zn}-pgsA^+$  merodiploid strain (+Zn) did not allow growth of  $\Delta rodZ$  transformants (Table 1, line 9). We conclude from genetic complementation along with the use of markerless alleles that phenotypes attributed to mutations in *rodZ* in this study are not caused by polarity on *pgsA* or other downstream genes.

### 2.3 | RodZ is required for normal cell shape and morphology of *S. pneumoniae*

To study primary *rodZ* mutant phenotypes without accumulating suppressors (Table 1), RodZ was depleted in  $\Delta rodZ//P_{Zn}-rodZ^+$  and  $\Delta rodZ//P_{Zn}-rodZ\text{-FLAG}$  merodiploid mutants (-Zn), and cultures were sampled at various times after depletion (Fig. 3 and 4, where F is used as an abbreviation for the FLAG tag here and elsewhere). RodZ depletion causes a decrease in apparent growth rate after  $\approx 4.5$  h, followed by a decrease in culture density at  $\approx 7$  h (Fig. 3A and 4A). In controls for depletion experiments, cells expressing functional RodZ-FLAG from the native locus grew at the same rate in BHI broth lacking or containing the Zn inducer (0.4 mM ZnCl<sub>2</sub> + 0.04 mM MnSO<sub>4</sub>), where 1/10 MnSO<sub>4</sub> was added to lessen Zn<sup>2+</sup> toxicity (Fig. S3A} (Jacobsen *et al.*, 2011, Perez *et al.*, 2021b, Tsui *et al.*, 2016), and cell morphology and cellular RodZ-FLAG amount were not appreciably altered by Zn addition (Fig. S3B and S3C). By 4 h of RodZ depletion, cells tended to become larger and more heterogeneous in shape, with some cells becoming round and others exhibiting pointed ends (Fig. 3B, 3C, and 4B). By 6 h of RodZ depletion, cell width and size increased significantly, and cells became more spherical with an average aspect ratio approaching 1 (Fig. 3B and 3C). Quantitative western blotting showed that RodZ-FLAG was not detectable by 3 h of depletion and that RodZ depletion for 4 h did not alter

the cellular amounts of MreC, bPBP2b, or bPBP2x (Fig. 4D). Depletion of RodZ also led to a moderate increase in the number of cells in chains (Fig. S4).

Depletion of RodZ for 4 h or 6 h is bacteriostatic and did not lead to a loss of cell viability, as determined by live-dead staining (Fig. 5) or by recovery of CFUs following RodZ depletion for at least 7 h (Fig. S5). Finally, we tested whether overexpression of RodZ affected growth or cell morphology of *S. pneumoniae*, as happens in *E. coli* and *C. crescentus* (Alyahya *et al.*, 2009, Bendezu *et al.*, 2009, Shiomi *et al.*, 2008). Overexpression of RodZ-FLAG by  $\approx$ 2.5 fold (Fig. S6C) did not have an appreciable effect on pneumococcal growth (Fig. S6A) or cell morphology (Fig. S6B and S6D), although more lysed cells were observed when RodZ-FLAG was overexpressed. Altogether, these results indicate that RodZ is required for normal morphology of pneumococcal cells. Notably, cell shape and size tend to be more heterogeneous for RodZ depletion than for depletion of other pneumococcal elongasome components, such as MreC, bPBP2b, or FtsEX, which results in chains of relatively uniform, spherical cells at 4 h (Berg *et al.*, 2013, Sham *et al.*, 2013, Tsui *et al.*, 2014).

#### **2.4 | The RodZ(*Spn*) HTH and TM domains, but not the DUF domain, are required for normal growth**

RodZ(*Spn*) has the same overall domain structure as RodZ from bacteria that express MreB homologs (*Introduction*; Fig. 1 and S1). Tn-seq of the WT strain demonstrated that viable insertions are obtained in the C-terminus of *rodZ(Spn)* starting with TA in the TAT (Y132) codon, resulting in a stop codon after AAC (N131) (Fig. 1D and 2A). Thus, the entire extracellular region of RodZ(*Spn*) from aa Y132-N273, including DUF4115 and the disordered extracellular domain proximal to the membrane are dispensable for growth in

BHI broth at 37°C. This conclusion was confirmed by deletion mutations constructed in a *rodZ*/ $\text{P}_{\text{Zn}}\text{-}rodZ^+$  merodiploid strain (Table 2, lines 6 and 7; Fig. 6). RodZ(M1-Q134) and RodZ(M1-T135) mutants form normal-sized colonies on TSAI-BA plates, as did other deletion mutants of the extracellular domains (Table 2; Fig. 6A). Cells of RodZ( $\Delta$ DUF) and RodZ(M1-Q195; lacking DUF and the C-terminal region) resemble WT cells in BHI broth at 37°C (Fig. 6B and S7). By contrast, the RodZ(M1-Q134) mutant forms wider, bigger cells than WT, indicative of partial RodZ function or instability, whereas RodZ(M1-T135) cells are mostly WT, with infrequent larger, wider cells (Fig. 6B). C-terminal FLAG-tagged WT RodZ was readily detected by western blotting (Fig. 4C). Curiously, truncated RodZ(M1-Q195) with a C-terminal FLAG-tag could not be detected by western blotting (Fig. 6), despite not showing growth or morphology phenotypes, suggesting C-terminal degradation in the absence of the DUF domain.

Transformation assays and growth characterization indicated that mutants lacking the TM, HTH, or the cytoplasmic linker domain of RodZ(*Spn*) are not viable (Table 2; Fig. 2A, 6A, and S8). Reduced RodZ( $\Delta$ HTH) mutant protein with a C-terminal FLAG-tag was detected in 4-h depletion experiments (Fig. 6A), consistent with lack of RodZ( $\Delta$ HTH) function and possibly decreased protein amount underlying its null mutant phenotype. Consistent with loss of function, the RodZ(HTH) domain mediates protein-protein interactions in B2H assays (see below). Changes of aromatic amino acids in RodZ(*Spn*) at three positions in Helix 4 of the HTH domain, which correspond to the MreB interaction interface in *E. coli* (van den Ent *et al.*, 2010), do not show growth phenotypes in *S. pneumoniae* (Fig. 6A and S9). In addition, amino-acid changes in the membrane-proximal pedestal region of bPBP2b failed to suppress  $\Delta$ rodZ lethality in *S. pneumoniae* (Table

S6), unlike the corresponding amino acid changes in *E. coli* bPBP2 that did suppress  $\Delta$ *rodZ* phenotypes (Rohs *et al.*, 2018). Finally, phosphorylation of S85 in RodZ(*Bsu*) was proposed to increase MreB filament density and growth (Sun & Garner, 2020). S85 of RodZ(*Bsu*) corresponds in alignment to E89 of RodZ(*Spn*) (dotted box, Fig. 1D; Fig. S1), which is not immediately adjacent to other serine or threonine residues. Phostag-PAGE analysis failed to detect phosphorylation of functional RodZ-HA<sup>3</sup> in *S. pneumoniae* (Fig. S10). From these combined results, we conclude that the cytoplasmic HTH and linker and the TM domain, but not the extracellular domains, of RodZ(*Spn*) are required for growth at 37°C under the conditions tested here and that amino acids important for RodZ function in *E. coli* and *B. subtilis* are not required in *S. pneumoniae* (see *Discussion*).

## 2.5 | RodZ(*Spn*) localizes with known pPG elongasome proteins throughout the pneumococcal cell cycle

The identical suppression pattern of  $\Delta$ *rodZ* and  $\Delta$ *mreC* in *S. pneumoniae* (Table 1) supports the hypothesis that RodZ is a member of the pPG elongasome. This hypothesis is further corroborated by protein co-localization analyses using immunofluorescence microscopy (IFM) as described in *Experimental procedures*. Strains expressing RodZ-FLAG<sup>3</sup> constructs or other epitope-tagged proteins from their native chromosomal loci were functional and did not exhibit aberrant growth or cell morphologies (Fig. S11). We used a previously published method to compare the average locations of two fluorescent epitope-tagged proteins relative to DAPI-stained nucleoids at four stages of division in pneumococcal cells growing exponentially in BHI broth at 37°C (Fig. 7) (Land *et al.*, 2013, Tsui *et al.*, 2014). This method also allows statistical comparisons of average midcell widths at different cell division stages as described in *Experimental procedures*.

By this analysis, RodZ co-localizes throughout the cell cycle with MreC and aPBP1a (Fig. 7A-7D), which have been implicated in pPG elongation in *S. pneumoniae* (Briggs *et al.*, 2021, Fenton *et al.*, 2016, Land & Winkler, 2011, Philippe *et al.*, 2014, Straume *et al.*, 2017, Tsui *et al.*, 2016). All three proteins localize at the midcell equator in Stage 1 cells, remain at the midcell septum in Stage 2 and 3 cells, and only appear at the new equators of daughter cells late in division at Stage 4. There is a very small displacement of midcell widths of RodZ-Myc from those of MreC-L-F<sup>3</sup> on the diagonal reference line (slope = 1), accompanied by statistically significant width differences for stage 1-3 cells (Fig. 7B). These slight differences likely indicate that the C-terminal epitope tag of RodZ extends further from the cell membrane than that of MreC (see below), with this apparent displacement possibly enhanced by the lengths of the two antibodies used in IFM (Perez *et al.*, 2021b). In contrast to RodZ, MreC, and aPBP1a, nascent FtsZ- rings move outward toward the future sites of the new equators throughout division and largely leave the septum in Stage 3 and 4 cells (Fig. 7E and 7F) (Perez *et al.*, 2019). We conclude that RodZ co-localizes with components of the pPG elongasome, which overlaps FtsZ localization in Stage 1 cells, but is different in later stages of the cell cycle. This conclusion is corroborated independently by high-resolution 3D-SIM of RodZ and FtsZ in cells at different division stages (Fig. S12).

## **2.6 | RodZ(*Spn*) forms complexes and interacts with proteins in the septal PG (sPG) and pPG synthesis machines and with PG synthesis regulators**

To gain more information about RodZ function in *S. pneumoniae*, we performed pairwise co-IP experiments using RodZ-FLAG and RodZ-FLAG<sup>3</sup> as bait proteins that were probed in western blots for complex formation with proteins involved in PG elongation, septation,

or cell division. Representative co-IP results are shown in Fig. 8A, quantitated in Table 3, and summarized in Fig. 8B and 8C. Additional supporting data are in Fig. S13 and S14. Strong complex formation was detected between RodZ and pPG elongasome proteins MreC and bPBP2b at some stage of division in non-synchronized cell cultures (Table 3). The experiment to probe for complexes between RodZ and RodA could not be performed, because cells expressing RodZ-FLAG<sup>3</sup> and HaloTag-RodA (HT-RodA) showed a synthetic lysis phenotype not observed in cells separately expressing the fusion proteins (Fig. S14A and S14B). Complexes were also detected between RodZ and protein regulators of PG synthesis (GpsB; StkP (Ser/Thr protein kinase); DivIVA), Class A PBPs (aPBP1a; aPBP2a), and MpgA (PG muramidase) (Briggs *et al.*, 2021, Massidda *et al.*, 2013). Consistent with these results, MreC, MpgA, or aPBP1a, each of which has been linked to pPG elongation in *S. pneumoniae* (Briggs *et al.*, 2021, Fenton *et al.*, 2016, Land & Winkler, 2011, Massidda *et al.*, 2013, Philippe *et al.*, 2014, Taguchi *et al.*, 2021, Tsui *et al.*, 2016), pulled down the same set of proteins (Table 3). RodZ was also detected in complexes with the sPG synthesis proteins bPBP2x (Fig. 8A) and FtsW (Fig. S14C) at some stage of cell division, possibly the initial equatorial ring of newly divided cells (Briggs *et al.*, 2021) or the outer pPG synthesis ring that also contains some bPBP2x, and presumably FtsW (Perez *et al.*, 2021a). In contrast, marginal or no complexes were detected between RodZ and FtsA, FtsZ, PhpP (protein phosphatase), or KhpAB (RNA-binding regulator) (Fig. 8 and S13C; Table 3) (Massidda *et al.*, 2013, Mura *et al.*, 2017, Perez *et al.*, 2019, Rued *et al.*, 2017, Stamsas *et al.*, 2017, Zheng *et al.*, 2017). Thus, an *in vivo* complex containing RodZ and KhpB was not detected, despite a previous report of an interaction in a B2H assay (Winther *et al.*, 2021).

B2H assays were performed in *E. coli* to test for direct interactions between WT RodZ (*Spn*) or truncated constructs lacking the HTH or DUF domain of RodZ(*Spn*) and the set of proteins mentioned above, as well as additional proteins not analyzed by co-IP (Fig. 9 and S15; Table S7). B2H assays revealed RodZ(*Spn*) self-interaction and a strong signal of interactions, usually bidirectional, between RodZ(*Spn*) and GpsB, MreC, MreD, MpgA, bPBP2b, RodA, aPBP1a, aPBP2a, bPBP2x, FtsW, EzrA, DivVA, or aPBP1b (Fig. 2D, 8C, and 9A). Weaker signals of unidirectional interaction or no interaction were detected by B2H between RodZ(*Spn*) and StkP, FtsA, or FtsZ (Fig. 9A). For comparison, B2H assays were performed to determine direct interactions of pPG elongasome proteins MreC(*Spn*) or MreD(*Spn*) with Class A PBPs. MreC interacts with itself and shows bidirectional interactions with aPBP1a, aPBP2a, or aPBP1b, whereas MreD also self-interacts and shows bidirectional interactions with aPBP1a, but unidirectional interactions with aPBP2a or aPBP1b (Fig. 2D and 9B).

Finally, B2H assays were used to determine whether the absence of the HTH or DUF domain reduces binding to the above-mentioned proteins. Compared to WT RodZ(*Spn*), the absence of the HTH or DUF domain does not completely abolish the interactions between the truncated RodZ variants and any of the numerous partners tested (Fig. S15; Table S7). For many of them, including MreC, MreD, MpgA, aPBP2a, and EzrA, the signal was unchanged compared to WT RodZ(*Spn*) at the endpoint of the assay (data not shown). Yet, the absence of the HTH domain significantly reduces the interactions of RodZ(*Spn*) with itself and several proteins, including GpsB, bPBP2b, RodA, bPBP2x, FtsW, DivVA, and aPBP1b (Fig. 9C and S15; Table S7). Although not essential in *S. pneumoniae* (Fig. 2 and 6; Table 2), the absence of the extracellular DUF domain also

Accepted Article

reduces the interactions with GpsB, bPBP2b, bPBP2x, or FtsW in the B2H assay (Fig. 9C and S15; Table S7). Together, we conclude that RodZ(*Spn*) is in complexes with numerous pPG elongasome proteins, PG synthesis regulatory proteins, and a few sPG synthesis proteins, possibly through direct interactions in some cases. Implications of these complexes to pneumococcal PG synthesis and division are considered further in *Discussion*.

## 2.7 | Depletion of RodZ(*Spn*) mislocalizes MreC, bPBP2b, and RodA, but not other pPG and sPG synthesis proteins

We tested the hypothesis that RodZ(*Spn*) organizes the assembly of pPG elongasome proteins. We first determined whether incorporation of a fluorescent D-amino acid (FDAA) changes in a *rodZ*(ΔDUF), *rodZ*(ΔHTH), or Δ*rodZ* merodiploid mutant after ectopically expressed WT RodZ is depleted (Fig. S16). FDAA incorporation indicates regions of active PBP transpeptidase activity during PG synthesis (Boersma *et al.*, 2015, Tsui *et al.*, 2014), but does not distinguish between sPG and pPG synthesis at the midcell of *S. pneumoniae* cells (Perez *et al.*, 2021a). As expected, FDAA labeling in Δ*rodZ*(DUF) cells depleted for RodZ (-Zn) is the same as that of cells expressing RodZ (+Zn or WT). FDAA is also similar in Δ*rodZ*(HTH) or Δ*rodZ* cells depleted of RodZ (-Zn inducer), although the RodZ depletion changes the cell size and morphology (Fig. S16). Results presented next show that RodZ depletion disrupts normal localization of MreC and the bPBP2b:RodA pPG synthase. Therefore, we interpret the FDAA labeling at midcell and equators of Δ*rodZ*(HTH) or Δ*rodZ* cells depleted of RodZ to reflect sPG synthesis, which is not disrupted by RodZ depletion. We conclude that RodZ depletion does not lead to widespread mislocalization of sPG synthesis, as occurs upon FtsZ, FtsA, or EzrA

depletion, where EzrA(*Spn*) acts as a positive regulator of FtsZ-ring formation in pneumococcus (Mura *et al.*, 2017, Perez *et al.*, 2021b).

We next constructed  $\Delta rodZ//P_{Zn}\text{-}rodZ^+$  merodiploid strains expressing from native chromosomal loci twelve other PG synthesis and division proteins fused to epitope tags, fluorescent reporter proteins, or a HaloTag (HT) (Fig S17-S22). Apart from three exceptions, we did not observe pronounced fusion-associated phenotypes that suppressed or exacerbated growth defects upon RodZ depletion (-Zn) in these strains. A sfGFP-MpgA fusion suppressed  $\Delta rodZ$  lethality (Fig. S18A and S18B), likely because of reduced MpgA enzymatic activity, which is known to bypass the requirement for the pPG elongasome in *S. pneumoniae* (Taguchi *et al.*, 2021, Tsui *et al.*, 2016). Conversely, GFP-MpgA or HT-bPBP2x fusion exacerbated the drop in OD<sub>620</sub> upon RodZ depletion, without overtly changing localization of the fusion proteins after 4 h of RodZ depletion (Fig. S18C and S22A).

Of the twelve proteins tested, aberrant localization upon RodZ depletion was only observed for MreC (Fig. 10A, 11, and S21), bPBP2b (Fig. 10B, S21, and S22B), and RodA (Fig. S22C) (summarized in Fig. 12). Mislocalization of MreC, bPBP2b, and RodA upon RodZ depletion was demonstrated by demographic analysis (Fig. 11, S21, and S22) and confirmed independently by IFM for MreC and bPBP2b (Fig. 10). By contrast, MpgA (Fig. S18) and aPBP1a (Fig. S20) (pPG synthesis); bPBP2x (Fig. S19 and S22D) (sPG synthesis); FtsZ (Fig. S19), MapZ (Fig. S19), EzrA (Fig. S19), and FtsA (Fig. S20) (Z-ring organization); and StkP (Fig. S20) and DivIVA (Fig. S19) (pPG and sPG synthesis) localize normally at midcell upon RodZ depletion (Fig. 12) (for functions, see (Briggs *et al.*, 2021, Massidda *et al.*, 2013, Straume *et al.*, 2021)). We conclude that RodZ(*Spn*) is

required for normal assembly and localization of MreC, bPBP2b, and RodA in the pPG elongasome.

To test this notion and further establish the assembly hierarchy, we determined protein localization upon MreC depletion. We first established that Zn inducer (0.4 mM ZnCl<sub>2</sub> + 0.4 mM MnSO<sub>4</sub>) does not affect growth or MreC amount in WT cells (Fig. S23). We then showed that MreC depletion for 4 h in a  $\Delta mreC//P_{Zn}\text{-}mreC^+$  merodiploid strain reduces MreC cellular amount to  $\approx 10\%$  of WT, but does not alter bPBP2b or bPBP2x cellular amount (Fig. S24). Depletion of MreC resulted in mislocalization of bPBP2b detected by demographic analysis of HaloTag-bPBP2b (Fig. 13) and by IFM (Fig. S25C). Likewise, demographic analysis showed that RodA mislocalizes upon MreC depletion (Fig. S26B). In contrast, RodZ (Fig. S25A), aPBP1a (Fig. S25B), and bPBP2x (Fig. S26C) remained mostly at their normal midcell positions upon MreC depletion. Together, these results support an assembly hierarchy wherein RodZ is required for MreC midcell localization, which in turn, is required for midcell localization of bPBP2b and RodA (Fig. 14A).

## 2.8 | RodZ(*Spn*), but not MreCD(*Spn*), displays a synthetic-viable genetic relationship with aPBP1b

Tn-seq analysis indicates the essentiality of the cytoplasmic N-terminal HTH and TM domains of RodZ(*Spn*) (above; Fig. 2A, row 1) and confirmed the essentiality of MreC(*Spn*) and MreD(*Spn*) (see above). Unexpectedly, Tn-seq analysis of a  $\Delta pbp1b$  mutant, which lacks aPBP1b of unknown function, indicates suppression of *rodZ* essentiality (*i.e.*, insertions throughout the HTH and TM domains), but not *mreCD* essentiality (Fig. 2A, row 2). Previous results and those reported here show that  $\Delta pbp1a$  suppresses the requirement for MreC, MreD, and RodZ (Table 1) (Fenton *et al.*, 2016,

Land & Winkler, 2011, Tsui *et al.*, 2016). Likewise,  $\Delta khpA$  and  $\Delta khpB$  mutations, which result in the absence of the major KhpAB RNA-binding regulatory protein (Hor *et al.*, 2020, Olejniczak *et al.*, 2022), suppress  $\Delta mreCD$  and  $\Delta rodZ$  mutations (Table 1) (Zheng *et al.*, 2017). These results are reiterated by Tn-seq analysis (Fig. 2A, row 3). Finally, in contrast to  $\Delta pbp1b$  or  $\Delta pbp1a$ , Tn-seq analysis shows that  $\Delta pbp2a$ , which lacks aPBP2a, fails to suppress the essentiality of *mreC*, *mreD*, or *rodZ* in *S. pneumoniae* (Fig. 2A, row 4). We conclude that there is an unanticipated synthetic-viable genetic relationship between null mutations of *pbp1b* and *rodZ*, but not between *pbp1b* and *mreCD* (Fig. 14B). By contrast, there is a different synthetic-viable genetic relationship between null mutations of *pbp1a* and *mreC*, *mreD*, or *rodZ* (Fig. 14C; Discussion).

We confirmed these synthetic-viable relationships detected by Tn-seq by independent transformation assays, in which  $\Delta rodZ$  or  $\Delta mreCD$  amplicons were transformed into deletion mutants of recipient strains (Fig 2B and 2C). Consistent with the Tn-seq results,  $\Delta pbp1b$  suppresses  $\Delta rodZ$ , but not  $\Delta mreCD$ ,  $\Delta pbp1a$  or  $\Delta khpB$  suppresses  $\Delta rodZ$  or  $\Delta mreCD$ , and  $\Delta pbp2a$  does not suppress  $\Delta rodZ$  or  $\Delta mreCD$  (Fig. 2B and 2C). This synthetic-viable genetic relationship between aPBP1b and RodZ could reflect a direct interaction between the proteins. To test this idea, we performed B2H assays. Indeed, aPBP1b interacts with itself and shows bidirectional interactions with RodZ, MreC, or aPBP1a (Fig. 2D), as well as unidirectional interactions with MreD, MpgA, aPBP2a, or EzrA. Altogether, these results implicate aPBP1b in the regulation of the pPG elongasome, possibly through direct interaction with RodZ, as discussed below.

### 3 | DISCUSSION

The essentiality of RodZ(*Spn*) has been controversial (Stamsas *et al.*, 2017, Straume *et al.*, 2017, Tsui *et al.*, 2016).  $\Delta rodZ$  mutants can be constructed in laboratory strain R6 and its derivatives (Martin-Galiano *et al.*, 2014, Straume *et al.*, 2017); however, these R6-derived strains contain dozens of mutations compared to progenitor D39 strain, including mutations in *pbp1a* (Land & Winkler, 2011, Lanie *et al.*, 2007). Moreover, full suppression of essential mutations in R6-strains requires additional unspecified mutations, besides those known in *pbp1a* (Land & Winkler, 2011), making genetic deconvolution problematic. Because of this genetic variance, R6-derived strains have significant differences in shape and the timing of cell division compared to progenitor D39 strains (Trouve *et al.*, 2021), indicating that R6-derived strains are not an exact model for mechanisms of PG synthesis and cell division that occur in their virulent progenitor D39 strain. Yet, *rodZ* has also been classified as non-essential in several Tn-seq studies of different *S. pneumoniae* serotype strains (Slager *et al.*, 2018, van Opijnen & Camilli, 2012). Tn-seq and deletion analyses (Fig. 2 and 6) presented here show that the entire extracellular domain corresponding to about 48% of *rodZ(Spn)* is dispensable, which may account for these previous misclassifications. The essentiality of *rodZ* and other members of the pPG elongasome, including *mreC*, *mreD*, *pbp2b*, and *rodA*, was confirmed by transformation assays of unencapsulated ( $\Delta cps$ ) *S. pneumoniae* D39 grown at 37°C (Table 1; Fig. S2C). *rodZ* was also confirmed to be essential by transformation assays of encapsulated D39 strains (Table 1) and by depletion assays of unencapsulated strains (Fig. 3-5). Analogous to the case in *E. coli* (Bendezu & de Boer, 2008), this essentiality is conditional in unencapsulated D39 strains. Mutants lacking components of the pneumococcal pPG elongasome (MreCD, bPBP2b, RodA, or RodZ) grow poorly at the lower temperature of

32°C under the growth conditions tested (Fig. S2). It remains to be tested whether this residual growth at 32°C, which is close to the that of the nasopharynx, is of physiological significance *in vivo*, because insertions in *mreC*, *pbp2b*, or *rodA* are not recovered in Tn-seq screens of a murine nasal colonization model (van Opijnen & Camilli, 2012).

In rod-shaped bacteria, RodZ acts as the linker between cytoplasmic MreB filaments and the largely extracellular Rod complex containing regulators MreC and MreD and the PG synthase complex consisting of an essential bPBP and SEDS-protein RodA (reviewed in (Rohs & Bernhardt, 2021)). Despite the absence of MreB, the overall structure of RodZ(*Spn*) is remarkably similar to that of RodZ in rod-shaped bacteria that have MreB (Fig. 1 and S1) (Ago & Shiomi, 2019, Alyahya *et al.*, 2009, Bendezu *et al.*, 2009, Shiomi *et al.*, 2008). Nevertheless, the TM and cytoplasmic domains, including the HTH domain, are essential for RodZ(*Spn*) function (Fig. 2 and 6; Table 2), similar to their importance in rod-shaped bacteria (Alyahya *et al.*, 2009, Bendezu *et al.*, 2009, Morgenstein *et al.*, 2015, Shiomi *et al.*, 2008). In rod-shaped bacteria, the HTH domain of RodZ binds to MreB, and changes in amino acids in one helix (Fig. 1 and S9) alter this interaction (Bendezu *et al.*, 2009, Morgenstein *et al.*, 2015, van den Ent *et al.*, 2010). However, amino acid changes at corresponding positions in RodZ(*Spn*) do not cause a detectable phenotype (Table 2; Fig. 6). In contrast to the HTH and TM domains, the RodZ(*Spn*) β-strand DUF domain and most of the extracellular unstructured linker (beyond amino acid 132) are dispensable for growth, although cell morphology is altered by truncation ending at amino acid Q134 (Fig. 2 and 6; Table 2). Deletion of the RodZ(*Spn*) DUF domain lessens interactions with a couple of proteins in B2H assays, including bPBP2b (Fig. 9C and S15A); however, these interactions, if they exist in pneumococcal cells, are dispensable.

Several lines of evidence presented here strongly link RodZ(*Spn*) to the elongasome that carries out pPG synthesis at the middle of dividing pneumococcal cells (Briggs *et al.*, 2021, Massidda *et al.*, 2013, Perez *et al.*, 2021a, Philippe *et al.*, 2014, Tsui *et al.*, 2014). Transformation assays show that  $\Delta rodZ(Spn)$  is suppressed by the same mutations that suppress  $\Delta mreC$ , including  $\Delta pbp1a$ , *mpgA*(Y488D),  $\Delta khpA$ , insertions in *khpB*, and overexpression of FtsA (Fig. 2; Table 1)) (Land & Winkler, 2011, Tsui *et al.*, 2016, Zheng *et al.*, 2017). MreC and MpgA are members of the pPG elongasome (Briggs *et al.*, 2021, Fenton *et al.*, 2016, Land & Winkler, 2011, Philippe *et al.*, 2014, Straume *et al.*, 2017, Tsui *et al.*, 2016), and KhpAB and FtsA amounts regulate the requirement for pPG elongasome in *S. pneumoniae* (Zheng *et al.*, 2017). Although CozE(*Spn*) also associates with proteins in the pPG elongasome (Fenton *et al.*, 2016), it is neither essential, nor is the poor growth of  $\Delta cozE$  mutants suppressed by  $\Delta pbp1a$ , *mpgA*(Y488D), or other mutations that suppress  $\Delta mreC$  and  $\Delta rodZ$  in transformation assays (Table 1). These results suggest different functions of MreC and RodZ from CozE in pPG elongation under the conditions tested here.

In addition, throughout the cell cycle, RodZ(*Spn*) colocalizes with pPG elongasome members MreC and aPBP1a (Fig. 7), which are genetically linked to pPG synthesis (see below) (Briggs *et al.*, 2021, Fenton *et al.*, 2016, Land & Winkler, 2011, Massidda *et al.*, 2013, Tsui *et al.*, 2014). These colocalization experiments were performed by IFM of exponentially growing cells expressing C-terminal RodZ-Myc, RodZ-FLAG, or RodZ-L-FLAG<sup>3</sup> fusions from the *rodZ* native locus. These constructs did not cause observable growth or morphology defects (Fig. S11 and S12). Attempts to construct numerous RodZ(*Spn*) N-terminal, C-terminal, or internal sandwich-fusions to different fluorescent-

protein reporters were unsuccessful, because the fusions were lethal, caused cell morphology defects, and/or showed diffuse fluorescence over entire cells (data not shown). Finally, depletion experiments of RodZ(*Spn*) or MreC(*Spn*) demonstrate that RodZ is required for MreC, bPBP2b, and RodA localization, whereas MreC is required for bPBP2b and RodA localization, but not for RodZ localization (Fig. 10-14). Together, these transformation assays, colocalization, and assembly hierarchy results establish that RodZ is a member of the pPG elongasome of *S. pneumoniae*.

RodZ(*Spn*) acting as a scaffold for the MreC/bPBP2b/RodA complex is analogous to its function in rod-shaped bacteria, where an assembly hierarchy has not yet been reported (Ago & Shiomi, 2019, Bendezu *et al.*, 2009, Morgenstein *et al.*, 2015, Rohs & Bernhardt, 2021). However, there are some specific differences in phenotypes that may reflect the absence of an MreB-dependent mechanism in *S. pneumoniae*. Depletion of RodZ(*Spn*) is bacteriostatic, halts growth, and leads to cell rounding, increased size, and slight chaining (Fig. 3-5 and S4-S5). Nonetheless, cells depleted for RodZ(*Spn*) are more heterogenous in shape and form shorter chains than cells depleted of MreC(*Spn*) (Land & Winkler, 2011), bPBP2b(*Spn*) (Berg *et al.*, 2013, Tsui *et al.*, 2014), or the regulated FtsEX:PcsB(*Spn*) PG hydrolase (Sham *et al.*, 2011, Sham *et al.*, 2013), which also localizes with the pPG elongasome (Perez *et al.*, 2021a) and may act as a remodeling space maker during PG synthesis (Bartual, *et al.*, 2014, Briggs *et al.*, 2021, Rued *et al.*, 2019, Sham *et al.*, 2011, Trouve *et al.*, 2021). These results suggest that RodZ(*Spn*) may have some functions distinct from MreC(*Spn*), as discussed below for aPBP1b (see Fig. 14B). In another example, activated mutants of bPBP2(*Eco*) largely bypass the requirement for regulators MreC, MreD, and RodZ, suggesting that MreB, bPBP2, and

RodA form the core of the *E. coli* elongasome (Rohs *et al.*, 2018). In contrast, corresponding amino acid changes in the pedestal region of bPBP2b(*Spn*) fail to suppress  $\Delta$ *rodZ* mutations (Table S6), raising the possibility that bPBP2(*Eco*) activation is dependent on MreB. Other differences in phenotypes suggest functional differences between RodZ in *S. pneumoniae* and *E. coli*. Overexpression of FtsZ(*Spn*) does not suppress  $\Delta$ *rodZ*(*Spn*) (Table 1), and overexpression of RodZ(*Spn*) does not alter cell shape (Fig. S6), in contrast to overexpression phenotypes reported in *E. coli* and *C. crescentus* (Alyahya *et al.*, 2009, Bendezu *et al.*, 2009, Shiomi *et al.*, 2008).

To further define the role of RodZ(*Spn*) in pPG synthesis by the elongasome, we performed co-IP and B2H assays (summarized in Fig. 8 and 9). B2H and bimolecular fluorescence complementation assays and genetic approaches have indicated that RodZ of rod-shaped bacteria interacts with MreB and with other components of the Rod complex, including MreC, MreD, bPBP2, and RodA (Ago & Shiomi, 2019, Alyahya *et al.*, 2009, Beilharz *et al.*, 2012, Morgenstein *et al.*, 2015, Shiomi *et al.*, 2013, van den Ent *et al.*, 2010). Likewise, RodZ(*Spn*) is found in complexes in unsynchronized pneumococcal cells with tested proteins bPBP2b, MreC, MpgA, and aPBP1a, which have been implicated in pPG elongation (Fig. 8; Table 3) (Briggs *et al.*, 2021, Philippe *et al.*, 2014, Straume *et al.*, 2021). Direct interactions were detected in B2H assays between RodZ(*Spn*) and these proteins and with other elongasome proteins MreD and RodA (Fig. 9), which were not tested in co-IP assays (Fig 8). In addition, complexes and direct interactions were detected for RodZ(*Spn*) and other aPBPs (aPBP2a and aPBP1b), PG synthesis regulators (GpsB and DivIVA), the sPG synthase components (bPBP2x and FtsW), and EzrA (Fig. 2, 8, and 9; Table 3). Based on B2H assays, many of these

interactions are mediated at some level by the cytoplasmic HTH domain of RodZ(*Spn*), but others are not (Fig. 9 and S15; Table S7). Phosphorylation of RodZ(*Spn*) by StkP was not detected by western blotting (Fig. S10) or by phosphoryl-proteomic analysis (Ulrych *et al.*, 2021).

The functions and timing of these putative interactions of RodZ(*Spn*) with proteins outside of the canonical elongasome remain to be determined. Pneumococcal GpsB is found in complexes with EzrA, MreC, aPBP2a, bPBP2b, and StkP, which itself is detected in complexes with MreC, bPBP2b, and bPBP2x, at currently unknown stages of cell division (Cleverley *et al.*, 2019, Rued *et al.*, 2017). The interactions and phenotypes of *gpsB* mutants suggest a model wherein GpsB activates protein phosphorylation by StkP and also balances sPG and pPG synthesis at the midcell of dividing pneumococcal cells (Cleverley *et al.*, 2019, Fleurie *et al.*, 2014b, Rued *et al.*, 2017). Moreover, a low level of bPBP2x is detected in the outer midcell pPG synthesis ring of *S. pneumoniae* (Briggs *et al.*, 2021, Perez *et al.*, 2021a, Tsui *et al.*, 2014). On the other hand, strong complexes containing RodZ(*Spn*) and FtsZ were not detected by co-IP (Fig. 8; Table 3) and no interactions between RodZ(*Spn*) and FtsZ were detected by B2H assays (Fig. 9), in contrast to what was reported in *E. coli* (Ago & Shiomi, 2019, Yoshii *et al.*, 2019). In this regard, *S. pneumoniae* lacks a homolog of newly characterized ZapG, which interacts with elongasome proteins, including RodZ(*Eco*), and divisome proteins (Mehla *et al.*, 2021). At best, only marginal complexes were detected containing RodZ(*Spn*) and FtsA, which is an actin homolog like MreB (Fig. 8). Altogether, the detected interactions and assembly patterns are consistent with RodZ(*Spn*) acting as a scaffold protein that may

link GpsB and EzrA to the assembly and function of the pneumococcal pPG elongasome (Fig. 14A).

A main finding from this study is the synthetic-viable genetic relationship specifically between RodZ and aPBP1b, but not between RodZ and MreCD in *S. pneumoniae* (Fig. 2 and 15). This is one of the first phenotypes that has been associated with pneumococcal aPBP1b, about which little is known (Briggs *et al.*, 2021, Ducret & Grangeasse, 2017, Straume *et al.*, 2021). The regulation and functions of Class A PBPs are not generally well understood in *S. pneumoniae* and other bacteria, but likely play roles during normal growth and stress conditions (Briggs *et al.*, 2021, Pazos & Vollmer, 2021, Rohs & Bernhardt, 2021, Straume *et al.*, 2021, Vigouroux *et al.*, 2020). aPBP1a and aPBP2a have a synthetic-lethal relationship, such that  $\Delta pbp1a \Delta pbp2a$  mutants are inviable (Paik *et al.*, 1999, Straume *et al.*, 2021). In addition, aPBP1a was shown previously to have a synthetic-viable relationship with the elongasome components MreC, MreD, and RodZ, such that  $\Delta pbp1a$  suppresses and allows growth of strains containing normally lethal  $\Delta mreC$ ,  $\Delta mreCD$ , or  $\Delta rodZ$  mutations (Fig. 2; Table 1) (Fenton *et al.*, 2016, Land & Winkler, 2011, Tsui *et al.*, 2016). Notably,  $\Delta pbp1a$  does not suppress  $\Delta pbp2b$  or  $\Delta rodA$ , indicating that aPBP2b and RodA are still required for viability in the absence of MreCD, RodZ, and aPBP1a (Tsui *et al.*, 2016). In contrast to aPBP1a, aPBP1b displays a synthetic-viable relationship only with RodZ, but not with MreCD, such that  $\Delta pbp1b$  suppresses  $\Delta rodZ$ , but does not suppress  $\Delta mreCD$  (Fig. 2A). This synthetic viable relationship was confirmed by transformation assays (Fig. 2B and 2C), and B2H assays indicate direct interactions between aPBP1b and RodZ, MreC, or aPBP1a (Fig. 2D). Tn-

seq data confirms that  $\Delta pbp1b$  also does not suppress knock-out insertions in *pbp2b* or *rodA* (data not shown).

Different models can account for the synthetic-viable relationships of aPBP1b and aPBP1a with components of the pPG elongasome. Our favored model postulates that some form of pPG synthesis is essential for pneumococcal viability and that failsafe mechanisms can bypass or modulate the function of the core RodZ-MreCD-bPBP2b-RodA elongasome (Fig. 14B and 14C). pPG synthesis may be essential, because it drives the composite MapZ/FtsZ/FtsA/EzrA nascent equatorial rings from midcell to the middle of daughter cells (Briggs *et al.*, 2021, Fleurie *et al.*, 2014a, Holeckova *et al.*, 2014, Perez *et al.*, 2019). The absence of aPBP1b induces the pneumococcal WalRK two-component system (TCS) regulon (Zheng *et al.*, 2017), which responds to cell wall stresses (Gutu *et al.*, 2010, Tsui *et al.*, 2016, Wayne *et al.*, 2012). Induction of the WalRK TCS increases transcript amounts of genes encoding PG hydrolases and PG-binding proteins (Ng *et al.*, 2005). Another possible change that may occur in the absence of aPBP1b is altered activity and/or interactions of aPBP1a, which associates with the core pPG elongasome and can provide alternate TP and GT activities (Fig. 8 and 9) (Briggs *et al.*, 2021, Land & Winkler, 2011, Philippe *et al.*, 2014, Tsui *et al.*, 2016). In a  $\Delta rodZ \Delta pbp1b$  mutant, these alternate activities and/or interactions are proposed to bypass the defects in pPG elongasome assembly in the absence of RodZ and allow the aPBP2b:RodA PG synthase and perhaps aPBP1a to carry out sufficient pPG synthesis for division and growth (Fig. 14B).

The absence of aPBP1a also induces the WalRK regulon (Zheng *et al.*, 2017), changes cell shape in culture (Land & Winkler, 2011, Tsui *et al.*, 2016), and possibly alters

the interactions and/or functions aPBP1b, which is associated with the pneumococcal pPG elongasome (Fig. 2). In a  $\Delta pbp1a \Delta mreCD \Delta rodZ$  mutant, alternate activities and/or interactions would bypass the defects in pPG elongasome assembly in the absence of RodZ and MreCD and allow the bPBP2b:RodA PG synthase and perhaps aPBP1b to carry out sufficient pPG synthesis for division and growth (Fig. 14C). Another putative component of failsafe, bypass mechanisms for pPG synthesis is the sPG synthase bPBP2x:FtsW. A majority of bPBP2x migrates in the inner ring of sPG synthesis at the leading edge of the closing septal annulus (Briggs *et al.*, 2021, Perez *et al.*, 2021a, Tsui *et al.*, 2014). However, some bPBP2x, and presumably FtsW, remains in the outer pPG synthesis ring and may provide an alternate pathway of pPG synthesis. Consistent with this notion, RodZ(*Spn*) associates with bPBP2x and FtsW (Fig. 8 and 9; Table 3). Finally, although aPBP2a also associates with the pPG elongasome (Fig. 8 and 9; Table 3), there is no genetic evidence that implicates aPBP2a in a bypass mechanism of pPG synthesis (Fig. 2), and  $\Delta pbp2a$  does not induce the WalRK TCS (Zheng *et al.*, 2017).

Other genetic patterns strongly support the idea of alternate, bypass mechanisms to maintain pPG synthesis in *S. pneumoniae*. The pPG elongasome-associated muramidase MpgA (formerly MltG(*Spn*)) (Fig. 8 and 9) is essential; yet,  $\Delta mpgA$  is suppressed by  $\Delta pbp1a$  (Taguchi *et al.*, 2021, Tsui *et al.*, 2016). Furthermore, a triple  $\Delta pbp1a \Delta mpgA \Delta pbp2b$  mutant lacks the core pPG elongasome, but is viable and forms elongated cells (Tsui *et al.*, 2016). In addition, a *mpgA*(Y488D) mutant, which expresses an MpgA with greatly reduced enzymatic activity (Taguchi *et al.*, 2021, Tsui *et al.*, 2016), bypasses the requirement for the core pPG elongasome, in that *mpgA*(Y488D)  $\Delta pbp2b$  and *mpgA*(Y488D)  $\Delta rodA$  mutants are viable and form elongated cells (Tsui *et al.*, 2016).

Yet, the *mpgA*(Y488D)  $\Delta pbp2b$   $\Delta pbp1a$  mutant is now inviable, which appears at odds with the phenotype of the  $\Delta pbp1a$   $\Delta mpgA$   $\Delta pbp2b$  mutant. This apparent discrepancy can be explained if aPBP1b mediates pPG bypass synthesis in the  $\Delta pbp1a$   $\Delta mpgA$   $\Delta pbp2b$  mutant, while aPBP1a mediates pPG bypass synthesis in the *mpgA*(Y488D)  $\Delta pbp2b$  mutant, where aPBP1a bypass activity is dependent on the physical presence, but not the activity, of MpgA(Y488D). Finally, the shape and size of WT and  $\Delta pbp1b$  cells grown in BHI broth are similar to those of  $\Delta pbp1b$   $\Delta rodZ$  mutants, with some heterogeneity, whereas  $\Delta pbp1a$   $\Delta rodZ$  cells have the distinctive shorter, narrower shape of  $\Delta pbp1a$  mutant cells compared to WT (data not shown) (Land & Winkler, 2011, Tsui et al., 2016). These data indicate that suppression of  $\Delta rodZ$  by  $\Delta pbp1b$  or  $\Delta pbp1a$  are not equivalent, consistent with different mechanisms. Taken together, these results support the hypothesis of multiple bypass pathways for essential pPG synthesis when the core pPG elongasome is incomplete or absent.

Another model for the synthetic-viable relationships of aPBP1b and aPBP1a with components of the pPG elongasome invokes direct regulation of aPBP activity, interactions, and/or localization (Fig. S27) (Land & Winkler, 2011, Tsui et al., 2016). In this model, RodZ(*Spn*) acts as a negative regulator of aPBP1b activity, interactions, and/or mislocalization. The absence of RodZ causes aPBP1b misregulation that contributes to cell lethality (Fig. S27A). Likewise, MreC, MreD, and RodZ would negatively regulate aPBP1a activity, interactions, and/or mislocalization. In the absence of MreC, MreD, or RodZ, aPBP1a misregulation contributes to cell lethality (Fig. S27B).

There are issues with this alternative model. First, to date, PBPs have been found to be positively regulated, rather than negatively regulated. For example, in *E. coli* the

activities of FtsI(bPBP3), bPBP2, aPBP1a, and aPBP1b are positively activated by FtsN, MreC, LpoA, and LpoB, respectively (Pazos & Vollmer, 2021, Pichoff *et al.*, 2019, Rohs & Bernhardt, 2021). In *S. pneumoniae*, aPBP2a is positively regulated by MacP and GpsB (Cleverley *et al.*, 2019, Fenton *et al.*, 2018). Second, aPBP misregulation alone is insufficient to account for cell lethality, because function of the bPBP2b:RodA pPG synthase is still essential (Fig. 14B and 14C), despite suppression of  $\Delta rodZ$  or  $\Delta mreCD$   $\Delta rodZ$  by  $\Delta pbp1b$  or  $\Delta pbp1a$ , respectively (Fig. 2). Third, aPBP1a localizes normally when RodZ or MreC is depleted (Fig. 12 and 13C). This result contrasts with a previous conclusion that aPBP1a mislocalizes in the absence of MreC (Fenton *et al.*, 2016). The different results may reflect the ectopic induction of potentially high levels of active GFP-aPBP1a in a  $\Delta mreC$  mutant, which is not tolerated, as opposed to the MreC depletion used here in a strain expressing epitope-tagged aPBP1a-FLAG from its chromosomal locus (Fig. S25B). Moreover, moderate ( $\approx$ 2-fold) overexpression of aPBP1a in a WT strain does not overtly affect normal cell morphology or growth (Averi McFarland; unpublished result). Finally, because the synthetic-viable relationships of the aPBPs with components of the pPG elongasome are different, it is difficult to reconcile a model postulating that absence of aPBP1b or aPBP1a in the  $\Delta rodZ$  or  $\Delta rodZ$   $\Delta mreCD$  mutant, respectively, solely decreases competition or interference with residual bPBP2b:RodA pPG synthase activity. For this type of model to work, there still needs to be differential regulation of aPBP1b or bPBP1a expression, activity, and/or interactions allowing bypass pPG synthesis. Therefore, current data supports alternate mechanisms leading to pPG bypass synthesis more than other models for these synthetic-viable genetic relationships.

The different synthetic-viable relationships of aPBP1b and aPBP1a with components of the pPG elongasome indicates functional fungibility during pPG synthesis in *S. pneumoniae*. This flexibility points to altered protein interactions and/or regulatory pathways that enable alternate pPG synthesis pathways. Some of these outcomes may be through direct interactions, while others may be indirect through additional proteins induced or regulated by stress responses. Along the same lines, CozE does not have a strong synthetic viable relationship with aPBP1a in transformation assays or in Tn-seq analyses (data not shown) under the conditions used here, and  $\Delta cozE$  was not suppressed by the array of mutations that suppress  $\Delta rodZ$  and  $\Delta mreC$  (Table 1). These shared and different functions and interactions of pPG elongasome members RodZ, MreC, MreD and CozE require further study at different stages of the pneumococcal cell cycle. Taken together, we conclude that both aPBP1a and aPBP1b play roles in the regulation of the pPG elongasome and possibly participate in pPG synthesis in *S. pneumoniae*. The action of RodZ(*Spn*) in assembly and function of the pPG elongasome and the roles of the aPBPs in WT and bypass pPG synthesis are important topics for future studies.

## 4 | EXPERIMENTAL PROCEDURES

### 4.1 | Strain construction and growth conditions

Bacterial strains used in this study are derivatives of the unencapsulated, *S. pneumoniae* serotype 2 strain D39W (Lanie *et al.*, 2007, Slager *et al.*, 2018), and are listed in Table S1. For strains containing antibiotic markers, linear DNA amplicons synthesized by fusion PCR were transformed into competent pneumococcal cells as described in (Land *et al.*,

2013, Tsui *et al.*, 2010, Tsui *et al.*, 2014). For antibiotic selection Trypticase soy agar II (modified; Becton-Dickinson) and 5% (vol/vol) defibrinated sheep blood (TSII-BA) plates were supplemented with the following final concentrations of antibiotics: 250 µg kanamycin/mL, 150 µg spectinomycin/mL, 0.3 µg erythromycin/mL, 200 µg streptomycin/mL, or 0.25 µg tetracycline/mL. Strains containing markerless mutations or insertions at the native site in the chromosome, e.g. *iht-pbp2b* markerless (i-tag-HaloTag (iHT) fused to bPBP2b (Perez *et al.*, 2019)), were constructed through two rounds of transformation via the Janus method, as described in (Sung *et al.*, 2001). Linkers used in construction of fluorochrome or epitope-tagged fusion proteins are listed in Table S2. All primers and templates used in this study are listed in Table S4. All strains were confirmed via PCR and sequencing. For overnight growth, BHI broth was inoculated with frozen glycerol stocks, serially diluted and propagated overnight for 12-13 hours at 37°C in an atmosphere of 5% CO<sub>2</sub>. Antibiotics were not added to the media. To start experiments, overnight cultures with an OD<sub>620</sub> of 0.1-0.4 (exponentially growing) were diluted to an OD<sub>620</sub> of 0.003 in fresh BHI, lacking antibiotics.

#### 4.2 | Tn-seq transposon library generation and insertion sequencing

Tn-seq was carried out using protocols in (Fenton *et al.*, 2016, van Opijken *et al.*, 2015) with the following modifications. A transposon insertion library was generated for each of the following strains: WT D39  $\Delta$ cps *rpsL1* (IU1824), isogenic  $\Delta$ *pbp1b* (IU14697),  $\Delta$ *khpB* (IU10592), and  $\Delta$ *pbp2a* (IU13256). Approximately 200,000 (WT,  $\Delta$ *pbp1b* and  $\Delta$ *khpB*) or 300,000 ( $\Delta$ *pbp2a*) transformants were pooled for each library (see Appendix A). Genomic DNA preparations were modified from the instructions provided by Qiagen for Gram-positive bacteria using a DNeasy blood and tissue kit (Qiagen 69504). 5 mL of cultures

at  $OD_{620} = 0.4$  were centrifuged for 10 min at  $5,000 \times g$  at room temperature and suspended in 180  $\mu L$  of enzymatic lysis buffer containing 20 mg/mL lysozyme, and incubated for 30 min at  $37^{\circ}C$ . 10  $\mu L$  of RNase A (Qiagen 19101, 100 mg/ml) was added, followed by a 5-min incubation at room temperature. Subsequent steps were as specified by the Qiagen manual, except that DNA was eluted with 100  $\mu L$  of water. Eluted genomic DNA and pMagellan6 DNA prepared with a QIAprep Spin Miniprep Kit (27104) were concentrated by ethanol precipitation to concentrations of more than 0.3  $\mu g/\mu L$  in ultrapure distilled water. *In vitro* transposition reactions were performed as described previously (van Opijnen *et al.*, 2015) with genomic DNA obtained from WT or mutant strains with the following modifications. A reaction mixture of 1  $\mu g$  genomic DNA, 1  $\mu g$  pMagellan6 DNA, and 3  $\mu L$  of purified MarC9 transposase prepared as specified in (van Opijnen *et al.*, 2015) was incubated at  $30^{\circ}C$  for 4h. Transposon junctions were repaired by using 1 $\mu L$  of 3 U/ $\mu L$  T4 DNA polymerase at  $12^{\circ}C$  for 30 min. All incubation steps were performed in a thermocycler. Ten independent 20  $\mu L$ -transposition products were prepared each time and stored at  $-20^{\circ}C$ . Starter cultures for transformation were prepared by growing frozen stocks of respective strains in 4 mL of BHI broth at  $37^{\circ}C$  with  $CO_2$  to  $OD_{620} \approx 0.15$ . The cultures were centrifuged for 3 min at  $16,000 \times g$  at room temperature, and pellets were resuspended in 400  $\mu L$  BHI broth mixed with 600  $\mu L$  25% glycerol. 50- $\mu L$  aliquots of starter cultures were stored at  $-80^{\circ}C$ .

Transposed DNA was transformed into CSP-1 induced competent WT or mutant strains and plated onto TSAll agar plates containing spectinomycin and catalase. On the day of transformation, recipient strains were grown from frozen starter cultures in 5 mL of BHI broth to  $OD_{620} \approx 0.03-0.04$ . TSAll agar (BBL 212305) plates containing spectinomycin

and catalase were prepared by pouring 17 mL of warm TSAll agar containing 150 µg/mL spectinomycin into each 100 x 15 mm plate. After solidification, 396 µL (13,000U to 15,000U) of catalase solution (Worthington, CAT # LS001896) were spread on the surface of each plate and dried for 30 min in a sterile hood. Transformation mixes were prepared by addition of 40 µL CSP-1 (50 ng/µL), 1 mL heat inactivated horse serum, 45 µL 40% glucose, to 9 mL BHI broth. 300 µL of cell culture at  $OD_{620} \approx 0.03-0.04$  were mixed with 700 µL of transformation mix. After incubation at 37°C for 10 min, 3-8 µL of respective transposed DNA were added to each transformation, and the mixtures were incubated at 37°C for 1 h. Transformations containing no DNA or 27 ng of genomic DNA obtained from IU2072 containing *spxR*::Mariner (Ramos-Montanez *et al.*, 2008) were used as negative or positive controls. 200 µL of transformed cell culture were spread on the surface of each prepared TSAll/spectinomycin/catalase plate, which were incubated at 37°C in 5% CO<sub>2</sub> for 20 h.

After 20 h of incubation, colonies were scraped from 50 plates and collected in 20 mL of BHI broth. Cell suspensions were centrifuged for 8 min at 3,000 x g at room temperature, and the pellets were resuspended in 3 mL BHI mixed with 2 mL 25% glycerol. From each transformation, twenty 250-µL of transposon library starter culture aliquots were stored at -80°C. For WT,  $\Delta pbp1b$ ,  $\Delta khpB$  strains, transposon library starter cultures were obtained from  $\approx 200,000$  colonies with 11, 2, and 5 independent transformations, respectively. For  $\Delta pbp2a$  strain, transposon library starter cultures were obtained from  $\approx 300,000$  colonies with 4 independent transformations. Transposon library starter cultures from different transformations were thawed and mixed together in proportion to the numbers of transformants obtained from each transformation. The

Accepted Article

combined starter cultures were diluted to  $OD_{620} \approx 0.005$  in 5 mL of BHI broth containing 180  $\mu$ g/mL spectinomycin and 5  $\mu$ L/mL Ec-oxyrase (Oxyrase, EC0005), and were grown at 37°C with 5 % CO<sub>2</sub> to  $OD_{620} \approx 0.4$ . 5 mL of culture at  $OD_{620} \approx 0.4$  were used to extract genomic DNA using DNeasy blood and tissue kit. 3  $\mu$ g of DNA from each sample was used for *MmeI* digestion, followed by ligation to adaptors described in (van Opijken *et al.*, 2015). The samples were further processed according to (Fenton *et al.*, 2016) and sequenced on the Illumina NextSeq 500 using a NextSeq 75 high sequencing kit at the Center for Genomics and Bioinformatics, Indiana University Bloomington. Sequencing reads were de-multiplexed and trimmed using the QIAGen CLC genomics workbench (version 11.0.1). Data were mapped and analyzed as described in (Fenton *et al.*, 2016). Insertion data were visualized graphically using the Artemis genome browser (version 10.2) (Carver *et al.*, 2012). Tn-seq primary data for the region between *mreD* (*spd\_2044*) and *spd\_2051*, the gene upstream *rodZ* (*spd\_2050*), are contained in Appendix A, including run summaries, number of reads per TA site in each gene, and count ratios for each gene in the indicated mutants compared to WT. P values for comparisons of the number of reads per TA site in each gene were calculated by the Mann-Whitney test using GraphPad Prism (9.2.0).

#### 4.3 | Growth of Zn-dependent depletion and merodiploid strains

Ectopic expression of *rodZ* or *mreC* was achieved from a zinc-inducible promoter (P<sub>Zn</sub>) in the *bgaA* site (Tsui *et al.*, 2016, Tsui *et al.*, 2014). 0.4 mM of ZnCl<sub>2</sub> and corresponding 1/10 concentration of MnSO<sub>4</sub> were added to TSAll-BA plates or BHI broth for inducing conditions. Mn<sup>2+</sup> was added to Zn<sup>2+</sup> conditions to prevent zinc toxicity (Jacobsen *et al.*, 2011, Perez *et al.*, 2021b, Tsui *et al.*, 2016). Depletion strains requiring ZnCl<sub>2</sub> for growth

were grown overnight in BHI broth in the presence of Zn inducer (0.4 mM ZnCl<sub>2</sub> + 0.04 mM MnSO<sub>4</sub>). For depletion/complementation experiments, overnight cultures (OD<sub>620</sub> of 0.1-0.4) supplemented with inducer were diluted to an OD<sub>620</sub> of 0.003 in 5 mL fresh BHI with or without inducer. Growth was monitored every 1 hour using a Genesys 2 spectrophotometer (Thermo Scientific) for 10 h. For these experiments, the point of resuspension serves as time zero, (T = 0). All growth curves and microscopy experiments were performed two or more times with similar results.

#### 4.4 | Transformation assays

Transformations were performed as detailed in (Rued *et al.*, 2017, Tsui *et al.*, 2016). All amplicons (experimental and control) contained ≈1 kb flanking region and were obtained from PCR reactions using primer pairs and templates listed in Table S4. Recipient strains were grown to OD<sub>620</sub> ≈0.03 from glycerol ice stock and 100 µL was added to 900 µL of transformation mix containing 10% (wt/vol) heat-treated horse serum, 0.18% (wt/vol) glucose, 100 ng CSP-1 (competence stimulatory peptide, type 1) mL<sup>-1</sup> and 9 mL of BHI. The mixture was incubated for 10 min at 37°C in the presence of 5% CO<sub>2</sub>. 30 or 100 ng of purified amplicon (for unencapsulated and encapsulated strains, respectively) was added to the transformation mixture and incubated for 1 h at 37°C in the presence of 5% CO<sub>2</sub>. A fraction or the entire final transformation mixture was added to 3 mL of soft agar containing the appropriate antibiotic (72 µL of 0.1 mg erythromycin mL<sup>-1</sup>, 36 µL of 0.1 mg spectinomycin mL<sup>-1</sup>, 60 µL of 100 mg streptomycin mL<sup>-1</sup>, or 120 µL of 50 mg kanamycin mL<sup>-1</sup>) and plated onto TSAll-BA plates. Unless explicitly stated, the numbers of colonies listed are normalized to 1 mL of transformation mixture. Transformants were incubated

overnight in the presence of 5% CO<sub>2</sub> for 20-24 h, at which time colony numbers and morphology were counted and evaluated.

#### **4.5 | Viable count (CFU) assays**

At various time points (3, 4, 5, 6, and 7.5 h) in depletion and complementation experiments, 100 µL of culture was suspended in 900 µL of 1X PBS and serially diluted from 10<sup>-1</sup> to 10<sup>-7</sup>. 100 µL of three selected dilutions were suspended in 3 mL of molten soft agar and poured onto TSAI<sup>II</sup>-BA plates with or without inducer, 0.4 mM Zn + 0.04 mM Mn. Solidified plates were incubated at 37°C in the presence 5% CO<sub>2</sub> for 20-24 h. Plates containing 30-300 CFUs were scored and counted with respect to colony number and size. CFU/mL values were calculated for each strain and condition.

#### **4.6 | Image Acquisition and processing**

For 2D-epifluorescence microscopy (eFM), 2D-immunofluorescence microscopy (IFM), and phase-contrast microscopy (PCM) experiments, images were taken using a Nikon E-400 epifluorescence phase-contrast microscope and 100X Nikon Plan Apo oil-immersion objective (numerical aperture, 1.40) connected to a CoolSNAP HQ2 charged-coupled device (CCD) camera (Photometrics). Images were analyzed with NIS-Elements AR software (Nikon). Micrographs were assembled using Adobe Illustrator and all images are to scale.

#### **4.7 | Cell length and width measurements**

Cell lengths and widths of strain growing exponentially in BHI broth were measured as previously described (Perez *et al.*, 2021b, Tsui *et al.*, 2016). For all strains, only ovoid-shape pre-divisional cells were measured. Unless indicated in the figure legends, more than 50 cells from one experiment were measured, and plotted with box and whiskers

plot (5 to 95 percentile whiskers). P values were obtained by one-way ANOVA analysis by using the Kruskal-Wallis test in GraphPad Prism program.

#### **4.8 | Live-dead staining and eFM**

Live/dead staining was performed using the BacLight Bacterial Viability kit (Syto9 and Propidium Iodide), according to the manufacturer's instructions (ThermoFisher Scientific, Cat. #L7007) and (Perez *et al.*, 2021b, Sham *et al.*, 2013). Briefly, 500 µL of cultures were harvested at 4 and 6 h of growth and centrifuged at 12,000 x g for 2.5 min at 25°C. Pellets were re-suspended in 50 µL of BHI broth plus 2 µL of a 1:1 (v/v) mixture of Syto-9 and propidium iodide, and incubated for 5 min in the dark at 22°C. As a control, heat killed cells (95° C for 5 min) were stained as described above for comparison. After incubation, samples were immediately imaged using both the Alexa 488 (EX 460-500, DM 505, and BA 510-560) and Alexa 568 (EX 532-587, DM 595, and BA 608-682) filters. The staining pattern of the sample was revealed by superimposing the corresponding Alexa 488 and Alexa 568 images upon one another within the NIS-Elements AR software (Nikon). A total of 200 cells were categorized based on the staining pattern for quantification of percentage of live vs dead cells.

#### **4.9 | FDAA (fluorescent D-amino acids) short-pulse labeling and eFM**

The FDAA TADA (tetramethylrhodamine 3-amino-D-alanine) synthesized as described in (Kuru *et al.*, 2012) was obtained from Michael VanNieuwenhze. Samples were processed as described in (Boersma *et al.*, 2015, Perez *et al.*, 2021a, Tsui *et al.*, 2014) with minor changes. Briefly, at 4 h of growth, 500 µL of culture was harvested and centrifuged at 16,000 x g for 5 min at room temperature. Cultures were washed twice with 500 µL ice cold 1X PBS. Pelleted via centrifugation (16,000× for 5 min) and re-suspended in 250 µL

of BHI broth containing TADA at a final concentration of 500  $\mu$ M. Working solutions of TADA in BHI were diluted from 500 mM stocks in DMSO, which were stored at -20°C. Samples were incubated for 5 min at 37°C. Cells were centrifuged for 2.5 min at 16 000 x g at 4°C, and washed twice in 1 mL of cold 1x PBS. Pellets were resuspended in 1 mL of 4% (wt/vol) paraformaldehyde (EMS; 157-4), followed by 15 min incubation at room temperature and 45 min incubation on ice in the dark. Fixed cells were centrifuged and washed three times with ice cold 1x PBS. After which cells were resuspended in 50-75  $\mu$ L of Slowfade Gold antifade reagent (Invitrogen; S36936), vortexed briefly, and applied to a glass slide. A glass coverslip was gently placed onto to the slide and the samples were cured overnight at 4° C, in the dark. To visualize TADA labeling, images were taken using eFM with a Texas-Red filter.

#### 4.10 | HaloTag labeling and eFM

To determine the localization pattern of the HaloTag-fusion proteins, cells were labeled with saturating TMR ligand and viewed by eFM as described in (Perez *et al.*, 2019, Perez *et al.*, 2021b). Briefly, strains with HT-domain fusions expressed from native chromosomal loci were grown in BHI broth as described above. At 4 h of growth, 0.5  $\mu$ L of working stock of TMR (500  $\mu$ M TMR ligand (Promega cat #G8252) in DMSO stored at -20° C) was added to 300  $\mu$ L of culture (final concentration = 0.83  $\mu$ M). Tubes were inverted gently three times and then incubated for 15 min at 37 °C in the dark in the absence of CO<sub>2</sub>. Cells were then collected by centrifugation at 14,000 x g for 2.5 min, washed once with 500  $\mu$ L of fresh BHI broth, re-pelleted (14,000 x g for 2.5 min), and resuspended in 15-20  $\mu$ L of fresh BHI broth. Cell shape and fluorescence localization patterns were imaged using PCM and eFM with a Texas-red filter.

**4.11 | Demograph generation.** Demographs showing protein fluorescence intensity as a function of cell length were generated using Microbe J (version 5.11s) (Ducret *et al.*, 2016, Perez *et al.*, 2019, Perez *et al.*, 2021b). Demographs were also generated from phase-contrast images corresponding to light scattering caused by the cell body as a function of cell length. For cells displaying WT size and morphology, the following “WT” parameters were used: (area [ $\mu\text{m}^2$ ] 0.53-max; length [ $\mu\text{m}$ ] 0.5-3.2; width ([ $\mu\text{m}$ ] 0.2-max; circularity [0-1] 0-max; curvature [0-max] 0-max; sinuosity [0-max] 0-max; angularity [rad] 0-0.38; solidity [0-max] 0.75-max; intensity [0-max] 0-6200; Z-score 2.0-max). Within a given WT field of cells, ≈3-5% of the population were excluded from automated selection by the program due to variables such as clustering of cells, size, shape defects, and/or out of plane of focus. These cells were not manually entered into the program. Stages of cells were classified by the degree of separation as described in (Perez *et al.*, 2019). For depletion conditions in which gross morphological changes occurred in both cell shape and size, the “WT” parameters did not fit to automated selection, leading to the exclusion of > 30 % of the cells from automated selection. Therefore, a separate set of “mutant” parameters were used: (area [ $\mu\text{m}^2$ ] 0.43-5; length [ $\mu\text{m}$ ] 0.3-5; width ([ $\mu\text{m}$ ] 0.4-max; circularity [0-1] 0-max; curvature [0-max] 0-0.45; sinuosity [0-max] 0-max; angularity [rad] 0-0.45; solidity [0-max] 0.75-max; intensity [0-max] 0-6200; Z-score 1.0-max). Complementation fields were analyzed using the “mutant” parameters.

#### **4.12 | IFM of strains expressing single epitope-tagged proteins**

IFM of cells harvested after 4 h of growth was performed as described in (Land *et al.*, 2013, Tsui *et al.*, 2016, Tsui *et al.*, 2014). Primary antibodies were: rabbit anti-FLAG polyclonal antibody (Sigma, F7425, 1:100 dilution) or rabbit anti-HA polyclonal antibody

(Invitrogen, 71–5500, 1:100 dilution). Secondary antibodies used were: anti-rabbit IgG conjugated to Alexa Fluor 488 (Life Technologies; A11034, 1:100 dilution). Control experiments did not detect labeling in untagged WT IU1824 or untagged depletion IU12738 ( $\Delta rodZ//P_{Zn}-rodZ^+$ ) and IU12345 ( $\Delta mreC//P_{Zn}-mreC^+$ ) strains. Protein localization patterns were visualized and scored across multiple fields for depletion/complementation conditions and WT backgrounds. Cells were scored in accordance with the key provided in the appropriate figure legends.

#### 4.13 | IFM of strains expressing two epitope-tagged proteins

For co-localization IFM studies, double epitope-tagged strains IU7072 (*rodZ-L-F<sup>3</sup> ftsZ-Myc*), IU7113 (*mreC-L-F<sup>3</sup> rodZ-Myc*), and IU7515 (*pbp1a-L-F<sup>3</sup> rodZ-Myc*) were grown exponentially to OD<sub>620</sub> ≈0.15–0.20 and processed as detailed in (Land *et al.*, 2013, Tsui *et al.*, 2016, Tsui *et al.*, 2014). Primary antibodies used were: anti-FLAG rabbit polyclonal antibody (dilution 1:100) and anti-Myc mouse monoclonal antibody (dilution 1:100). Secondary antibodies used were: goat anti-rabbit conjugated to Alexa Fluor 488 (1:100) or goat anti-mouse-Alexa Fluor 568 (1:100). Primary and secondary antibody incubations were for 2 h at 37°C, and 1 h at 24°C, respectively. DNA in nucleoids was stained with SlowFade Gold Antifade reagent with DAPI (Life Technologies, S36939). Image analysis was performed using a point-and-click IMA-GUI organized in MATLAB (The Mathworks) as described in (Land *et al.*, 2013, Tsui *et al.*, 2014). Pneumococcal cells were manually aligned and binned into four division stages 1 to 4: pre-, early-, mid- and late-divisional, within the program by eye. The mean cell outline (phase-contrast image) and fluorescence intensities of DNA or tagged-proteins were measured and represented graphically as previously performed in (Land *et al.*, 2013), where n is the number of cells

at a particular division stage averaged from two independent biological replicates. Widths of bands at midcell were measured and statistically compared as described in (Tsui *et al.*, 2014) and the legend to Fig. 7.

#### **4.14 | Structured-illumination microscopy (3D-SIM)**

IFM images were taken using the Deltavision OMX Super Resolution system located in the Indiana University Bloomington Light Microscopy Imaging Center (LMIC) as detailed in (Tsui *et al.*, 2014). Briefly, the system is equipped with four Photometrics Cascade II EMCCD cameras that allow simultaneous four-color imaging, and is controlled by DV-OMX software, with image processing by Applied Precision softWoRx 6.0. software. For information:

<http://www.indiana.edu/~lmic/microscopes/index.html#OMX>

#### **4.15 | Western blotting and immunodetection.**

Cell lysates were prepared by the SEDS lysis-buffer (0.1% deoxycholate (vol/vol), 150 mM NaCl, 0.2% SDS (vol/vol), 15 mM EDTA pH 8.0)) method as described in (Cleverley *et al.*, 2019). Briefly, bacteria were grown exponentially in 5 mL BHI broth to an  $OD_{620} \approx 0.1\text{-}0.2$ . Aliquots of 1.0-2.0 mL were centrifuged (5 min, 16,000  $\times g$  at 4°C), and cell pellets were washed once with 4°C PBS. Frozen pellets collected from 1.8 mL of cultures at  $OD_{620} = 0.16$  were suspended in 80  $\mu L$  of SEDS lysis buffer. Samples collected from different volumes or at different  $OD_{620}$  readings were resuspended in volumes of SEDS lysis buffer proportional to the culture volumes and cell densities. Cell lysis was performed by incubation at 37°C in a shaking block at 300 rpm for 15 min. Protein concentrations of lysed samples were determined with Bio-Rad DC™ protein assay kit. Samples were denatured with 2x Laemmeli SDS loading buffer (Bio-Rad) plus  $\beta$ -mercaptoethanol (5% vol: vol) at 95°C for 10 min. 3-10  $\mu g$

of total crude lysate per sample was loaded onto a 4-15% precast gradient SDS-PAGE gel (Bio-Rad) and subjected to electrophoresis. Amounts of crude lysates loaded and primary antibodies are specified for individual experiments.

Sources of antibodies used for western blotting are as below. Primary antibodies used are anti-HaloTag monoclonal antibody (Promega, G921A, 1:1000), and the following polyclonal rabbit antibodies: anti- FLAG (Sigma, F7425, 1:2,000); anti-HA (Invitrogen, 71–5500, 1:1,000); anti-Myc (ThermoFisher Scientific, PA1-981, 1:1,000); anti-GFP (Invitrogen, A11122, 1:1,400); anti-StkP ((Beilharz *et al.*, 2012), 1:10,000); anti-PhpP ((Beilharz *et al.*, 2012), 1:5,000); anti-MreC ((Land & Winkler, 2011), 1:5,000); anti-FtsZ ((Lara *et al.*, 2005), 1:20,000); anti-FtsA ((Lara *et al.*, 2005), 1:20,000); anti-bPBP2b ((Perez *et al.*, 2021a), 1:10,000); anti-bPBP2x ((Perez *et al.*, 2021a), 1:10,000); anti-GpsB ((Cleverley *et al.*, 2019), 1:2,000); anti-aPBP2a ((Cleverley *et al.*, 2019), 1:5,000); and anti-DivIVA ((Fadda *et al.*, 2007), 1:5,000). Anti-aPBP1a (1:5,000) was generated with purified aPBP1a (aa S37 to P719) and showed no signal at 94 kDa in lysate prepared from a  $\Delta pbp1a$  strain. Secondary antibodies used were anti-mouse IgG conjugated to horseradish peroxidase (Invitrogen, SA1-100, 1:3300), anti-rabbit IgG conjugated to horseradish peroxidase (GE healthcare NA93AV, 1:10,000), or Licor IR Dye800 CW goat anti-rabbit (926-32211, 1:14,000). Chemiluminescence signals obtained with secondary HRP-conjugated antibodies were detected using IVIS imaging system as described previously (Wayne *et al.*, 2010). IR signals obtained with Licor IR Dye800 CW secondary antibody was detected with Azure biosystem 600.

#### **4.16 | Depletion experiments with quantitative western blotting**

Depletion of proteins expressed from a Zn<sup>2+</sup>-inducible prompter ( $P_{Zn}$ ) was performed as described in (Perez *et al.*, 2021b, Tsui *et al.*, 2016) with the following modifications. Merodiploid strains IU12345 ( $\Delta mreC/P_{Zn}\text{-}mreC^+$ ) and IU10947 ( $\Delta rodZ/P_{Zn}\text{-}rodZ\text{-}F$ ) require 0.4 mM Zn + 0.04 mM Mn in BHI broth for growth and ectopic induction of MreC or RodZ-F, respectively. To measure protein amounts during depletion of MreC, or RodZ-F, IU1824 (WT), IU12345 ( $\Delta mreC/P_{Zn}\text{-}mreC^+$ ), IU14594 ( $rodZ\text{-}F$ ) and IU10947 ( $\Delta rodZ/P_{Zn}\text{-}rodZ\text{-}F$ ) were diluted from overnight cultures (IU12345 and IU10947 supplemented with Zn inducer (0.4 mM ZnCl<sub>2</sub> + 0.04 mM MnSO<sub>4</sub>) and re-suspended to an OD<sub>620</sub> ≈ 0.003 in fresh BHI broth ± Zn inducer. Cultures were harvested at 3 or 4 h of growth, and processed for western blotting as described above. To ensure western blots were quantitative, standard curves were generated by loading a range of protein amounts on the lanes, and labeled for anti-MreC, or anti-FLAG for RodZ-F (Perez *et al.*, 2021a). A protein amount corresponding to the mid-range of the standard curve was loaded for each targeted protein. 3 µg of cell lysate were loaded for the detection of bPBP2x or bPBP2b, 3 or 6 µg for detection of MreC, and 10 µg for the detection of RodZ-F. For the detection of RodZ-F during depletion, Licor IR Dye800 CW goat anti-rabbit secondary antibody (926-32211)(1:14,000) was used, and IR signal was detected with Azure biosystem 600. In addition, signals obtained with anti-F antibody were normalized with total protein stain in each lane using Totalstain Q-NC reagent from Azure.

#### 4.17 | Phos-tag SDS-PAGE and western blotting

This method is based on the mobility shift of phosphorylated proteins in SDS-PAGE with polyacrylamide-bound Mn<sup>2+</sup>-Phos-tag (Kinoshita *et al.*, 2006). Phosphorylated proteins in gels are visualized as slower migrating bands compared to corresponding

unphosphorylated proteins. Phos-tag SDS-PAGE and standard Western blotting were carried out as described previously with modifications (Wayne *et al.*, 2012). Overnight BHI broth cultures were diluted and grown up to  $OD_{620} \approx 0.2$  in 30 mL of BHI. Cells were centrifuged at 14,500  $\times g$  for 5 min at 4°C, and all subsequent steps were performed at 4°C. Pellets were lysed using a FastPrep homogenizer (MP biomedicals) in cold lysis buffer (20 mM Tris-HCl pH 7.0 and 1 protease inhibitor tablet (ThermoFisher Scientific) per 10 mL buffer). Cell lysates were resolved by 10 % SDS-PAGE supplemented with 75  $\mu M$  Phos-tag acrylamide (AAL-107; Wako) and 100  $\mu M$  MnCl<sub>2</sub>, and standard 10 % SDS-PAGE as control. Volumes of loaded samples were normalized to  $OD_{620}$  of harvested cultures (for  $OD_{620} \approx 0.2$ , 30  $\mu L$  of the sample was loaded). Gel electrophoresis was carried out for 3h. RodZ-HA<sup>3</sup> was detected by western blotting as described above using anti-HA as the primary antibody.

#### 4.18 | Co-immunoprecipitation (Co-IP) assays

Co-IP assays were performed as previously described in (Perez *et al.*, 2019, Perez *et al.*, 2021b, Rued *et al.*, 2017). Briefly, cultures were grown exponentially to an  $OD_{620} \approx 0.2$ -0.3 in 400 mL of BHI broth, concentrated 20-fold in 4°C PBS, and cross-linked with 0.1 % paraformaldehyde for 1h at 37°C. After quenching with 1 M glycine and a wash with PBS, pellets were re-suspended in 2 mL of cold lysis buffer (50 mM Tris-HCl pH 7.4, 150 mM NaCl, 1 mM EDTA, 1% Triton X100 (v/v) containing protease inhibitor, and homogenized in lysing matrix B tubes (MP Biomedicals) in a FastPrep homogenizer. One mL of lysate (input sample, normalized to  $\approx 2$ -5 mg/mL) was added to 50  $\mu L$  of anti-FLAG magnetic beads (Sigma, M8823) and incubate for 2h at 4°C with rotation. 100  $\mu L$  of FLAG elution solution containing 150 ng 3X FLAG peptide/ $\mu L$  (Sigma, F4799) was used to elute FLAG-

Accepted Article

tagged proteins and other associated proteins (output elution samples). Input or output samples were mixed with 2x Laemmli sample buffer (Bio-Rad) containing 10% (vol/vol) β-mercaptoethanol (Sigma), and were heated at 95°C for 1 h to break cross-links, with the exception of IU8918 (*ftsW-L-gfp*) and IU16126 (*ftsW-L-gfp rodZ-L-F<sup>3</sup>*), when the samples were not heated. For most samples, 4-6 µL of input mixed with sample buffer was loaded onto pre-cast SDS-PAGE 4-15% gels (Bio-Rad), resulting in ≈4-9 µg of cell lysate. For the output (elutions), 15 or 25 µL of samples mixed with sample buffer were loaded. Proteins were detected using standard western blotting and immunodetection methods described above. All pair-wise co-IP experiments were performed independently 2-6 times.

#### 4.19 | Bacterial two-hybrid (B2H) assays

B2H assays were performed as described before (Cleverley *et al.*, 2019, Perez *et al.*, 2021b, Rued *et al.*, 2017) with the following modifications. The hybrid plasmids used in the B2H assays are listed in Table S3. For cloning, the target genes were amplified by PCR from *S. pneumoniae* D39 chromosomal DNA (or its derivatives) using the primers listed in Table S4. PCR fragments for *rodZ*(ΔHTH), *rodZ*(ΔDUF) and *pbp1b* were purified, digested with the appropriate restriction enzymes and cloned into the corresponding sites of the pKT25/pUT18C vectors to generate plasmids encoding the corresponding hybrid proteins fused at the C-terminal ends of the T25/T18 fragments. *E. coli* DH5α or XL1-blue transformants were selected on LB agar plates containing ampicillin (100 µg/mL) or kanamycin (50 µg/mL) and 0.4% glucose to repress leaky expression (Karimova *et al.*, 2005). The correct sequence of each construct was verified by double-strand sequencing, using primers listed in Table S4. B2H vectors pKT25/pUT18C containing *rodZ*, *mreC*,

*mpgA*, *pbp1a*, *pbp2b*, *rodA*, *pbp2a*, *pbp2x*, *ftsW*, and *ftsA* and vectors pKNT25/pUT18 containing *ftsZ*, *ezrA*, *gpsB*, *divIVA*, *stkP* and *mreD* were previously constructed and reported (Cleverley *et al.*, 2019, Krupka *et al.*, 2012, Perez *et al.*, 2021b, Rued *et al.*, 2017). Each pair of plasmids was co-transformed into the *E. coli* *cya*<sup>-</sup> BTH101 strain and co-transformation mixtures were spotted directly onto LB agar plates supplemented with ampicillin (100 µg/mL), kanamycin (50 µg/mL) and X-Gal (60 µg/mL), followed by incubation at 30°C. Plasmid pairs pKT25/pUT18C and pKT25-zip/pUT18C-zip were used as negative and positive controls, respectively. Plates were inspected and photographed after 24 h and 40 h. In the case of time course experiments, B2H plates were inspected for color development after 24, 30 and 36 h of incubation at 30°C and scored similarly as reported in (Bendezu *et al.*, 2009). All the B2H experiments were performed at least twice.

## ACKNOWLEDGEMENTS

We thank Kevin Bruce, Jiaqi Zheng, and other members of the Winkler lab for discussions about this work; Jim Powers and Sidney Shaw (Indiana University Bloomington) for advice about light microscopy; Jason Rosch (St. Jude's) and Tim van Opijnen (Boston College) for Tn-seq protocols; Mike VanNieuwenhze (Indiana University Bloomington) for TADA FDAA reagent; and Suzanne Walker and David Rudner (Harvard Medical School) for antibodies against pneumococcal PG synthesis proteins. This work was supported by NIH Grants R35GM131767 (to MEW), R01GM141242 (to XW), Predoctoral Grant F31AI138430 (to MML), and NIH Equipment Grant S10OD024988 (to the Indiana University Bloomington (IUB) Light Microscopy Imaging Center); and by institutional research funds from the CIBIO Department of the University of Trento (to OM).

## **CONFLICT OF INTEREST**

The authors declare that they have no conflicts of interests.

## **AUTHOR CONTRIBUTIONS**

MML, HCTT, and MEW contributed to the conception or design of this study. MML, IM, MJ, ZAY, MB, AZ, ZR, XW, OM, HCTT, and MEW contributed to the acquisition, analysis, and interpretation of the data. MML, OM, HCTT, and MEW contributed to the writing of the manuscript with input from the other authors.

## **DATA AVAILABILITY**

The data that support the findings of this study are available in Appendix A and from the corresponding authors upon reasonable request.

## **ORCID**

Melissa M. Lamanna <https://orcid.org/0000-0002-6535-7903>

Orietta Massidda <https://orcid.org/0000-0001-8823-2372>

Zhongqing Ren: <https://orcid.org/0000-0003-1788-5362>

Ho-Ching T. Tsui <https://orcid.org/0000-0003-0849-874X>

Malcolm E. Winkler <https://orcid.org/0000-0002-1482-2588>

Xindan Wang: <https://orcid.org/0000-0001-6458-180X>

## **REFERENCES**

- Aaron, M., Charbon, G., Lam, H., Schwarz, H., Vollmer, W., and Jacobs-Wagner, C. (2007) The tubulin homologue FtsZ contributes to cell elongation by guiding cell wall precursor synthesis in *Caulobacter crescentus*. *Mol Microbiol* **64**: 938-952.
- Ago, R., and Shiomi, D. (2019) RodZ: a key-player in cell elongation and cell division in *Escherichia coli*. *AIMS Microbiol* **5**: 358-367.
- Alyahya, S.A., Alexander, R., Costa, T., Henriques, A.O., Emonet, T., and Jacobs-Wagner, C. (2009) RodZ, a component of the bacterial core morphogenic apparatus. *Proc Natl Acad Sci U.S.A.* **106**: 1239-1244.
- Aravind, L., Anantharaman, V., Balaji, S., Babu, M.M., and Iyer, L.M. (2005) The many faces of the helix-turn-helix domain: transcription regulation and beyond. *FEMS Microbiol Rev* **29**: 231-262.
- Barendt, S.M., Land, A.D., Sham, L.T., Ng, W.L., Tsui, H.C., Arnold, R.J., and Winkler, M.E. (2009) Influences of capsule on cell shape and chain formation of wild-type and *pcsB* mutants of serotype 2 *Streptococcus pneumoniae*. *J Bacteriol* **191**: 3024-3040.
- Bartual, S.G., Straume, D., Stamsås, G.A., Munoz, I. G., Alfonso, C., Martinez-Ripoll, M., Håvarstein, L.S., and Hermoso, J.A. (2014) Structural basis of PcsB-mediated cell separation in *Streptococcus pneumoniae*. *Nat Comm* **5**: 3842. Doi: 10.1038/ncomms4842.
- Beilharz, K., Novakova, L., Fadda, D., Branny, P., Massidda, O., and Veening, J.W. (2012) Control of cell division in *Streptococcus pneumoniae* by the conserved Ser/Thr protein kinase StkP. *Proc Natl Acad Sci U.S.A.* **109**: E905-913.
- Bendezu, F.O., and de Boer, P.A. (2008) Conditional lethality, division defects, membrane involution, and endocytosis in mre and mrd shape mutants of *Escherichia coli*. *J Bacteriol* **190**: 1792-1811.
- Bendezu, F.O., Hale, C.A., Bernhardt, T.G., and de Boer, P.A. (2009) RodZ (YfgA) is required for proper assembly of the MreB actin cytoskeleton and cell shape in *E. coli*. *EMBO J* **28**: 193-204.

- Berg, K.H., Stamsas, G.A., Straume, D., and Havarstein, L.S. (2013) Effects of low PBP2b levels on cell morphology and peptidoglycan composition in *Streptococcus pneumoniae* R6. *J Bacteriol* **195**: 4342-4354.
- Boersma, M.J., Kuru, E., Rittichier, J.T., VanNieuwenhze, M.S., Brun, Y.V., and Winkler, M.E. (2015) Minimal peptidoglycan (PG) turnover in wild-type and PG hydrolase and cell division mutants of *Streptococcus pneumoniae* D39 growing planktonically and in host-relevant biofilms. *J Bacteriol* **197**: 3472-3485.
- Bratton, B.P., Shaevitz, J.W., Gitai, Z., and Morgenstein, R.M. (2018) MreB polymers and curvature localization are enhanced by RodZ and predict *E. coli*'s cylindrical uniformity. *Nat Commun* **9**: 2797.
- Briggs, N.S., Bruce, K.E., Naskar, S., Winkler, M.E., and Roper, D.I. (2021) The pneumococcal divisome: dynamic control of *Streptococcus pneumoniae* cell division. *Front Microbiol* **12**: 737396.
- Bush, K., and Bradford, P.A. (2016) beta-Lactams and beta-lactamase inhibitors: An Overview. *Cold Spring Harb Perspect Med* **6**: a025247.
- Carver, T., Harris, S.R., Berriman, M., Parkhill, J., and McQuillan, J.A. (2012) Artemis: an integrated platform for visualization and analysis of high-throughput sequence-based experimental data. *Bioinformatics* **28**: 464-469.
- CDC. (2019) Antibiotic resistance threats in the United States, 2019. Atlanta, GA: U.S. Department of Health and Human Services, CDC. <http://www.cdc.gov/drugresistance/Biggest-Threats.html>.
- Cho, H., Wivagg, C.N., Kapoor, M., Barry, Z., Rohs, P.D.A., Suh, H., Marto, J.A., Garner, E.C., and Bernhardt, T.G. (2016) Bacterial cell wall biogenesis is mediated by SEDS and PBP polymerase families functioning semi-autonomously. *Nat Microbiol* **1**: 16172.
- Cleverley, R.M., Rutter, Z.J., Rismundo, J., Corona, F., Tsui, H.T., Alatawi, F.A., Daniel, R.A., Halbedel, S., Massidda, O., Winkler, M.E., and Lewis, R.J. (2019) The cell cycle regulator GpsB functions as cytosolic adaptor for multiple cell wall enzymes. *Nat Commun* **10**: 261.

- Colavin, A., Shi, H., and Huang, K.C. (2018) RodZ modulates geometric localization of the bacterial actin MreB to regulate cell shape. *Nat Commun* **9**: 1280.
- Daitch, A.K., and Goley, E.D. (2020) Uncovering unappreciated activities and niche functions of bacterial cell wall enzymes. *Curr Biol* **30**: R1170-R1175.
- den Blaauwen, T., Andreu, J.M., and Monasterio, O. (2014) Bacterial cell division proteins as antibiotic targets. *Bioorg Chem* **55**: 27-38.
- Dion, M.F., Kapoor, M., Sun, Y., Wilson, S., Ryan, J., Vigouroux, A., van Teeffelen, S., Oldenbourg, R., and Garner, E.C. (2019) *Bacillus subtilis* cell diameter is determined by the opposing actions of two distinct cell wall synthetic systems. *Nat Microbiol* **4**: 1294-1305.
- Ducret, A., and Grangeasse, C. (2017) Bacterial physiology: wrapping the cell in a CozE shell. *Nat Microbiol* **2**: 16262.
- Ducret, A., Quardokus, E.M., and Brun, Y.V. (2016) MicrobeJ, a tool for high throughput bacterial cell detection and quantitative analysis. *Nat Microbiol* **1**: 16077.
- Egan, A.J.F., Errington, J., and Vollmer, W. (2020) Regulation of peptidoglycan synthesis and remodelling. *Nat Rev Microbiol* **18**: 446-460.
- Errington, J., and Wu, L.J. (2017) Cell cycle machinery in *Bacillus subtilis*. *Subcell Biochem* **84**: 67-101.
- Evans, R., O'Neill, M., Pritzel, A., Antropova, N., Senior, A., Green, T., Žídek, A., Bates, R., Blackwell, S., Yim, J., Ronneberger, O., Bodenstein, S., Zielinski, M., Bridgland, A., Potapenko, A., Cowie, A., Tunyasuvunakool, K., Jain, R., Clancy, E., Kohli, P., Jumper, J., and Hassabis, D. (2021) Protein complex prediction with AlphaFold-Multimer. *bioRxiv* doi: <https://doi.org/10.1101/2021.10.04.463034>.
- Fadda, D., Santona, A., D'Ulisse, V., Ghelardini, P., Ennas, M.G., Whalen, M.B., and Massidda, O. (2007) *Streptococcus pneumoniae* DivIVA: localization and interactions in a MinCD-free context. *J Bacteriol* **189**: 1288-1298.
- Fenton, A.K., El Mortaji, L., Lau, D.T., Rudner, D.Z., and Bernhardt, T.G. (2016) CozE is a member of the MreCD complex that directs cell elongation in *Streptococcus pneumoniae*. *Nat Microbiol* **2**: 16237.

- Fenton, A.K., Manuse, S., Flores-Kim, J., Garcia, P.S., Mercy, C., Grangeasse, C., Bernhardt, T.G., and Rudner, D.Z. (2018) Phosphorylation-dependent activation of the cell wall synthase PBP2a in *Streptococcus pneumoniae* by MacP. *Proc Nat Acad Sci U.S.A.* **115**: 2812-2817.
- Fleurie, A., Lesterlin, C., Manuse, S., Zhao, C., Cluzel, C., Lavergne, J.P., Franz-Wachtel, M., Macek, B., Combet, C., Kuru, E., VanNieuwenhze, M.S., Brun, Y.V., Sherratt, D., and Grangeasse, C. (2014a) MapZ marks the division sites and positions FtsZ rings in *Streptococcus pneumoniae*. *Nature* **516**: 259-262.
- Fleurie, A., Manuse, S., Zhao, C., Campo, N., Cluzel, C., Lavergne, J.-P., Freton, C., Combet, C., Guiral, S., Soufi, B., Macek, B., Kuru, E., VanNieuwenhze, M.S., Brun, Y.V., Di Guilmi, A.-M., Claverys, J.P., Galinier, A., and Grangeasse, C. (2014b) Interplay of the serine/threonine-kinase StkP and the paralogs DivIVA and GpsB in pneumococcal cell elongation and division. *PLoS Genet.* **10**: e1004275.doi:10.1371/journal.pgen.1004275.
- Gutu, A.D., Wayne, K.J., Sham, L.T., and Winkler, M.E. (2010) Kinetic characterization of the WalRKSpn (VicRK) two-component system of *Streptococcus pneumoniae*: dependence of WalkSpn (VicK) phosphatase activity on its PAS domain. *J Bacteriol* **192**: 2346-2358.
- Hakenbeck, R. (2014) Discovery of beta-lactam-resistant variants in diverse pneumococcal populations. *Genome Med* **6**: 72.
- Hakenbeck, R., Bruckner, R., Denapaité, D., and Maurer, P. (2012) Molecular mechanisms of beta-lactam resistance in *Streptococcus pneumoniae*. *Future Microbiol* **7**: 395-410.
- Holeckova, N., Doubravova, L., Massidda, O., Molle, V., Buriankova, K., Benada, O., Kofronova, O., Ulrych, A., and Branny, P. (2014) LocZ is a new cell division protein involved in proper septum placement in *Streptococcus pneumoniae*. *mBio* **6**: e01700-01714.
- Hor, J., Garriss, G., Di Giorgio, S., Hack, L.M., Vanselow, J.T., Forstner, K.U., Schlosser, A., Henriques-Normark, B., and Vogel, J. (2020) Grad-seq in a Gram-positive

bacterium reveals exonucleolytic sRNA activation in competence control. *EMBO J* **39**: e103852.

- Hussain, S., Wivagg, C.N., Szwedziak, P., Wong, F., Schaefer, K., Izore, T., Renner, L.D., Holmes, M.J., Sun, Y., Bisson-Filho, A.W., Walker, S., Amir, A., Lowe, J., and Garner, E.C. (2018) MreB filaments align along greatest principal membrane curvature to orient cell wall synthesis. *Elife* **7**: e32471.
- Jacobsen, F.E., Kazmierczak, K.M., Lisher, J.P., Winkler, M.E., and Giedroc, D.P. (2011) Interplay between manganese and zinc homeostasis in the human pathogen *Streptococcus pneumoniae*. *Metalomics* **3**: 38-41.
- Jumper, J., Evans, R., Pritzel, A., Green, T., Figurnov, M., Ronneberger, O., Tunyasuvunakool, K., Bates, R., Zidek, A., Potapenko, A., Bridgland, A., Meyer, C., Kohl, S.A.A., Ballard, A.J., Cowie, A., Romera-Paredes, B., Nikolov, S., Jain, R., Adler, J., Back, T., Petersen, S., Reiman, D., Clancy, E., Zielinski, M., Steinegger, M., Pacholska, M., Berghammer, T., Bodenstein, S., Silver, D., Vinyals, O., Senior, A.W., Kavukcuoglu, K., Kohli, P., and Hassabis, D. (2021) Highly accurate protein structure prediction with AlphaFold. *Nature* **596**: 583-589.
- Karimova, G., Dautin, N., and Ladant, D. (2005) Interaction network among *Escherichia coli* membrane proteins involved in cell division as revealed by bacterial two-hybrid analysis. *J Bacteriol* **187**: 2233-2243.
- Kemege, K.E., Hickey, J.M., Barta, M.L., Wickstrum, J., Balwalli, N., Lovell, S., Battaile, K.P., and Hefty, P.S. (2015) *Chlamydia trachomatis* protein CT009 is a structural and functional homolog to the key morphogenesis component RodZ and interacts with division septal plane localized MreB. *Mol Microbiol* **95**: 365-382.
- Kinoshita, E., Kinoshita-Kikuta, E., Takiyama, K., and Koike, T. (2006) Phosphate-binding tag, a new tool to visualize phosphorylated proteins. *Mol Cell Proteomics* **5**: 749-757.
- Krupka, M., Rivas, G., Rico, A.I., and Vicente, M. (2012) Key role of two terminal domains in the bidirectional polymerization of FtsA protein. *J Biol Chem* **287**: 7756-7765.
- Kumar, S., Mollo, A., Kahne, D., and Ruiz, N. (2022) The bacterial cell wall: from Lipid II flipping to polymerization. *Chem Rev* **122**: 8884-8910.

- Kuru, E., Hughes, H.V., Brown, P.J., Hall, E., Tekkam, S., Cava, F., de Pedro, M.A., Brun, Y.V., and VanNieuwenhze, M.S. (2012) *In situ* probing of newly synthesized peptidoglycan in live bacteria with fluorescent D-amino acids. *Angew Chem Int Ed Engl* **51**: 12519-12523.
- Lamanna, M.M., and Maurelli, A.T. (2022) What Is Motion? Recent advances in the study of molecular movement patterns of the peptidoglycan synthesis machines. *J Bacteriol* **204**: e0059821.
- Land, A.D., Tsui, H.C., Kocaoglu, O., Vella, S.A., Shaw, S.L., Keen, S.K., Sham, L.T., Carlson, E.E., and Winkler, M.E. (2013) Requirement of essential Pbp2x and GpsB for septal ring closure in *Streptococcus pneumoniae* D39. *Mol Microbiol* **90**: 939-955.
- Land, A.D., and Winkler, M.E. (2011) The requirement for pneumococcal MreC and MreD is relieved by inactivation of the gene encoding PBP1a. *J Bacteriol* **193**: 4166-4179.
- Lanie, J.A., Ng, W.L., Kazmierczak, K.M., Andrzejewski, T.M., Davidsen, T.M., Wayne, K.J., Tettelin, H., Glass, J.I., and Winkler, M.E. (2007) Genome sequence of Avery's virulent serotype 2 strain D39 of *Streptococcus pneumoniae* and comparison with that of unencapsulated laboratory strain R6. *J Bacteriol* **189**: 38-51.
- Lara, B., Rico, A.I., Petruzzelli, S., Santona, A., Dumas, J., Biton, J., Vicente, M., Mingorance, J., and Massidda, O. (2005) Cell division in cocci: localization and properties of the *Streptococcus pneumoniae* FtsA protein. *Mol Microbiol* **55**: 699-711.
- Lewis, K. (2020) The science of antibiotic discovery. *Cell* **181**: 29-45.
- Liechti, G., Kuru, E., Packiam, M., Hsu, Y.P., Tekkam, S., Hall, E., Rittichier, J.T., VanNieuwenhze, M., Brun, Y.V., and Maurelli, A.T. (2016) Pathogenic *Chlamydia* lack a classical sacculus but synthesize a narrow, mid-cell peptidoglycan ring, regulated by MreB, for cell division. *PLoS Pathog* **12**: e1005590.
- Ling, L.L., Schneider, T., Peoples, A.J., Spoering, A.L., Engels, I., Conlon, B.P., Mueller, A., Schaberle, T.F., Hughes, D.E., Epstein, S., Jones, M., Lazarides, L.,

- Steadman, V.A., Cohen, D.R., Felix, C.R., Fetterman, K.A., Millett, W.P., Nitti, A.G., Zullo, A.M., Chen, C., and Lewis, K. (2015) A new antibiotic kills pathogens without detectable resistance. *Nature* **517**: 455-459.
- Lund, V.A., Wacnik, K., Turner, R.D., Cotterell, B.E., Walther, C.G., Fenn, S.J., Grein, F., Wollman, A.J., Leake, M.C., Olivier, N., Cadby, A., Mesnage, S., Jones, S., and Foster, S.J. (2018) Molecular coordination of *Staphylococcus aureus* cell division. *Elife* **7**: e32057.
- Martin-Galiano, A.J., Yuste, J., Cercenado, M.I., and de la Campa, A.G. (2014) Inspecting the potential physiological and biomedical value of 44 conserved uncharacterised proteins of *Streptococcus pneumoniae*. *BMC Genomics* **15**: 652.
- Massidda, O., Novakova, L., and Vollmer, W. (2013) From models to pathogens: how much have we learned about *Streptococcus pneumoniae* cell division? *Environ Microbiol* **15**: 3133-3157.
- Meeske, A.J., Riley, E.P., Robins, W.P., Uehara, T., Mekalanos, J.J., Kahne, D., Walker, S., Kruse, A.C., Bernhardt, T.G., and Rudner, D.Z. (2016) SEDS proteins are a widespread family of bacterial cell wall polymerases. *Nature* **537**: 634-638.
- Mehla, J., Liechti, G., Morgenstein, R.M., Caufield, J.H., Hosseinnia, A., Gagarinova, A., Phanse, S., Goodacre, N., Brockett, M., Sakhawalkar, N., Babu, M., Xiao, R., Montelione, G.T., Vorobiev, S., den Blaauwen, T., Hunt, J.F., and Uetz, P. (2021) ZapG (YhcB/DUF1043), a novel cell division protein in gamma-proteobacteria linking the Z-ring to septal peptidoglycan synthesis. *J Biol Chem* **296**: 100700.
- Morgenstein, R.M., Bratton, B.P., Nguyen, J.P., Ouzounov, N., Shaevitz, J.W., and Gitai, Z. (2015) RodZ links MreB to cell wall synthesis to mediate MreB rotation and robust morphogenesis. *Proc Nat Acad Sci U.S.A.* **112**: 12510-12515.
- Muchova, K., Chromikova, Z., and Barak, I. (2013) Control of *Bacillus subtilis* cell shape by RodZ. *Environ Microbiol* **15**: 3259-3271.
- Mura, A., Fadda, D., Perez, A.J., Danforth, M.L., Musu, D., Rico, A.I., Krupka, M., Denapaite, D., Tsui, H.T., Winkler, M.E., Branny, P., Vicente, M., Margolin, W., and Massidda, O. (2017) Roles of the Essential Protein FtsA in Cell Growth and Division in *Streptococcus pneumoniae*. *J Bacteriol* **199**: e00608-16.

- Accepted Article
- Ng, W.L., Tsui, H.C., and Winkler, M.E. (2005) Regulation of the *pspA* virulence factor and essential *pcrB* murein biosynthetic genes by the phosphorylated VicR (YycF) response regulator in *Streptococcus pneumoniae*. *J Bacteriol* **187**: 7444-7459.
- Olejniczak, M., Jiang, X., Basczok, M.M., and Storz, G. (2022) KH domain proteins: Another family of bacterial RNA matchmakers? *Mol Microbiol* **117**: 10-19.
- Ouellette, S.P., Lee, J., and Cox, J.V. (2020) Division without binary fission: cell division in the FtsZ-less *Chlamydia*. *J Bacteriol* **202** e00252-20.
- Ozbaykal, G., Wollrab, E., Simon, F., Vigouroux, A., Cordier, B., Aristov, A., Chaze, T., Matondo, M., and van Teeffelen, S. (2020) The transpeptidase PBP2 governs initial localization and activity of the major cell-wall synthesis machinery in *E. coli*. *Elife* **9** e50629.
- Paik, J., Kern, I., Lurz, R., and Hakenbeck, R. (1999) Mutational analysis of the *Streptococcus pneumoniae* bimodular class A penicillin-binding proteins. *J Bacteriol* **181**: 3852-3856.
- Pazos, M., Peters, K., Casanova, M., Palacios, P., VanNieuwenhze, M., Breukink, E., Vicente, M., and Vollmer, W. (2018) Z-ring membrane anchors associate with cell wall synthases to initiate bacterial cell division. *Nat Commun* **9**: 5090.
- Pazos, M., and Vollmer, W. (2021) Regulation and function of class A Penicillin-binding proteins. *Curr Opin Microbiol* **60**: 80-87.
- Perez, A.J., Boersma, M.J., Bruce, K.E., Lamanna, M.M., Shaw, S.L., Tsui, H.T., Taguchi, A., Carlson, E.E., VanNieuwenhze, M.S., and Winkler, M.E. (2021a) Organization of peptidoglycan synthesis in nodes and separate rings at different stages of cell division of *Streptococcus pneumoniae*. *Mol Microbiol* **115**: 1152-1169.
- Perez, A.J., Cesbron, Y., Shaw, S.L., Bazan Villicana, J., Tsui, H.T., Boersma, M.J., Ye, Z.A., Tovpeko, Y., Dekker, C., Holden, S., and Winkler, M.E. (2019) Movement dynamics of divisome proteins and PBP2x:FtsW in cells of *Streptococcus pneumoniae*. *Proc Nat Acad Sci U.S.A.* **116**: 3211-3220.
- Perez, A.J., Villicana, J.B., Tsui, H.T., Danforth, M.L., Benedet, M., Massidda, O., and Winkler, M.E. (2021b) FtsZ-Ring regulation and cell division are mediated by

- essential EzrA and accessory proteins ZapA and ZapJ in *Streptococcus pneumoniae*. *Front Microbiol* **12**: 780864.
- Philippe, J., Vernet, T., and Zapun, A. (2014) The elongation of ovococci. *Microb Drug Resist* **20**: 215-221.
- Pichoff, S., Du, S., and Lutkenhaus, J. (2019) Roles of FtsEX in cell division. *Res Microbiol* **170**: 374-380.
- Rajagopal, M., and Walker, S. (2017) Envelope Structures of Gram-positive bacteria. *Curr Top Microbiol Immunol* **404**: 1-44.
- Ramos-Montanez, S., Tsui, H.C., Wayne, K.J., Morris, J.L., Peters, L.E., Zhang, F., Kazmierczak, K.M., Sham, L.T., and Winkler, M.E. (2008) Polymorphism and regulation of the *spxB* (pyruvate oxidase) virulence factor gene by a CBS-HotDog domain protein (SpxR) in serotype 2 *Streptococcus pneumoniae*. *Mol Microbiol* **67**: 729-746.
- Ranjit, D.K., Liechti, G.W., and Maurelli, A.T. (2020) Chlamydial MreB directs cell division and peptidoglycan synthesis in *Escherichia coli* in the absence of FtsZ activity. *mBio* **11**: e03222-19.
- Rohs, P.D.A., and Bernhardt, T.G. (2021) Growth and division of the peptidoglycan matrix. *Annu Rev Microbiol* **75**: 315-336.
- Rohs, P.D.A., Buss, J., Sim, S.I., Squyres, G.R., Srisuknimit, V., Smith, M., Cho, H., Sjodt, M., Kruse, A.C., Garner, E.C., Walker, S., Kahne, D.E., and Bernhardt, T.G. (2018) A central role for PBP2 in the activation of peptidoglycan polymerization by the bacterial cell elongation machinery. *PLoS Genet* **14**: e1007726.
- Rohs, P.D.A., Qiu, J.M., Torres, G., Smith, M.D., Fivenson, E.M., and Bernhardt, T.G. (2021) Identification of potential regulatory domains within the MreC and MreD components of the cell elongation machinery. *J Bacteriol* **203**: e00493-20.
- Rued, B.E., Alcorlo, M., Edmonds, K.A., Martínez-Caballero, S., Straume, D., Fu, Y., Bruce, K.E., Wu, H., Håvarstein, L.S., Hermoso, J.A., Winkler, M.E., and Giedroc, D. P. (2019). Structure of the large extracellular loop of FtsX and its interaction with the essential peptidoglycan hydrolase PcsB in *Streptococcus pneumoniae*. *mBio* **10**: e02622-18. doi: 10.1128/mBio.02622-18.

- Rued, B.E., Zheng, J.J., Mura, A., Tsui, H.T., Boersma, M.J., Mazny, J.L., Corona, F., Perez, A.J., Fadda, D., Doubravova, L., Buriankova, K., Branny, P., Massidda, O., and Winkler, M.E. (2017) Suppression and synthetic-lethal genetic relationships of  $\Delta gpsB$  mutations indicate that GpsB mediates protein phosphorylation and penicillin-binding protein interactions in *Streptococcus pneumoniae* D39. *Mol Microbiol* **103**: 931-957.
- Saraiva, B.M., Sorg, M., Pereira, A.R., Ferreira, M.J., Caulat, L.C., Reichmann, N.T., and Pinho, M.G. (2020) Reassessment of the distinctive geometry of *Staphylococcus aureus* cell division. *Nat Commun* **11**: 4097.
- Sham, L.T., Barendt, S.M., Kopecky, K.E., and Winkler, M.E. (2011) Essential PcsB putative peptidoglycan hydrolase interacts with the essential FtsXSpn cell division protein in *Streptococcus pneumoniae* D39. *Proc Nat Acad Sci U.S.A.* **108**: E1061-1069.
- Sham, L.T., Jensen, K.R., Bruce, K.E., and Winkler, M.E. (2013) Involvement of FtsE ATPase and FtsX extracellular loops 1 and 2 in FtsEX-PcsB complex function in cell division of *Streptococcus pneumoniae* D39. *mBio* **4** e00431-13.
- Sham, L.T., Tsui, H.C., Land, A.D., Barendt, S.M., and Winkler, M.E. (2012) Recent advances in pneumococcal peptidoglycan biosynthesis suggest new vaccine and antimicrobial targets. *Curr Opin Microbiol* **15**: 194-203.
- Shiomi, D., Sakai, M., and Niki, H. (2008) Determination of bacterial rod shape by a novel cytoskeletal membrane protein. *EMBO J* **27**: 3081-3091.
- Shiomi, D., Toyoda, A., Aizu, T., Ejima, F., Fujiyama, A., Shini, T., Kohara, Y., and Niki, H. (2013) Mutations in cell elongation genes *mreB*, *mrdA*, and *mrdB* suppress the shape defect of RodZ-deficient cells. *Mol Microbiol* **87**: 1029-1044.
- Sjodt, M., Brock, K., Dobihal, G., Rohs, P.D.A., Green, A.G., Hopf, T.A., Meeske, A.J., Srisuknimit, V., Kahne, D., Walker, S., Marks, D.S., Bernhardt, T.G., Rudner, D.Z., and Kruse, A.C. (2018) Structure of the peptidoglycan polymerase RodA resolved by evolutionary coupling analysis. *Nature* **556**: 118-121.
- Sjodt, M., Rohs, P.D.A., Gilman, M.S.A., Erlandson, S.C., Zheng, S., Green, A.G., Brock, K.P., Taguchi, A., Kahne, D., Walker, S., Marks, D.S., Rudner, D.Z., Bernhardt,

- T.G., and Kruse, A.C. (2020) Structural coordination of polymerization and crosslinking by a SEDS-bPBP peptidoglycan synthase complex. *Nat Microbiol* **5**: 813-820.
- Slager, J., Aprianto, R., and Veening, J.W. (2018) Deep genome annotation of the opportunistic human pathogen *Streptococcus pneumoniae* D39. *Nucleic Acids Res* **46**: 9971-9989.
- Stamsas, G.A., Straume, D., Ruud Winther, A., Kjos, M., Frantzen, C.A., and Havarstein, L.S. (2017) Identification of EloR (Spr1851) as a regulator of cell elongation in *Streptococcus pneumoniae*. *Mol Microbiol* **105**: 954-967.
- Straume, D., Piechowiak, K.W., Kjos, M., and Havarstein, L.S. (2021) Class A PBPs: It is time to rethink traditional paradigms. *Mol Microbiol* **116**: 41-52.
- Straume, D., Stamsas, G.A., Berg, K.H., Salehian, Z., and Havarstein, L.S. (2017) Identification of pneumococcal proteins that are functionally linked to penicillin-binding protein 2b (PBP2b). *Mol Microbiol* **103**: 99-116.
- Sun, Y., and Garner, E. (2020) PrkC modulates MreB filament density and cellular growth rate by monitoring cell wall precursors. *bioRxiv*: 10/1101/2020.08.28.272336.
- Sung, C.K., Li, H., Claverys, J.P., and Morrison, D.A. (2001) An *rpsL* cassette, janus, for gene replacement through negative selection in *Streptococcus pneumoniae*. *App Env Microbiol* **67**: 5190-5196.
- Taguchi, A., Page, J.E., Tsui, H.T., Winkler, M.E., and Walker, S. (2021) Biochemical reconstitution defines new functions for membrane-bound glycosidases in assembly of the bacterial cell wall. *Proc National Acad Sci U.S.A.* **118**: e2103740118.
- Trouve, J., Zapun, A., Arthaud, C., Durmort, C., Di Guilmi, A.M., Soderstrom, B., Pelletier, A., Grangeasse, C., Bourgeois, D., Wong, Y.S., and Morlot, C. (2021) Nanoscale dynamics of peptidoglycan assembly during the cell cycle of *Streptococcus pneumoniae*. *Curr Biol* **31**: 2844-2856 e2846.
- Tsui, H.C., Mukherjee, D., Ray, V.A., Sham, L.T., Feig, A.L., and Winkler, M.E. (2010) Identification and characterization of noncoding small RNAs in *Streptococcus pneumoniae* serotype 2 strain D39. *J Bacteriol* **192**: 264-279.

- Accepted Article
- Tsui, H.C., Zheng, J.J., Magallon, A.N., Ryan, J.D., Yunck, R., Rued, B.E., Bernhardt, T.G., and Winkler, M.E. (2016) Suppression of a deletion mutation in the gene encoding essential PBP2b reveals a new lytic transglycosylase involved in peripheral peptidoglycan synthesis in *Streptococcus pneumoniae* D39. *Mol Microbiol* **100**: 1039-1065.
- Tsui, H.T., Boersma, M.J., Vella, S.A., Kocaoglu, O., Kuru, E., Peceny, J.K., Carlson, E.E., VanNieuwenhze, M.S., Brun, Y.V., Shaw, S.L., and Winkler, M.E. (2014) Pbp2x localizes separately from Pbp2b and other peptidoglycan synthesis proteins during later stages of cell division of *Streptococcus pneumoniae* D39. *Mol Microbiol* **94**: 21-40.
- Ulrych, A., Fabrik, I., Kupcik, R., Vajrychova, M., Doubravova, L., and Branny, P. (2021) Cell wall stress stimulates the activity of the protein kinase StkP of *Streptococcus pneumoniae*, leading to multiple phosphorylation. *J Mol Biol* **433**: 167319.
- van Beilen, J., Blohmke, C.J., Folkerts, H., de Boer, R., Zakrzewska, A., Kulik, W., Vaz, F.M., Brul, S., and Ter Beek, A. (2016) RodZ and PgsA play intertwined roles in membrane homeostasis of *Bacillus subtilis* and resistance to weak organic acid stress. *Front Microbiol* **7**: 1633.
- van den Ent, F., Johnson, C.M., Persons, L., de Boer, P., and Lowe, J. (2010) Bacterial actin MreB assembles in complex with cell shape protein RodZ. *EMBO J* **29**: 1081-1090.
- van Opijnen, T., and Camilli, A. (2012) A fine scale phenotype-genotype virulence map of a bacterial pathogen. *Genome Res* **22**: 2541-2551.
- van Opijnen, T., Lazinski, D.W., and Camilli, A. (2015) Genome-wide fitness and genetic interactions determined by Tn-seq, a high-throughput massively parallel sequencing method for microorganisms. *Curr Protoc Microbiol* **36**: 1E 3 1-1E 3 24.
- van Teeseling, M.C.F. (2021) Elongation at midcell in preparation of cell division requires FtsZ, but Not MreB nor PBP2 in *Caulobacter crescentus*. *Front Microbiol* **12**: 732031.
- Vigouroux, A., Cordier, B., Aristov, A., Alvarez, L., Ozbaykal, G., Chaze, T., Oldewurtel, E.R., Matondo, M., Cava, F., Bikard, D., and van Teeffelen, S. (2020) Class-A

penicillin binding proteins do not contribute to cell shape but repair cell-wall defects. *Elife* **9**: e51998.

- Vollmer, W., Massidda, O., and Tomasz, A. (2019) The cell wall of *Streptococcus pneumoniae*. *Microbiol Spectr* **7**: 10.1128/microbiolspec.GPP3-0018-2018.
- Wayne, K.J., Li, S., Kazmierczak, K.M., Tsui, H.C., and Winkler, M.E. (2012) Involvement of WalK (VicK) phosphatase activity in setting WalR (VicR) response regulator phosphorylation level and limiting cross-talk in *Streptococcus pneumoniae* D39 cells. *Mol Microbiol* **86**: 645-660.
- Weiser, J.N., Ferreira, D.M., and Paton, J.C. (2018) *Streptococcus pneumoniae*: transmission, colonization and invasion. *Nat Rev Microbiol* **16**: 355-367.
- Wheeler, R., Mesnage, S., Boneca, I.G., Hobbs, J.K., and Foster, S.J. (2011) Super-resolution microscopy reveals cell wall dynamics and peptidoglycan architecture in ovococcal bacteria. *Mol Microbiol* **82**: 1096-1109.
- Winther, A.R., Kjos, M., Herigstad, M.L., Havarstein, L.S., and Straume, D. (2021) EloR interacts with the lytic transglycosylase MltG at midcell in *Streptococcus pneumoniae* R6. *J Bacteriol* **203**: e00691-20.
- Yoshii, Y., Niki, H., and Shiomi, D. (2019) Division-site localization of RodZ is required for efficient Z ring formation in *Escherichia coli*. *Mol Microbiol* **111**: 1229-1244.
- Young, K.D. (2006) The selective value of bacterial shape. *Microbiol Mol Biol Rev* **70**: 660-703.
- Zapun, A., Vernet, T., and Pinho, M.G. (2008) The different shapes of cocci. *FEMS Microbiol Rev* **32**: 345-360.
- Zheng, J.J., Perez, A.J., Tsui, H.T., Massidda, O., and Winkler, M.E. (2017) Absence of the KhpA and KhpB (JAG/EloR) RNA-binding proteins suppresses the requirement for PBP2b by overproduction of FtsA in *Streptococcus pneumoniae* D39. *Mol Microbiol* **106**: 793-814.

**TABLES**

**Table 1.**  $\Delta rodZ$  has a similar suppression pattern as  $\Delta mreC$ , but not to  $\Delta cozE$ , in transformation assays at 37°C<sup>a</sup>

Recipient strain and condition	Genotype	Number of colonies at 22 h after transformation with deletion amplicons <sup>b</sup>		
		$\Delta rodZ$	$\Delta mreC$	$\Delta cozE$
<b>IU1824 (D39 <i>cps</i> <i>rpsL1</i>) unencapsulated genetic background</b>				
1. IU1824 -Zn	WT	0 <sup>c</sup>	0 (3)	>500 tiny (4)
2. IU1824 +Zn <sup>e,f</sup>		0 <sup>d</sup> (3)	0 (2)	>500 tiny (2)
3. IU9613 -Zn	<i>rodZ</i> <sup>+</sup> // $\Delta bgaA::P_{Zn}$ - <i>rodZ</i>	0 <sup>c</sup> (6)	0 (3)	>500 tiny (1)
4. IU9613 +Zn <sup>e</sup>		>500 (6)	0 (3)	>500 tiny (1)
5. IU10220 -Zn	<i>mreC</i> <sup>+</sup> // $\Delta bgaA::P_{Zn}$ - <i>mreC</i>	0 <sup>c</sup> (3)	0 (4)	>500 tiny (1)
6. IU10220 +Zn <sup>e</sup>		0 <sup>d</sup> (3)	>500 (4)	>500 tiny (1)
7. IU12681 -Zn	<i>cozE</i> <sup>+</sup> // $\Delta bgaA::P_{Zn}$ - <i>cozE</i>	0 <sup>c</sup> (1)	0 (1)	>500 tiny (2)
8. IU12681 +Zn <sup>e</sup>		0 <sup>d</sup> (1)	0 (1)	>500 normal (2)
9. IU6741	$\Delta pbp1a$	>500 (2)	>500 (2)	>500 tiny (2)
10. IU9760	<i>mpgA</i> (Y488D) (formerly <i>mltG</i> )	>500 (2)	>500 (2)	<300 tiny (2)
11. IU9036	$\Delta khpA$	>500 (2)	>500 (3)	>500 tiny (2)
12. IU12719	<i>ftsA</i> <sup>+</sup> // $\Delta bgaA::P_{ftsA}$ - <i>ftsA</i>	>500 <sup>h</sup> (2)	>500 (2)	>500 tiny (1)
13. IU12310 -Zn	<i>ftsA</i> <sup>+</sup> // $\Delta bgaA::P_{Zn}$ - <i>ftsA</i>	0 <sup>c</sup> (1)	0 <sup>g</sup> (2)	nd
14. IU12310 +Zn <sup>f</sup>		>500 <sup>h</sup> (2)	>500 <sup>g</sup> (2)	nd
15. IU12286 -Zn	<i>ftsZ</i> <sup>+</sup> // $\Delta bgaA::P_{Zn}$ - <i>ftsZ</i>	0 <sup>c</sup> (3)	0 (2)	>500 tiny (1)
16. IU12286 +Zn <sup>f</sup>		0 <sup>d</sup> (3)	0 (2)	>500 tiny (1)
<b>R6 unencapsulated laboratory strain background</b>				
17. R6 (EL59)	WT	>500 (2)	>500 (1)	>500 small (2)
<b>D39 <i>cps</i><sup>+</sup> encapsulated background</b>				
18. IU1690	<i>cps</i> <sup>+</sup>	<12 colonies <sup>i</sup> (5)	<2 (3)	≈300 small (2)

19. IU1781	<i>cps<sup>+</sup> rpsL1</i>	≈40 colonies <sup>i</sup> ; various sizes (7)	<5 (2)	≈300 small (2)
------------	------------------------------	---	--------	----------------

**$\Delta$ cps and *cps<sup>+</sup> ΔrodZ/P<sub>Zn</sub>-rodZ<sup>+</sup> merodiploid strains depleted or containing RodZ***

		Number of colonies 22 h after transformation with markerless <i>rodZ</i> Δ(21-257 aa) amplicon <sup>j</sup>	
		Transformation condition	
Recipient strain	Genotype	-Zn	+Zn
20. IU12515	D39 $\Delta$ cps <i>rpsL1</i> $\Delta$ rodZ::P <sub>c</sub> -[kan- <i>rpsL</i> <sup>+</sup> ]// $\Delta$ bgaA::P <sub>Zn</sub> -rodZ	<5; various sizes (2)	>300 WT size (2)
21. IU15645	D39 <i>cps<sup>+</sup> rpsL1</i> $\Delta$ rodZ::P <sub>c</sub> -[kan- <i>rpsL</i> <sup>+</sup> ]// $\Delta$ bgaA::P <sub>Zn</sub> -rodZ	<16; various sizes (2)	≈300 WT size (2)

<sup>a</sup>Recipient strains were constructed as described in Table S1. Transformations and visualization of colonies normalized to 1 mL of transformation mixture were performed as described in *Experimental procedures*. All transformation experiments were performed with no added DNA as the negative control and with a  $\Delta$ p<sub>bpb1b</sub> amplicon containing the same antibiotic selection as the positive control. 30 ng of purified amplicons were used for each transformation. The volumes of transformation mixture plated (100-500  $\mu$ L) were adjusted to provide ≈150-300 colonies with  $\Delta$ p<sub>bpb1b</sub> amplicons. Transformations with control  $\Delta$ p<sub>bpb1b</sub> or  $\Delta$ spd\_1874 amplicons yielded >500 colonies for  $\Delta$ cps strains per 1 mL of transformation mixture. Transformants were confirmed by PCR reactions.

<sup>b</sup>Results are presented as the number and appearance of colonies (amplicon used, number of biological replicates (n)). Unless specified, the sizes of colonies were similar to those obtained with the  $\Delta$ p<sub>bpb1b</sub> amplicon. Amplicons generated with primers and

genomic DNA templates listed in Tables S1 and S4 were:  $\Delta rodZ::P_c\text{-}aad9$ ,  $\Delta rodZ::P_c\text{-}erm$ ,  $\Delta rodZ::P_c\text{-}[kan\text{-}rpsL^+]$ ,  $\Delta mreC::P_c\text{-}erm$ ,  $\Delta cozE::P_c\text{-}erm$ , and  $\Delta cozE::P_c\text{-}cat$ . Similar results were obtained with amplicons with different antibiotics markers when transformed into D39  $\Delta cps\ rpsL1$  background strains.

<sup>c</sup>Fast-growing suppressors (<5 colonies per plate) were occasionally seen for the WT or merodiploid strains under the non-inducing condition.

<sup>d</sup>Faint colonies were present when transformation was carried out in the presence of Zn. However, these colonies are not viable when re-streaked on TSAll-BA plates containing antibiotics.

<sup>e</sup>Zn inducer (0.4 mM ZnCl<sub>2</sub> + 0.04 mM MnSO<sub>4</sub>) was added to BHI growth media to induce RodZ, MreC, or CozE expression in merodiploid strains before transformation, and in the transformation mixes, which were then divided into soft agar and TSAll-BA plates containing or lacking Zn inducer (0.4 mM ZnCl<sub>2</sub> + 0.04 mM MnSO<sub>4</sub>).

<sup>f</sup>0.5 mM ZnCl<sub>2</sub> + 0.05 mM MnSO<sub>4</sub> (Zn) was used in the transformations to induce FtsA or FtsZ expression.

<sup>g</sup> $\Delta mreCD<>aad9$  amplicon was used instead of  $\Delta mreC::P_c\text{-}erm$  amplicon for these transformations.

<sup>h</sup>No transformants were obtained previously when a promoterless  $\Delta rodZ<>aad9$  amplicon was used to transform IU12310 (D39  $\Delta cps\ rpsL1\ \Delta bgaA::P_{Zn}\text{-}ftsA$ ) in the presence of Zn inducer (Zheng *et al.*, 2017). We reprised this transformation with amplicons that contain a promoter in front of antibiotic-resistance genes ( $\Delta rodZ::P_c\text{-}aad9$  or  $\Delta rodZ::P_c\text{-}erm$ ) and obtained > 500 transformants (row 15). In addition, we obtained >500 transformants of promoter-containing amplicons into strains that constitutively express *ftsA* (rows 13). Two reasons could explain these different outcomes. First, the lack of transformants obtained before could be due to insufficient expression of the in-frame antibiotic resistance gene inserted into the *rodZ* reading frame. Alternatively,  $\Delta rodZ::P_c\text{-}aad9$  and  $\Delta rodZ::P_c\text{-}erm$  constructs may be polar and increase transcription of the downstream genes (*pgsA*, *cbiO1*, *cbiO2*, *cbiQ*, *mreC* and *mreD*; Fig. 1A), which may somehow cause *ftsA*

Accepted Article

overexpression to suppress the lethality of *rodZ* deletion. We did not distinguish between these two explanations in this study.

<sup>i</sup>*ΔrodZ::P<sub>c</sub>-aad9* amplicons used in these transformations.

<sup>j</sup>Markerless *rodZ* Δ(21-257 aa) amplicon was generated with primers and genomic DNA templates listed in Tables S1 and S3.

**Table 2.** The RodZ(*Spn*) HTH and TM domains are essential, while the extracellular domain, including DUF, is dispensable

Condition	Results 20-24 h			
	Initial transformation <sup>a</sup>		Re-streak	
	-Zn	+Zn	-Zn	+Zn
<b>Recipient strain:</b> $\Delta\text{rodZ}::\text{P}_c\text{-}[\text{kan-rpsL}^+]\text{/}\text{P}_{\text{Zn}}\text{-}\text{rodZ}^+$				
<b>Amplicon</b>				
1. <i>rodZ</i> <sup>+</sup> (1-273 aa) <sup>b</sup> positive control	>300, WT	>300, WT	WT	WT
2. No DNA negative control	0	0	ND <sup>c</sup>	ND <sup>c</sup>
3. <i>rodZ</i> (1-261 aa)	>300, WT	>300, WT	WT	WT
4. <i>rodZ</i> (1-195 aa)	>300, WT	>300, WT	WT	WT
5. <i>rodZ</i> Δ(196-261 aa) = ΔDUF	>300, WT	>300, WT	WT	WT
6. <i>rodZ</i> (1-135 aa)	>300, WT	>300, WT	WT	WT
7. <i>rodZ</i> (1-134 aa)	>300, WT	>300, WT	WT	WT
8. <i>rodZ</i> Δ(1-103 aa)	<5 <sup>d</sup>	>300, WT	≈10-20 Heterogeneous μcolonies; green sheen	WT
9. <i>rodZ</i> (1-72 aa)	<5 <sup>d</sup>	>300, WT	≈10-20 Heterogeneous μcolonies; green sheen	WT
10. <i>rodZ</i> Δ(21-257 aa) <sup>e</sup> = ΔRodZ	<5 <sup>d</sup>	>300, WT	<5 <sup>d</sup>	WT
11. <i>rodZ</i> Δ(4-68 aa) = ΔHTH	<5 <sup>d</sup>	>300, WT	<5 <sup>d</sup>	WT
12. <i>rodZ</i> <sup>+</sup> -FLAG	>300, WT	>300, WT	WT	WT
13. <i>rodZ</i> (Y51A F55A Y59A)- FLAG	>300, WT	>300, WT	WT	WT

<sup>a</sup>Amplicons were transformed into merodiploid strain  $\Delta\text{rodZ}::\text{P}_c\text{-}[\text{kan-rpsL}^+]\text{/}\text{P}_{\text{Zn}}\text{-}\text{rodZ}^+$  (IU12515), replacing the  $\Delta\text{rodZ}::\text{P}_c\text{-}[\text{kan-rpsL}^+]$  cassette at the native chromosomal locus. Prior to transformation,  $\Delta\text{rodZ}::\text{P}_c\text{-}[\text{kan-rpsL}^+]\text{/}\text{P}_{\text{Zn}}\text{-}\text{rodZ}^+$  (IU12515) was grown in BHI

Accepted Article

broth containing Zn inducer (0.4 mM ZnCl<sub>2</sub> and 0.04 mM MnSO<sub>4</sub>). Transformation experiments were first performed with fusion amplicons and repeated one or more times with sequence-verified amplicons obtained from strains: IU12696 ( $\Delta$ HTH), IU12699 ( $\Delta$ DUF), IU12738 ( $\Delta$ rodZ), IU12792 (rodZ(1-72)), IU12794 (rodZ(1-261)), IU12797 (rodZ(1-195)), IU12799 (rodZ(1-135)), IU12800 (rodZ(1-103)), IU12803 (rodZ(1-134)), or IU15628 (rodZ(Y51A F55A Y59A)-F). Transformation mixtures were added to soft agar  $\pm$ Zn inducer and subsequently plated onto TSAII-BA plates  $\pm$ Zn inducer. As the positive control, a rodZ<sup>+</sup> amplicon was transformed into the recipient -Zn inducer. Negative controls lacked amplicon DNA in transformation mixtures. Plates were incubated at 37°C in the presence of 5% CO<sub>2</sub> for 20-24 h before being scored for colony number and morphology. The number of colonies is normalized to 1 mL of transformation mixture. “ $\mu$ colonies” (micro-colonies) were barely visible by eye, but observed with a dissecting microscope. “green-sheen” refers to shiny green coloration observed on top of the blood agar, possibly due to partial hemolysis. Transformations were done at least twice independently with similar results.

<sup>b</sup>aa, amino acid.

<sup>c</sup>ND, not determined.

<sup>d</sup><5, indicates 0-4 colonies of different sizes.

<sup>e</sup>Similar Zn inducer-dependent growth occurred when the rodZ  $\Delta$ (21-257aa) amplicon was transformed into encapsulated strain IU15645 (D39 cps<sup>+</sup> rpsL1  $\Delta$ rodZ::P<sub>c</sub>-[kan-rpsL<sup>+</sup>]//  $\Delta$ bgaA::P<sub>Zn</sub>-rodZ)  $\pm$  Zn inducer.

**Table 3.** RodZ, MreC, MpgA, and aPBP1a are in complexes with key components of the peripheral and septal PG synthesis machines and division regulators StkP, GpsB, and DivIVA

Prey proteins tested	Primary antibodies	Ratio of prey protein band/background <sup>a</sup>				
		Bait protein				
		RodZ-F <sup>b</sup>	RodZ-L-F3 <sup>c</sup>	MreC-L-F3	MpgA-F	PBP1a-F
MreC	Anti-MreC	24 ± 1 (2)	100 ± 11 (3)	NA <sup>d</sup>	22 ± 9 (3)	19 ± 8 (3)
bPBP2b	Anti-PBP2b	26 ± 24 (2)	63 ± 28 (5)	47 ± 17 (6)	13 ± 10 (3)	13 ± 11 (3)
aPBP1a	Anti-PBP1a	11 ± 8 (2)	61 ± 28 (6)	41 ± 15 (6)	22 ± 10 (4)	NA <sup>d</sup>
aPBP2a	Anti-PBP2a	29 ± 5 (2)	34 ± 10 (4)	20 ± 6 (4)	ND <sup>e</sup>	ND <sup>e</sup>
GpsB	Anti-GpsB	24 ± 6 (2)	51 ± 20 (5)	26 ± 10 (4)	38 ± 22 (3)	16 ± 9 (2)
StkP	Anti-StkP	20 (1)	23 ± 3 (3)	14 ± 1 (4)	34 ± 13 (3)	28 ± 12 (3)
DivIVA	Anti-DivIVA	7.9 (1)	18 ± 1.5 (3)	4.3 ± 0.9 (3)	53 ± 30 (2)	6.8 ± 2.3 (2)
bPBP2x	Anti-PBP2x	4.8 ± 2.5 (2)	8.7 ± 2.3 (4)	10 ± 4 (4)	12 ± 4 (4)	15 ± 7 (3)
MpgA-HA	Anti-HA	ND <sup>e</sup>	8.6 ± 3.1 (3)	ND <sup>e</sup>	ND <sup>e</sup>	ND <sup>e</sup>
FtsW-L-GFP	Anti-GFP	ND <sup>e</sup>	4.5 ± 1.1 (3)	ND <sup>e</sup>	ND <sup>e</sup>	ND <sup>e</sup>
FtsA	Anti-FtsA	2.0 ± 0.0 (2)	1.9 ± 0.4 (3)	1.2 ± 0.1 (4)	4.5 ± 0.7 (3)	1.6 ± 0.1 (3)
FtsZ	Anti-FtsZ	1.1 (1)	1.7 ± 0.3 (3)	1.0 ± 0.0 (4)	2.0 ± 0.6 (3)	1.1 ± 0.1 (3)
PhpP	Anti-PhpP	0.9 (1)	1.0 ± 0.0 (3)	1.1 ± 0.1 (4)	1.1 ± 0.0 (3)	1.2 ± 0.1 (3)

Prey proteins tested	Primary antibody	Bait protein		
		PBP1a-F	KhpA-L-F3	KhpB-L-F3
RodZ-HA <sup>3</sup>	Anti-HA	8.6 ± 0.3 (2)	1.2 ± 0.0 (2)	1.4 ± 0.0 (2)

<sup>a</sup>Quantification and summary of RodZ interactions investigated in *S. pneumoniae* using Co-IP assay. Interaction ratios were obtained from co-IP experiments and western blot analysis as described in *Experimental procedures*. The interaction ratio is the mean ± SEM ((n), number of biological replicates) value of the prey band signal divided by that of the signal obtained from a non-FLAG tagged sample. A mean ratio of band intensity ≥ 2 between FLAG-tagged and non-FLAG-tagged samples was considered indicative of protein interaction. Co-IP experiments are performed with lysates obtained from non-

FLAG-tagged WT strain (IU1945), and isogenic FLAG-tagged strains *rodZ*-L-F<sup>3</sup> (IU6291), which contains three tandem FLAG tags, *mreC*-L-F<sup>3</sup> (IU4970), *mpgA*-F (IU7403), or *pbp1a*-F (IU5840) as bait, or from non-FLAG-tagged WT parent strain (IU1824), and isogenic *rodZ*-F markerless (IU14594). Co-IP elution samples were probed with native antibodies to detect prey proteins bPBP2b, aPBP1a, bPBP2x, StkP, DivIVA, MreC, GpsB, FtsA, FtsZ and PhpP (Fig. 8). RodZ/aPBP2a and MreC/aPBP2a complexes were detected with IU1945 (WT), K166 ( $\Delta pbp2a$ ), IU4970 (*mreC*-L-F<sup>3</sup>), IU17817 (*mreC*-L-F<sup>3</sup>  $\Delta pbp2a$ ), IU6291 (*rodZ*-L-F<sup>3</sup>), and IU17821 (*rodZ*-L-F<sup>3</sup>  $\Delta pbp2a$ ) (Fig. S13A). RodZ/MpgA complex was examined with strains IU7399 (*mpgA*-HA) and IU7584 (*rodZ*-L-F<sup>3</sup> *mpgA*-HA), and anti-HA antibody to detect MpgA-HA as prey (Fig. S13B). Strains used for examining complexes of aPBP1a/RodZ, KhpA/RodZ, and KhpB/RodZ interaction using PBP1a-F, KhpA-L-F3, and KhpB-L-F3 as bait were IU11828 (*rodZ*-HA<sup>3</sup>), IU11925 (*rodZ*-HA<sup>3</sup> *pbp1a*-F), IU17873 (*rodZ*-HA<sup>3</sup> *khpA*-L-F<sup>3</sup>) and IU17877 (*rodZ*-HA<sup>3</sup> *khpB*-L-F<sup>3</sup>), with the use of anti-HA to detect the prey protein RodZ-HA<sup>3</sup> (Fig. S13C). Strains IU8918 (*ftsW*-L-gfp), IU16026 (*rodZ*-L-F<sup>3</sup> *ftsW*-L-gfp), and an anti-GFP antibody were used for detection of RodZ/FtsW interaction (Fig. S14C).

<sup>b</sup>*rodZ*-F markerless (IU14594) construct has no polar effect on the expression of the downstream gene *mreC*.

<sup>c</sup>IU6291 (*rodZ*-L-F<sup>3</sup>-P<sub>Cerm</sub>) strain showed polar effect of increased expression (5-9-fold) of *mreC*, which is downstream of *rodZ*. IU6291 shows no growth or morphological phenotypes compared to its *rodZ*<sup>+</sup> WT parent (Fig. S11).

<sup>d</sup>NA, not applicable, since MreC-L-F3 or PBP1a-F were used as bait.

<sup>e</sup>ND, not determined.

## FIGURE LEGENDS

**Figure 1. Location and domains of RodZ(*Spn*).** (A) *rodZ* (*spd\_2050*) is predicted to be a member of operon\_816 in the *Spn* D39 chromosome (Slager *et al.*, 2018). Operon\_816 consists of *spd\_2052* (putative Zinc protease), *spd\_2051* (putative M16 family peptidase), *rodZ*, *pgsA* (CDP-diacylglycerol-glycerol-3-phosphate 3-phosphatidyltransferase), *cbiO2*, *cbiO1*, *cbiQ* (putative ATPase and transmembrane components of a cobalt ABC transporters), *mreC*, and *mreD*. (B) 2D protein structure of RodZ(*Spn*). Black line indicates residues that are not part of known domains. The intracellular helix-turn-helix (HTH) domain, transmembrane (TM), and extracellular domain of unknown function (DUF 4115) are depicted as blue, green, and orange, respectively, and intrinsically disordered regions are represented as gray boxes. The HTH and DUF domains are predicted to be in alpha helices and beta sheets, respectively, by AlphaFold2 (Jumper *et al.*, 2021). TM domain was determined with TMHMM server. The positively charged juxta-membrane region of the intracellular linker is shown as a yellow box (+++). SSS symbolizes multiple serine residues in the extracellular linker. (C). Predicted 3D structure of RodZ(*Spn*) generated using the AlphaFold2 webserver. (D) Amino acid sequence of RodZ(*Spn*). Color coding is as described in (B), except that the multiple serine residues are bolded and the positive juxta-membrane is both bolded and highlighted in yellow. Y51 and F55 within Helix 4 of the HTH domain (red boxes) correspond to the positions of aromatic amino acids that interact with MreB in *E. coli* (see Fig. S1) (van den Ent *et al.*, 2010). E89 (dotted box) corresponds to the position of S85 in RodZ(*Bsu*) that may be phosphorylated (Sun & Garner, 2020). The red bar between N131 and Y132 marks the first TA site in a TAT (Y132) codon with a Tn-Mariner insertion

Accepted Article

recovered by Tn-seq of the WT strain (Fig. 2). The junction of the Tn insertion creates a TAA stop codon, indicating that RodZ(M1-N131) is viable.

**Figure 2. Tn-seq analysis reveals suppression of  $\Delta rodZ$ , but not  $\Delta mreCD$ , lethality by  $\Delta pbp1b$  deletion.** (A) Tn-Seq transposon insertion profile for the genome region covering *spd\_2051*, *rodZ*, *pgsA*, *cbiO2*, *cbiO1*, *cbiQ*, *mreC*, and *mreD* of mini-Mariner *Magellan6* transposon (Tn) into the genomes of WT (D39 *Δcps rpsL1*, IU1824),  $\Delta pbp1b$  (IU14697),  $\Delta khpB$  (IU10592), or  $\Delta pbp2a$  (IU13256) strains. *In vitro* transposition reactions, containing purified genomic DNA, *Magellan6* plasmid DNA, and purified MarC9 mariner transposase, transformation, harvesting of transposon-inserted mutants, NextSeq 75 high-output sequencing, and analysis were performed as described in *Experimental procedures*. (B) Transformation assay confirming that  $\Delta pbp1b$  suppresses RodZ, but not MreCD, essentiality. Results were obtained 40 h after transformation of WT,  $\Delta pbp1b$ ,  $\Delta khpB$ ,  $\Delta pbp2a$ , or  $\Delta pbp1a$  (IU6741) strains with linearized  $\Delta rodZ::P_c-aad9$ ,  $\Delta mreCD<>aad9$ , or positive control  $\Delta bgaA::P_c erm$  amplicons. Numbers of transformants were normalized to correspond to 1 mL of transformation mixture. Similar results were obtained in two or more independent experiments. Similar results were obtained after 24 h of incubation, except that colonies  $\Delta rodZ \Delta pbp1b$  transformants were fainter in appearance than at 40 h, and <10  $\Delta rodZ$  colonies were obtained in the WT and  $\Delta pbp2a$  backgrounds (data not shown). (C) Appearance of colonies of the WT or  $\Delta pbp1b$  strain 40 h after transformation with the  $\Delta rodZ::P_c-aad9$  amplicon. (D) aPBP1b interacts with RodZ, MreC, MreD, EzrA, MpgA, aPBP1a, and aPBP2a as well as with itself (circular arrow) in B2H assays. Agar plates were photographed after 40 h at 30°C. B2H assays were performed as described in *Experimental procedures*.

**Figure 3. Depletion of RodZ results in cell rounding, indicative of a defect in peripheral PG synthesis.** (A) Representative growth curves of IU1824 (WT) and depletion/complementation strain IU12738 ( $\Delta rodZ//P_{Zn}\text{-}rodZ^+$ ) with or lacking Zn inducer (0.4 mM ZnCl<sub>2</sub> + 0.04 mM MnSO<sub>4</sub>). IU1824 or IU12738 was grown overnight in BHI broth at 37°C lacking or with Zn inducer, respectively. Samples were re-suspended in fresh BHI  $\pm$ Zn inducer to an OD<sub>620</sub> ≈ 0.003. Arrows indicate times (3 h, 4 h, and 6 h) at which samples were taken for phase-contrast microscopy. (B) Representative micrographs of IU1824 (WT) and IU12738 ( $\Delta rodZ//P_{Zn}\text{-}rodZ^+$ ) grown in the presence or absence of Zn inducer and sampled after 4 h or 6 h. All images are at the same magnification (scale bar = 1  $\mu\text{m}$ ). (C) Box-and-whiskers plots (5 to 95 percentile) of cell length, width, aspect ratio, and relative volume measured for IU1824 grown in the absence of Zn inducer, and IU12738 grown in the presence or absence of Zn inducer for 3 h, 4 h, and 6 h. For each time point, ≈50-80 cells per sample were measured, and statistical analysis was conducted using the non-parametric, one-way ANOVA Kruskal-Wallis test in GraphPad Prism. Statistical comparisons were carried out for IU12738 grown in the presence or absence of Zn inducer compared to the WT control at the respective time points. \*\*\*, p < 0.001; ns, non-significant. Results shown are representative from one of at least three independent biological replicates.

**Figure 4. RodZ levels decrease to an undetectable level upon depletion for 3 h.** (A) Representative growth curves of *rodZ*-FLAG (IU14594) and depletion strain  $\Delta rodZ//P_{Zn}\text{-}rodZ$ -FLAG (IU10947) with or lacking Zn inducer (0.4 mM ZnCl<sub>2</sub> + 0.04 mM MnSO<sub>4</sub>), where “F” is used as an abbreviation for the FLAG tag. IU14594 or IU10947 was grown overnight in BHI lacking or with Zn inducer, respectively, and diluted into BHI with

no Zn for IU14594, and into BHI with or lacking Zn for IU10947. Cultures were sampled at 3 or 4 h for Western analysis (arrows). (B) Representative micrographs of IU14594 (*rodZ*-F; -Zn) and IU 10947 ( $\Delta rodZ//P_{Zn}$ -*rodZ*-F; +Zn or -Zn) sampled at 4 h. Scale bar = 1  $\mu$ m (all images are at the same magnification). (C) Representative quantitative Western blot showing RodZ-F amount expressed from the native chromosomal site in IU14594 or from the ectopic site in the presence or absence of Zn inducer in IU10947 ( $\Delta rodZ//P_{Zn}$ -*rodZ*<sup>+</sup>-F) sampled at 3h and 4h. 10  $\mu$ g of crude cell lysates were loaded in the left 6 lanes, and 2, 5, or 15  $\mu$ g were loaded in the right three lanes to generate a standard curve for quantitation. SDS-PAGE and western blotting were carried out as described in *Experimental procedures* using Licor IR Dye800 CW secondary antibody detected with an Azure Biosystem 600. Signals obtained with anti-FLAG antibody were normalized for total protein in each lane using Totalstain Q-NC (Azure Scientific). Normalized ratios indicate RodZ-F protein amounts (mean  $\pm$  SEM) from 3h or 4h samples for IU10947 relative to IU14594 at 4h. (D) MreC, bPBP2b, and bPBP2x protein levels are not altered by RodZ depletion. Protein samples were obtained from IU14594 (*rodZ*-F WT), or IU10947 ( $\Delta rodZ//P_{Zn}$ -*rodZ*-F) grown in the presence or absence of Zn inducer for 4 h. 3  $\mu$ g of crude cell lysates were loaded in each lane. SDS-PAGE and Western blotting were carried out with primary antibodies to MreC, bPBP2b, or bPBP2x. Chemiluminescence signals obtained with secondary HRP-conjugated antibodies were detected using an IVIS imaging system. Ratios indicate protein amounts (average  $\pm$  SEM) in IU10947 ( $\Delta rodZ//P_{Zn}$ -*rodZ*<sup>+</sup>-F) relative to those in IU14594 (WT) from 2 independent biological replicates.

**Figure 5. Cells depleted of RodZ(*Spn*) for 6 h remain viable.** (A) Representative phase-contrast and 2D-epifluorescence microscopy (eFM) images of cells of WT (IU1824; left panels) or the  $\Delta rodZ//P_{Zn}-rodZ^+$  merodiploid strain (IU12738; right panels) depleted for RodZ (-Zn) or replete with RodZ (+Zn) for 4 h and stained for live (green) and dead (red; indicative of membrane permeability) cells. Cells were grown as described in Fig. 3A and stained with the Live-Dead BacLight Bacterial Viability Kit (Syto9 and Propidium Iodide) as described in *Experimental procedures*. Most exponentially growing WT cells are alive (green), while WT cells heat-killed by boiling for 5 min at 95°C are dead (red). RodZ depleted (-Zn) or RodZ replete (+Zn) cells are mostly alive (green) at 4 h. All images are at the same magnification (scale bar = 1  $\mu$ m). (B) Quantitation of the percentage of live or dead WT (IU1824) cells growing exponentially (-Zn) or boiled (control), and *rodZ*( $\Delta$ DUF)// $P_{Zn}$ -*rodZ* (IU12699), *rodZ* ( $\Delta$ HTH)// $P_{Zn}$ -*rodZ* (IU12696), or  $\Delta rodZ//P_{Zn}-rodZ$  (IU12738) cells grown in the presence (+Zn; RodZ $^+$ ) or absence (-Zn; mutant RodZ and/or RodZ depleted) of inducer (0.4 mM ZnCl<sub>2</sub> + 0.04 mM MnSO<sub>4</sub>) for 4 h or 6 h. 200 cells were examined and scored for each sample. Except for the boiled control cells, most cells remained viable. Data are averaged ( $\pm$  SEM) from 2 independent experiments, except for the 6 h time points of IU12699 and IU12738, which are from a single experiment.

**Figure 6. Amino Acids 1-131 of RodZ are required for growth of *Spn*.** (A) Amplicons harboring *rodZ* truncation or codon-changing alleles were transformed into merodiploid strain IU12515 ( $\Delta rodZ::P_c-[kan-rpsL^+]$  // $P_{Zn}-rodZ^+$ ) to replace the Janus cassette ( $\Delta rodZ::P_c-[kan-rpsL^+]$ ) as described in *Experimental procedures* and Table 2. Effects of RodZ truncations were determined by transformation assays on TSAll-blood agar plates with or lacking Zn inducer (0.4 mM ZnCl<sub>2</sub> + 0.04 mM MnSO<sub>4</sub>). Colony

Accepted Article

numbers, sizes, and morphologies were evaluated compared to *rodZ*<sup>+</sup> transformants after 20-24 h incubation at 37°C (see legend to Table 1 for experimental details). “μcolonies” (micro colonies) were barely visible by eye, but observed using a low power microscope. “Green-sheen” refers to a shiny green pattern observed on top of the blood agar that may be due to partial hemolysis. Similar results were obtained in two independent transformation experiments (Table 2). The red bar between N131 and Y132 in the RodZ(1-135) and RodZ(1-134) entries marks the first TA site with a TnMariner insertion recovered by Tn-seq of the WT strain (see Fig. 2). Cell shapes and sizes were determined for WT and merodiploid mutants depleted for RodZ (see Fig. 3; Fig. S7; panel (B), below; Fig. S8; and Fig. S9). Relative amounts of corresponding truncated RodZ proteins fused to a C-terminus FLAG tag were determined by quantitative western blotting probed with anti-FLAG antibody as described in *Experimental procedures*. Proteins samples were obtained from strains IU14594 (*rodZ*-F at native chromosomal locus), IU13457 (*rodZ*-F//P<sub>Zn</sub>-*rodZ*<sup>+</sup>), IU13655 (*rodZ*(ΔDUF)-F//P<sub>Zn</sub>-*rodZ*<sup>+</sup>), IU13660 ((*rodZ*(1-134)-F//P<sub>Zn</sub>-*rodZ*<sup>+</sup>), and IU13705 (*rodZ*(ΔHTH)-F//P<sub>Zn</sub>-*rodZ*<sup>+</sup>) (see Table S1). Strains were grown in BHI broth +Zn inducer overnight, followed by growth for 4 h in BHI media lacking or containing Zn inducer as described in Fig. 3. Values in the last column are amounts of truncated F-tagged RodZ variants grown -Zn relative to the amount of RodZ-F in IU14594. Although IU13655 (*rodZ*(ΔDUF)-F//P<sub>Zn</sub>-*rodZ*<sup>+</sup>) and IU13660 ((*rodZ*(1-134)-F//P<sub>Zn</sub>-*rodZ*<sup>+</sup>) were viable -Zn inducer, RodZ(ΔDUF)-F and RodZ(1-134)-F proteins were not detected in samples grown ± Zn, consistent with cleavage of the FLAG tag off the truncated RodZ variants lacking the C-terminal DUF domain. (B) Representative micrographs of IU1824 (WT parent), and *rodZ* truncation mutants IU12794 (*rodZ*(1-261)//P<sub>Zn</sub>-*rodZ*<sup>+</sup>), IU12797

(rodZ(1-195)//P<sub>Zn</sub>-rodZ<sup>+</sup>), IU12799 (rodZ(1-135)//P<sub>Zn</sub>-rodZ<sup>+</sup>), and IU12803 (rodZ(1-134)//P<sub>Zn</sub>-rodZ<sup>+</sup>), which grow in the absence of Zn inducer. Cells were imaged during exponential growth at an OD<sub>620</sub> ≈0.1-0.15 after ≈2.5-3.0 h of growth. Representative growth curves of truncated RodZ variants are shown in Fig. S9D. Shapes and sizes were categorized as described for panel (A), above. Only the RodZ(M1-Q134) mutant showed significant changes in relative median cell volume and average width ( $\pm$  SEM) compared to WT (n = 50 cells for each strain). \*\*\*, P<0.001 by the non-parametric, one-way ANOVA Kruskal-Wallis test in GraphPad Prism. RodZ(M1-T135) mutant cells resembled WT, except for an occasional bigger, wider cell.

**Figure 7. RodZ localizes with MreC and aPBP1a of the peripheral PG synthesis machine.** (A) Composite image displaying localization patterns of MreC and RodZ through four stages of pneumococcal growth and division. Images were obtained by dual-labeling immunofluorescence microscopy (IFM). To construct composite images, n > 30 cells from each division stage were averaged and quantified as described in *Experimental procedures*. (A) IU7113 (*mreC-L-F<sup>3</sup> rodZ-Myc*) IFM was probed with DAPI (DNA) and anti-FLAG and anti-Myc antibodies as detailed in *Experimental procedures*. (B) Scatter plot of the paired widths of RodZ compared to MreC constructed using the IMA-GUI program described in *Experimental procedures*. The dotted line intercepts the origin with slope = 1 and indicates the expected distribution if RodZ and MreC widths are identical. Differences between paired widths were calculated for cells at each division stage, and one-sample student's *t*-tests were performed to determine whether mean differences in widths were significantly different from the null hypothesis value of zero (NS, not significant; \*\*, P <0.01) (Tsui *et al.*, 2014). (C) Composite image of RodZ and aPBP1a

Accepted Article

localization in IFM of IU7515 (*pbp1a-L-F<sup>3</sup>* *rodZ*-Myc) probed with DAPI and anti-Myc and anti-FLAG antibodies. (D) Scatter plot of paired width analysis of aPBP1a compared to RodZ. (E) Composite image of RodZ and FtsZ localization in IFM of IU7072 (*rodZ-L-F<sup>3</sup>* *ftsZ*-Myc) probed with DAPI and anti-FLAG and anti-Myc antibodies. (F) Scatter plot of paired width analysis of FtsZ compared to RodZ. \*\*\*P value <0.001. Data were obtained from two independent experiments for each comparison.

**Figure 8. RodZ, MreC, MpgA (formerly MltG), and aPbp1a are in complexes with components of the peripheral and septal PG machines, class A PBPs, and cellular regulators StkP, GpsB, and DivIVA.** Co-IP experiments using non-FLAG-tagged WT strain (IU1945) or FLAG-tagged strains RodZ-L-F<sup>3</sup> (IU6291), MreC-L-F<sup>3</sup> (IU4970), MpgA-F (IU7403), or PBP1a-F (IU5840) as bait were probed with native antibodies to detect prey proteins bPBP2b, aPBP1a, bPBP2x, StkP, DivIVA, MreC, GpsB, FtsA, FtsZ and PhpP as described in *Experimental procedures*. Prey proteins were detected in all cell lysates (input; left lanes). In elution output samples (right lanes), prey proteins are undetectable for the WT non-FLAG-tagged control strain, but are present in different relative amounts in samples of the FLAG-tagged strains. The top blot was probed with anti-FLAG primary antibody for detection bait proteins. For most blots, 4 µl (4-6 µg) of each lysate sample (input) were loaded on the left lanes, while 15 µL of each elution output sample (after mixing 1:1 2x Laemmli buffer) were loaded on the right lanes. For detection of GpsB, 6 µl (6 µg) of lysate sample and 25 µL of output were loaded. Two bands are detected with anti-GpsB antibody in the input and output samples, possibly due to failure of heating to reverse crosslinking of GpsB monomers. The bottom band corresponds to GpsB monomer (~13 kDa), whereas the top band is likely a GpsB dimer

( $\approx$ 26 kDa). Bands detected with anti-MreC or anti-aPBP1a in MreC-L-F3 or Pbp1a-F strains were F-tagged bait proteins. For detection of MreC-L-F3 or Pbp1a-F in output elution samples, 3  $\mu$ l of samples were loaded to each lane. The relative amount of MreC was 5-9-fold higher in the input lysate of *rodZ*-L-F<sup>3</sup>-P<sub>c</sub>*erm* (IU4970; MreC row) compared to that from the untagged WT strain (shown in adjacent lane) or lysate obtained from the markerless *rodZ*-F strain (IU14594, data not shown), suggesting that the P<sub>c</sub> promoter present in the *rodZ*-L-F<sup>3</sup>-P<sub>c</sub>*erm* construct leads to overexpression of downstream genes, including *mreC*. Nevertheless, the Co-IP results using the *rodZ*-F markerless strain lacking an antibiotic-resistance cassette (IU14594) were similar to those for the *rodZ*-L-F<sup>3</sup>-P<sub>c</sub>*erm* strain (IU4970) (data not shown). Co-IP experiments were performed 2-6 times with similar results (See Table 3 for quantitation). (B) Interaction map of RodZ in cells detected by co-IP. (C) Proteins that were weakly or not detected in complex with RodZ by co-IP.

**Figure 9. RodZ interacts with numerous cell elongation and division proteins as well as with itself in B2H assays.** (A) RodZ interacts with GpsB, MreC, MreD, MpgA, bPBP2b, RodA, aPBP1a, aPBP2a, bPBP2x, FtsW, EzrA, and DivIVA in both directions, and with StkP and FtsA with a lower signal and only in one direction. Also, RodZ self-interaction is shown (circular arrow). B2H assays were performed as described in *Experimental procedures*. Agar plates were photographed after 40 h at 30°C. See Fig. S15 for earlier time points at 24 h, 30 h, and 36 h. Control experiments showed that all tested proteins exhibited self-interaction, indicative of functional intactness for interaction (data not shown). (B) MreC and MreD interact with aPBP1a and aPBP2a and also self-interact (circular arrows). Agar plates were photographed after 40 h at 30°C. The punctate

Accepted Article

appearance of the spot showing MreD self-interaction is likely due to high toxicity of the *S. pneumoniae mreD* hybrid constructs in *E. coli*. (C) Summary of decreased interactions of *Spn* RodZ(ΔHTH) and RodZ(ΔDUF) compared to RodZ WT with certain PG synthesis and division proteins in B2H assays. Data are shown in Fig. S15.

**Figure 10. Depletion of RodZ leads to the mislocalization of MreC and bPBP2b detected by IFM.** Representative images showing localization of MreC (A) or bPbp2b (C) after depletion of RodZ for 4 h of growth, which reduced RodZ to an undetectable amount (Fig. 3C). Phase contrast and 2D IFM was performed as described in *Experimental procedures* using antibody to the FLAG or HA tags. Strains used: (A) WT IU14458 (*mreC-L-F<sup>3</sup>*) and merodiploid strain IU14158 (*mreC-L-F<sup>3</sup> ΔrodZ//P<sub>Zn</sub>-rodZ<sup>+</sup>*); (C): WT IU14455 (*pbp2B-HA*) and merodiploid strain IU14131 (*pbp2B-HA ΔrodZ//P<sub>Zn</sub>-rodZ<sup>+</sup>*). Quantification of localization patterns of MreC (B) and bPBP2b (D) observed at 4h in the WT and after RodZ depletion. For each sample and condition, 100 cells were manually examined and scored according to the key. Data are averaged (± SEM) from 2 independent experiments.

**Figure 11. Depletion of RodZ leads to the mislocalization of MreC detected by 2D-eFM.** IU16920 (*iht-mreC ΔrodZ//P<sub>Zn</sub>-rodZ<sup>+</sup>*; where *iht* refers to the i-tag-HaloTag (Perez *et al.*, 2019)) was grown overnight in the presence of Zn inducer (0.4 mM ZnCl<sub>2</sub> + 0.04 mM MnSO<sub>4</sub>) and diluted into fresh medium to OD<sub>620</sub> ≈0.003 containing (complementation) or lacking (depletion) Zn inducer. At 4 h, localization of iHT-MreC was determined following saturation labeling of the iHT domain with HT-TMR ligand by 2D-epifluorescence microscopy (eFM) as described in *Experimental procedures*. (A) Representative micrographs showing iHT-MreC localization. (B) Demographs displaying fluorescence intensity of iHT-MreC localization in the absence (-Zn; RodZ depletion) or

presence (+Zn; RodZ present) of inducer. n, number of cells aligned and displayed in each demograph. Microscopy and demographics are representative of 3 independent biological replicates. (C) Bar graph displaying iHT-MreC localization patterns. For each sample and condition, 100 cells were manually examined and scored according to the key. Data are averaged ( $\pm$  SEM) from 2 independent experiments.

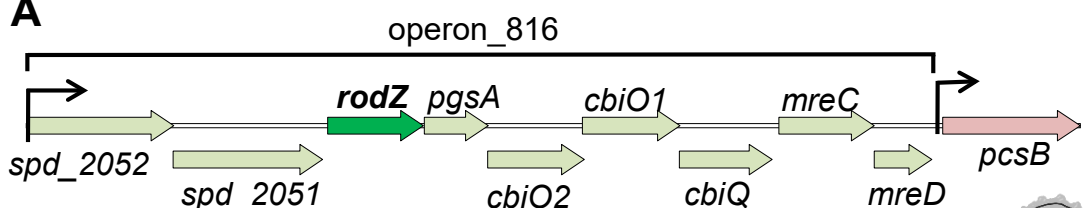
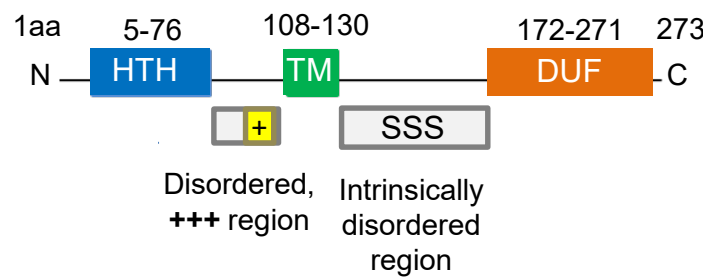
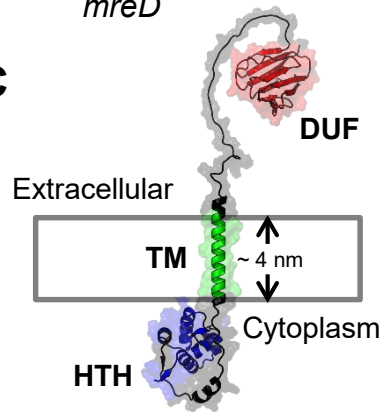
**Figure 12. Summary of localization patterns of PG synthesis and division proteins after RodZ depletion (-Zn) for 4 h.** Among the peripheral PG synthesis machine components, the morphogenic protein MreC and the PG synthase components bPBP2b (TPase) and RodA (GTase) require RodZ for localization, while the localization of MpgA (formerly MltG(*Spn*) muramidase and Class A PBP1a was unchanged by RodZ depletion. MreC, bPBP2b, and RodA localized normally in the presence of Zn inducer (Fig. 10, 11, and S22). Localization of other cell division and PG synthesis proteins (bPBP2x, FtsZ, FtsA, MapZ, EzrA, StkP and DivIVA) were unaffected by RodZ depletion. Representative micrographs of localization studies are shown in Fig. 10, 11, S18, S19, S20, and S22. 100 cells were scored by eye within a given field in each experiment using the indicated key. Data are averaged ( $\pm$  SEM) from 2 or more independent experiments of each strain. Strains used: IU16058 (*iht-pbp2b*), IU16060 (*iht-rodA*), IU16920 (*iht-mreC*), IU14433 (*gfp-mpgA*), IU14496 (*pbp1a-FLAG*), IU14160 (*stkP-FLAG<sup>2</sup>*), IU12993 (*ftsZ-sfgfp*), IU13061 (*divIVA-gfp*), IU13062 (*gfp-mapZ*), IU13058 (*ezrA-sfgfp*), IU13000 (*isfgfp-pbp2x*), and IU17022 (*FLAG-ftsA*) in the  $\Delta rodZ//P_{Zn}-rodZ^+$  background (see Table S1), which was depleted for RodZ as in Fig. 3.

**Figure 13. Depletion of MreC leads to mislocalization of bPBP2b and RodA, but not RodZ.** For localization of bPBP2b, IU16281 (*iht-pbp2b*  $\Delta mreC //P_{Zn}-mreC^+$ ) was

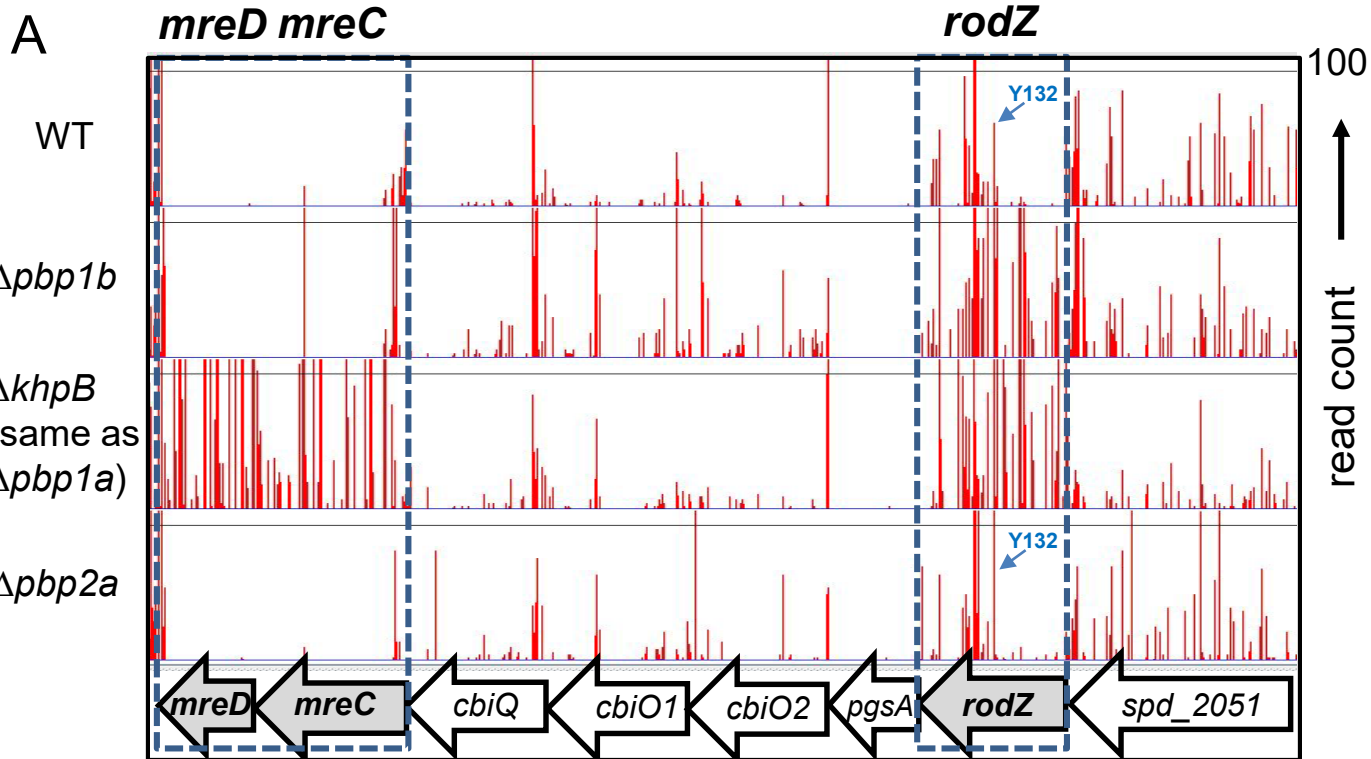
grown overnight in the presence of Zn inducer (0.4 mM  $\text{Cl}_2 \text{Zn}$  + 0.04 mM  $\text{MnSO}_4$ ) and diluted into fresh medium containing (complementation) or lacking (depletion) Zn inducer to  $\text{OD}_{620} \approx 0.003$ . After 4 h, iHT-PBP2b was labeled with a saturating concentration of a HT-TMR ligand, and localized in cells by 2D-epifluorescence microscopy (eFM) as described in *Experimental procedures*. (A) Representative micrographs of iHT-PBP2b localization under MreC complementation or depletion conditions. (B) Demographs displaying fluorescence intensity of iHT-PBP2b localization upon MreC depletion (-Zn) or in the presence of MreC (+Zn) for the number of cells (n) aligned and displayed in each demograph. Microscopy and demographs are representative of 3 independent biological replicates. (C) Bar graph displaying localization patterns of bPBP2b, RodA, RodZ, aPBP1a, and bPBP2x after MreC depletion (-Zn). For each sample and condition, 100 cells were manually examined and scored according to the key. Data are averaged ( $\pm$  SEM) from 2 independent experiments. Strains used: IU16281 (*iht-pbp2b*), IU16283 (*iht-rodA*), IU14598 (*rodZ*-FLAG), IU15901 (*pbp1a*-FLAG), and IU16326 (*iht-pbp2x*) in the  $\Delta mreC/\text{P}_{\text{Zn}}\text{-}mreC^+$  background (see Table S1). Representative micrographs of proteins other than bPBP2b are in Fig. S21, S25, and S26.

**Figure 14. Models of (A) the assembly hierarchy of the pPG core elongasome mediated by RodZ(*Spn*) and (B and C) bypass pPG synthesis to account for the synthetic-viable genetic relationships between Class A PBPs and pPG elongasome components in *S. pneumoniae*.** (A) Results presented here establish RodZ(*Spn*) as an essential scaffolding protein required for the assembly and function of the pPG elongasome. The assembly hierarchy is based on RodZ depletion experiments, protein interaction assays, and genetic relationships described in *Results*. Depletion of RodZ

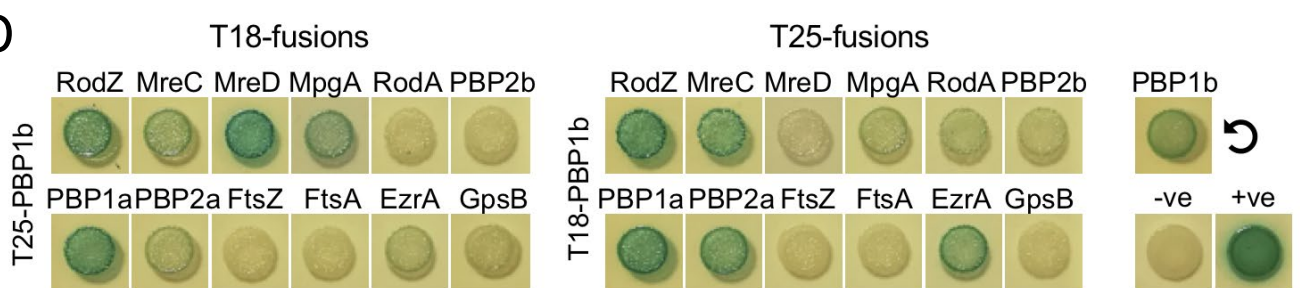
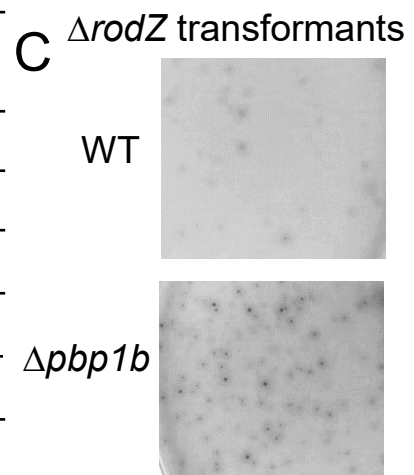
leads to mislocalization of bPBP2b, RodA, and MreC, which are members of the core pPG elongasome, but not aPBP1a, StkP, FtsA, PBP2x, or MpgA (formerly MltG(*Spn*)). In turn, depletion of MreC leads to mislocalization of bPBP2b and RodA, but not RodZ or bPBP2x. Hence, depletion of RodZ results in incomplete assembly of the pPG elongasome. Structures of pneumococcal RodZ:MreC, RodZ:MreC:MreD, bPBP2b:RodA, and bPBP2b:RodZ complexes were predicted by AlphaFold-Multimer (Evans, *et al.*, 2021) and aligned by PyMOL, Version 2.0 (Schrödinger, LLC) into a model of the core elongasome in *S. pneumoniae*. Synthetic-viable genetic relationship between RodZ(*Spn*) and aPBP1b and interaction experiments described in *Results* implicate aPBP1b in pPG elongasome regulation and possibly in pPG synthesis. Interaction experiments show that RodZ(*Spn*) interacts with GpsB and EzrA, which have been proposed to play roles in the interface between cell division and PG synthesis in *S. pneumoniae* (Cleverley *et al.*, 2019, Perez *et al.*, 2021b, Rued *et al.*, 2017). See text for additional details. (B)  $\Delta pbp1b$  suppresses  $\Delta rodZ$ , but not  $\Delta mreCD$ , and MreCD, bPBP2b, and RodA are still required for viability. (C)  $\Delta pbp1a$  suppresses  $\Delta rodZ$ ,  $\Delta mreC$ , or  $\Delta mreCD$ , and bPBP2b and RodA are still required for viability. A favored model postulates that some form of pPG synthesis is required for pneumococcal viability because of the proposed role of pPG synthesis in positioning future equatorial Z-rings in daughter cells. When functions of the WT RodZ-MreCD-bPBP2b-RodA core elongasome (panel (A), above) are impaired, failsafe mechanisms bypass or modulate the function of the pPG elongasome as indicated and restore division and growth. See text for additional details and alternative models for these synthetic-viable phenotypes.

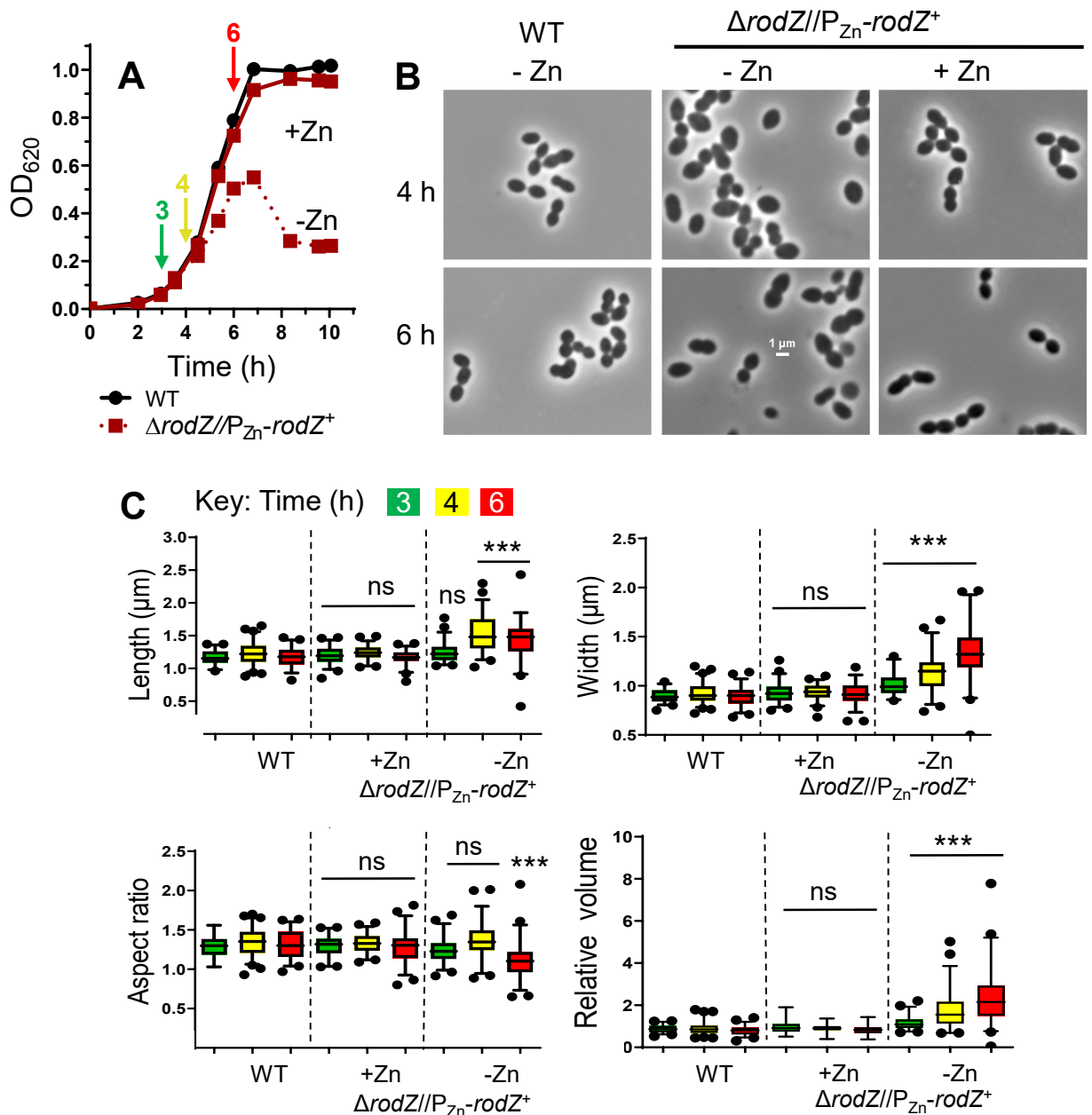
**A****B****C****D**

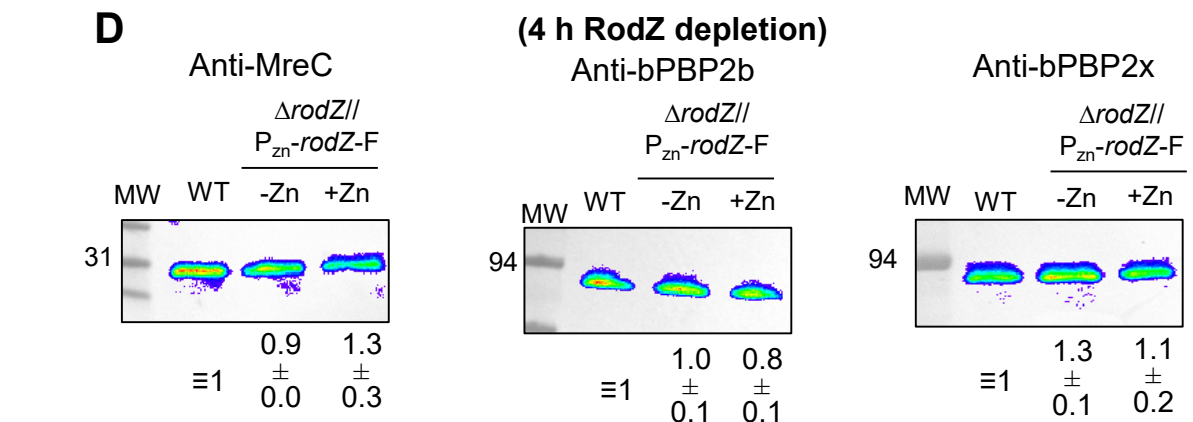
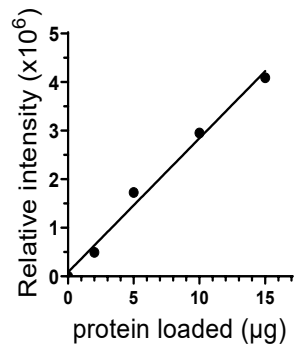
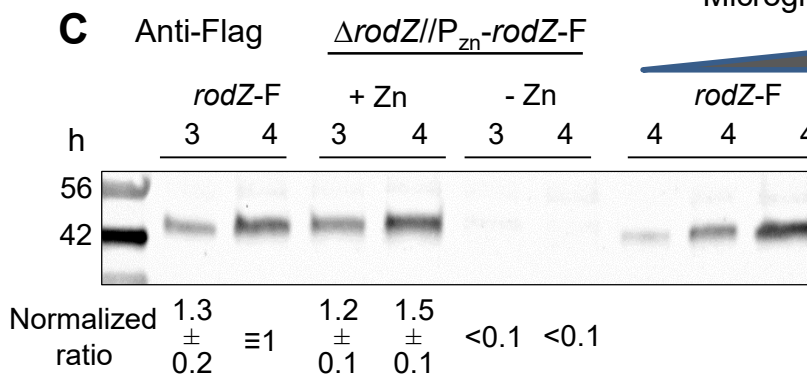
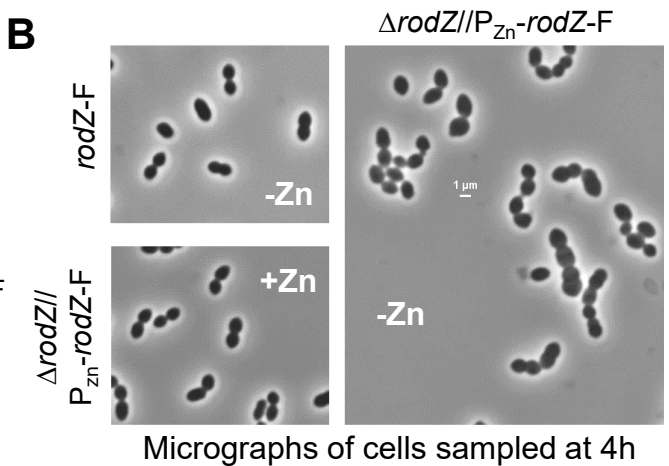
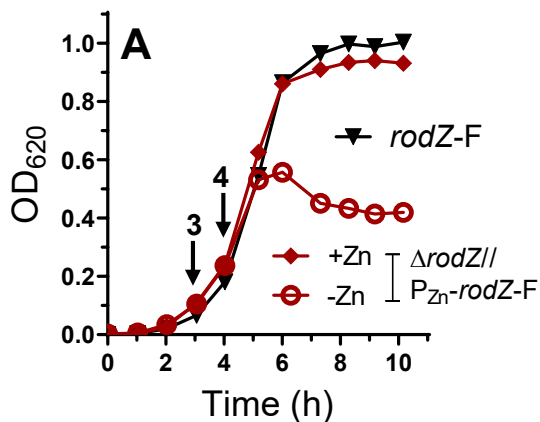
MRKKTIGEVLRALARINQQLSLDELQKKTEIQLDMLEAMEADDFDQLPSPF  
YTRSFLKKYWAVELDDQIVLDAYDSGSMITYEEVDVDEDELTGRRRSSK  
KKKKKTTSFLPLFYFILFALSILIFVTYYVWNYIQTQPEEPSLSNYSVQSTS  
STSSVPHSSSSSSSSSSIESAISVSGEGNHVEIAYKTSKETVKLQLAVSDVTS  
WVSVSESELEGVTLSPKKKSAEATVATKSPVTITLGVVKGVDLTVDNQT  
VDSLKLTAQTGQITVTFTKN

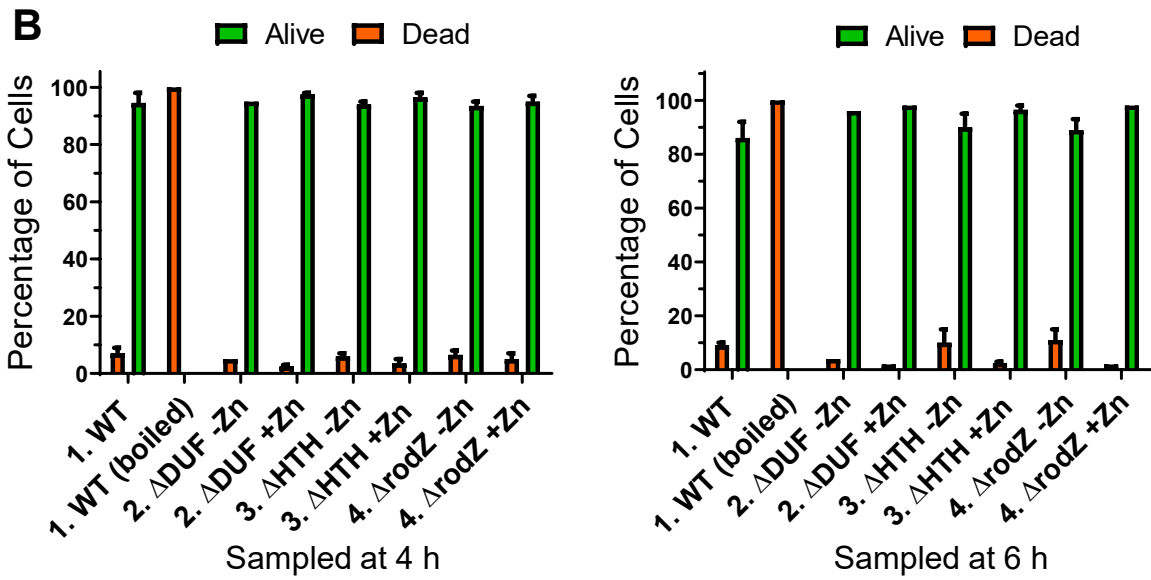
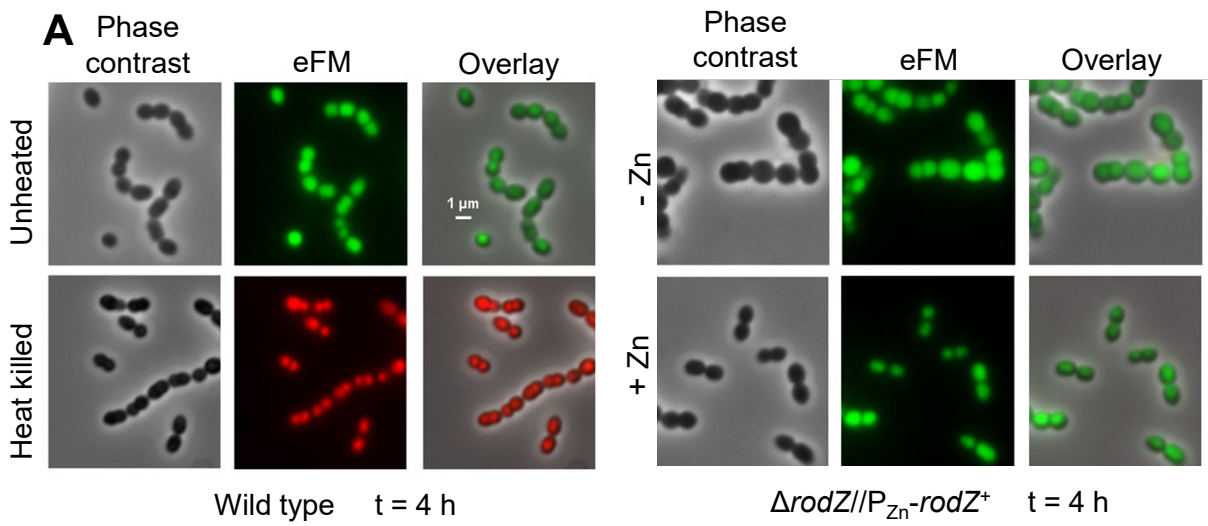


Recipient strain	# of colonies 40 h after transformation with amplicons		
	$\Delta rodZ$	$\Delta mreCD$	$\Delta bgaA$
WT	<30	0	>500
$\Delta pbp1b$	>500	0	>500
$\Delta khpB$	>500	>500	>500
$\Delta pbp2a$	<30	0	>500
$\Delta pbp1a$	>500	>500	>500









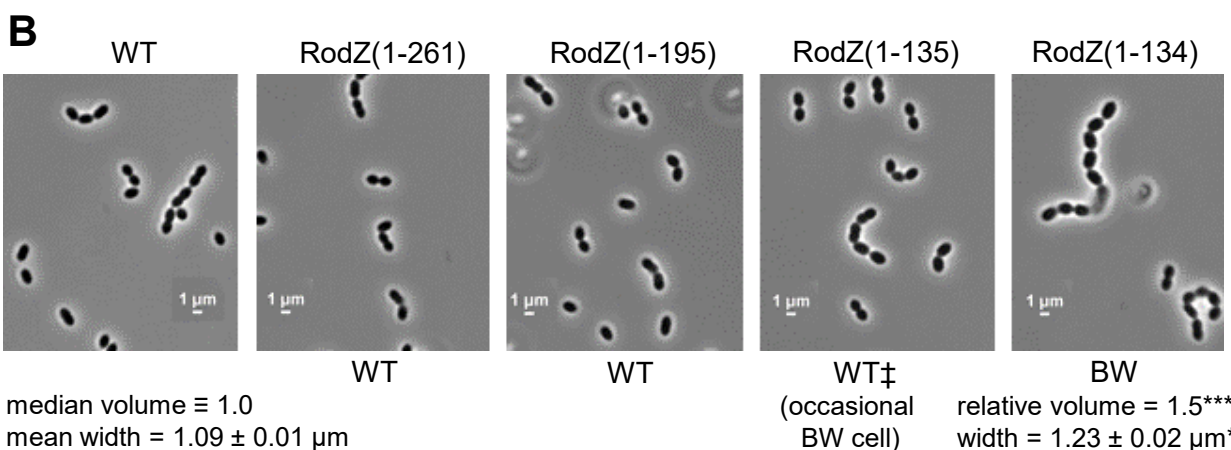
**A**

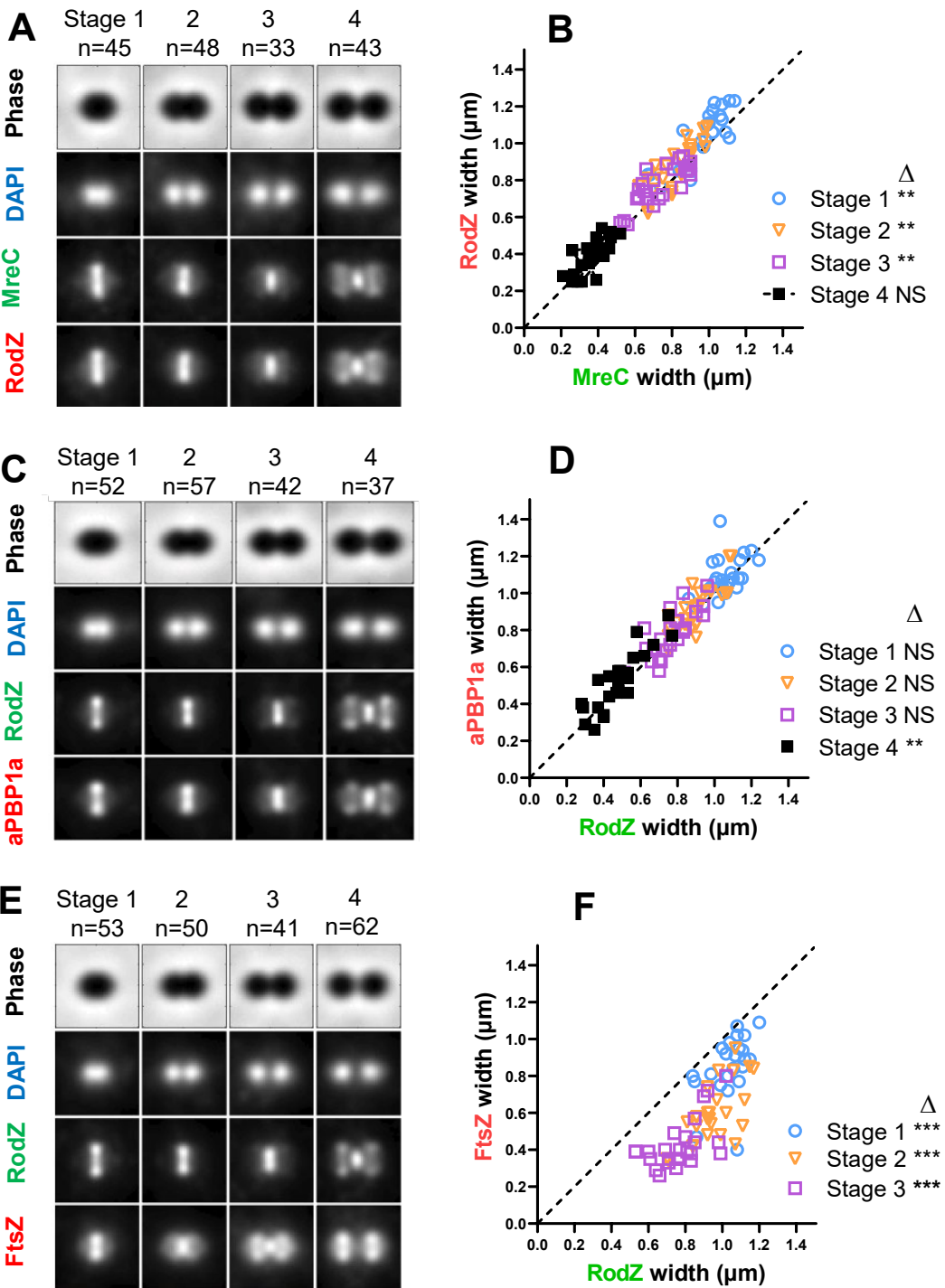
			Mutation lethal?	Colony morphology	Cell shape/size	F-tagged protein expression level
RodZ(1-273)	aa 5-76    108-130    172-271 WT	1 HTH TM DUF 273		WT	WT	0.9 ± 0.1
RodZ(1-261)		261	No	WT	WT	not done (nd)
RodZ(1-195)		195	No	WT	WT	nd
ΔDUF		(Δ196-261)	No	WT	WT	0 (n=3)
RodZ(1-135)			No	WT	WT‡	nd
RodZ(1-134)			No	WT	BW	0 (n=3)
RodZ(1-103)			Yes	μcolony & green-sheen	not done (nd)	nd
RodZ(1-72)			Yes	μcolony & green-sheen	nd	nd
ΔRodZ	(Δ21-257)		Yes	no colonies	ΔRodZ	nd
ΔHTH	(Δ4-68)		Yes	no colonies	ΔRodZ	0.24 ± 0.1
RodZ (Y51A F55A Y59A)			No	WT	WT	nd

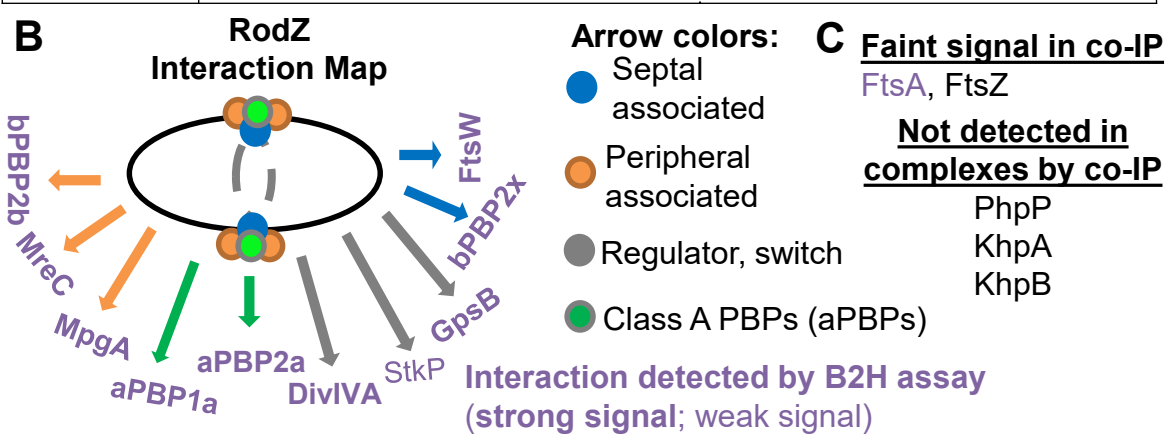
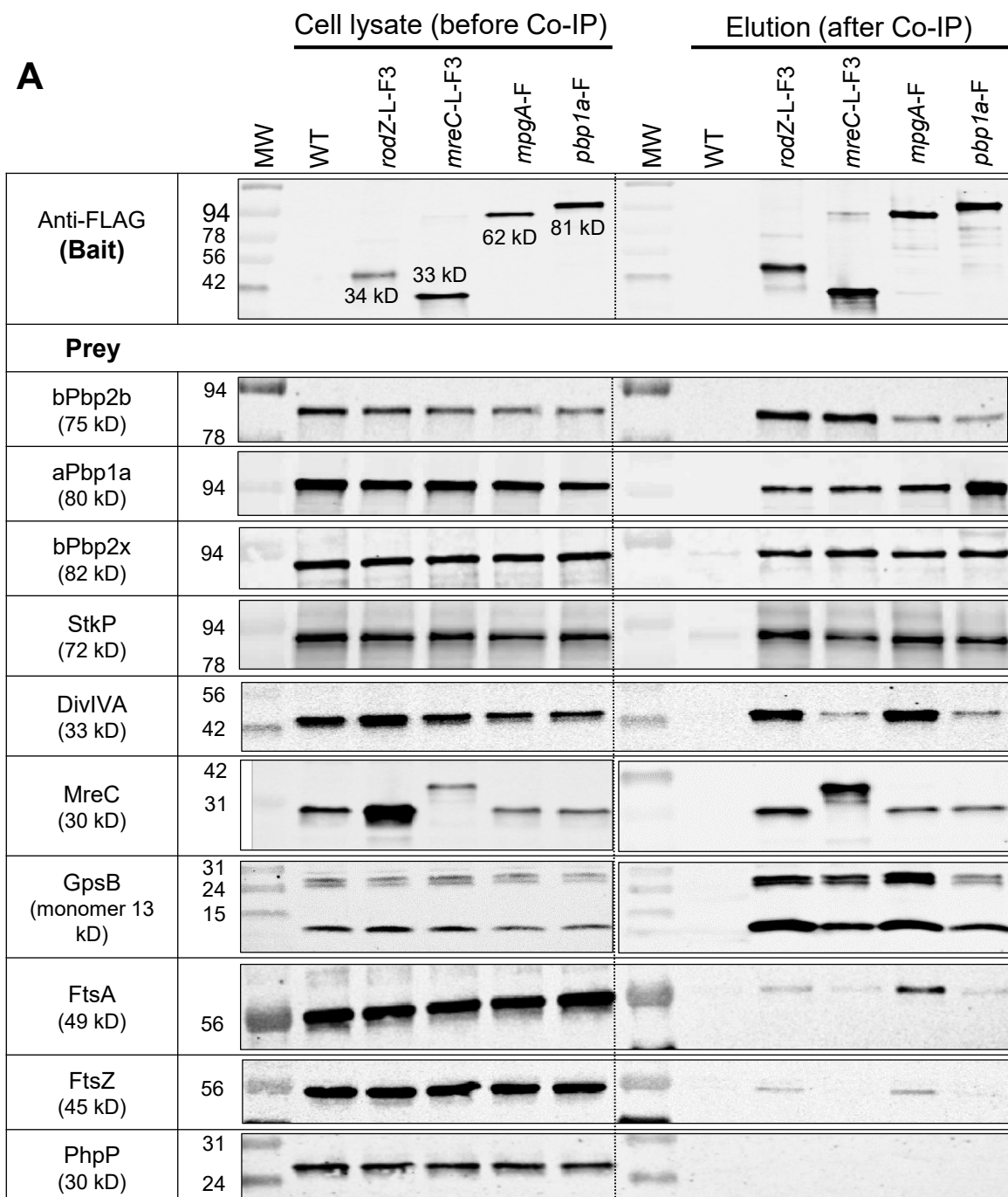
Key:

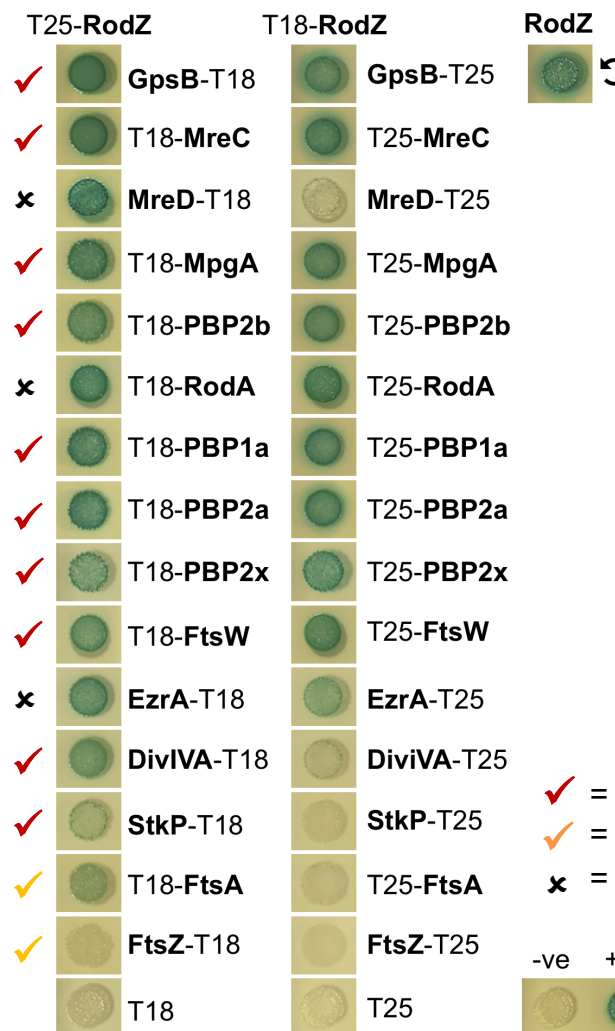
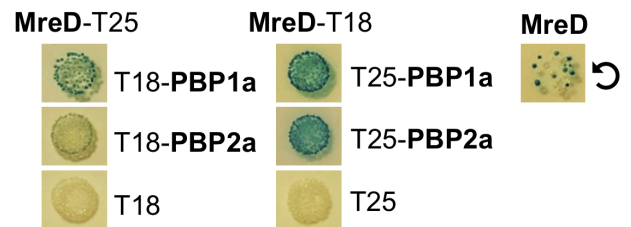
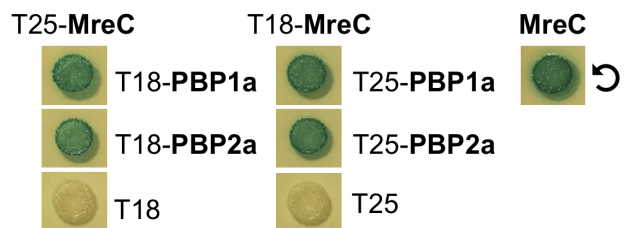
- ↓ = stop codon
- - - = deleted region
- ||| = Y51A F55A Y59A in HTH (Helix 4)

WT, wild-type or similar to WT  
 WT‡, occasional BW cell  
 BW, bigger, wider cell than WT  
 ΔRodZ, similar to ΔRodZ mutant



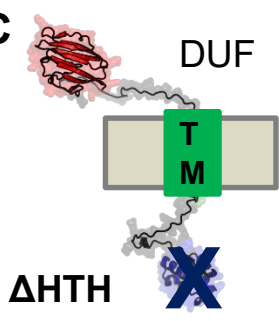




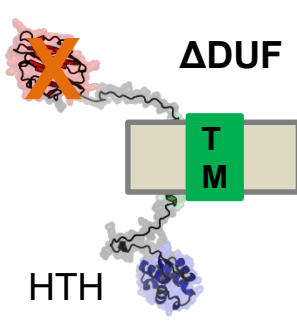
**A****B**

- ✓ = detected in co-IP
- ✗ = weak in co-IP
- ✗ = co-IP not performed

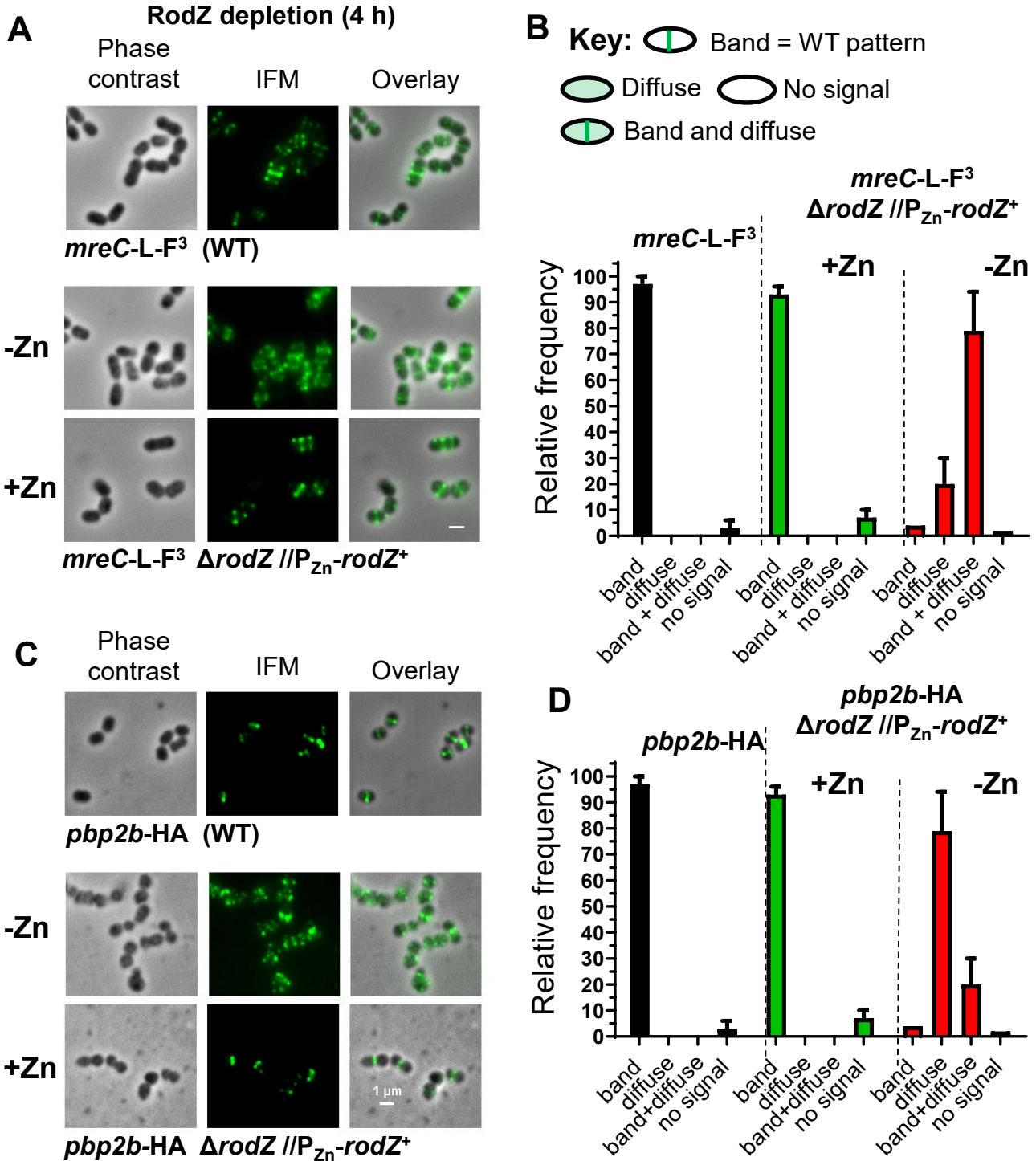
-ve      +ve

**C**

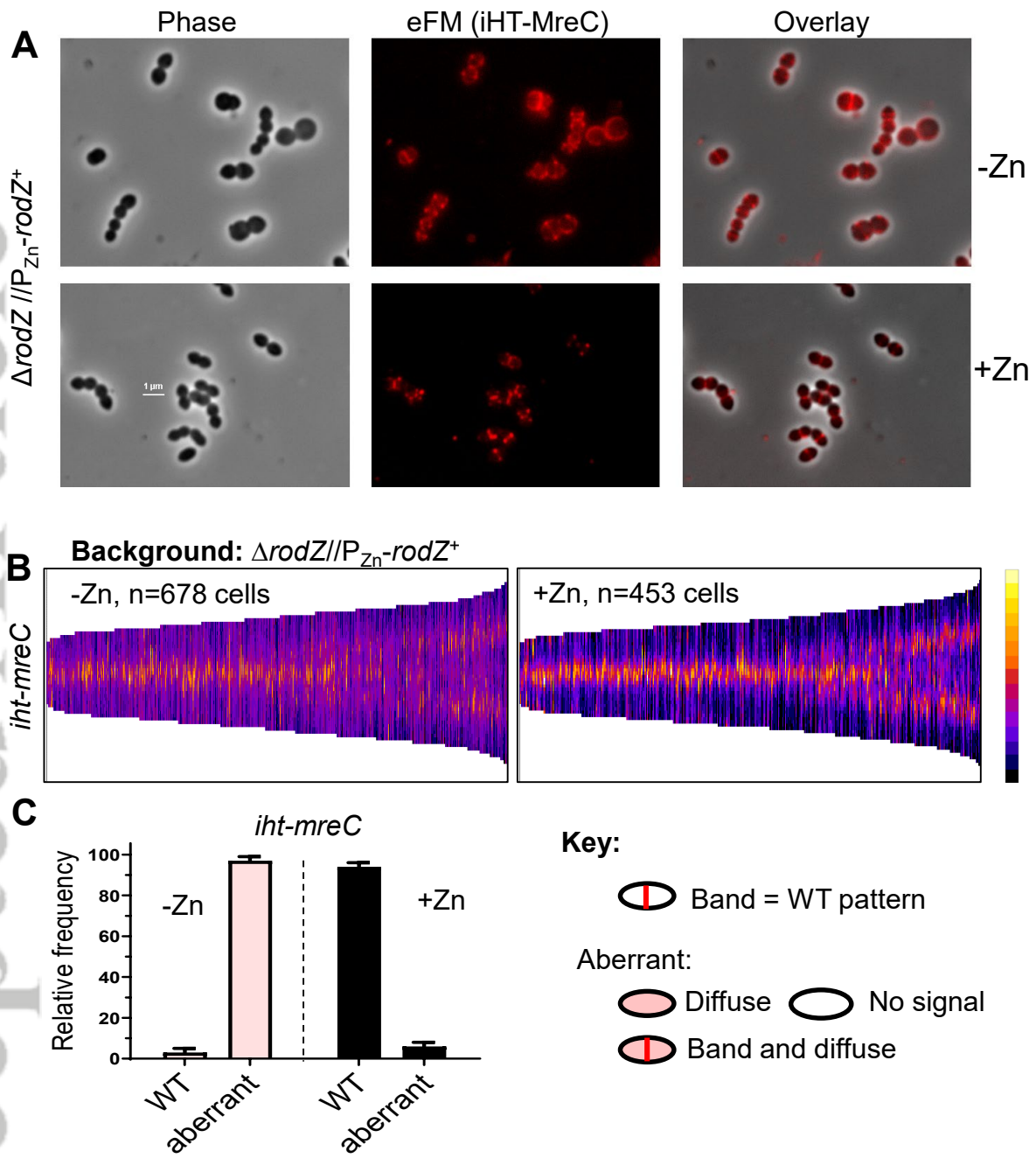
Decreased interaction with:  
 Itself (RodZ WT)  
 GpsB  
 bPBP2b, RodA  
 bPBP2x, FtsW  
 DivIVA  
 aPBP1b



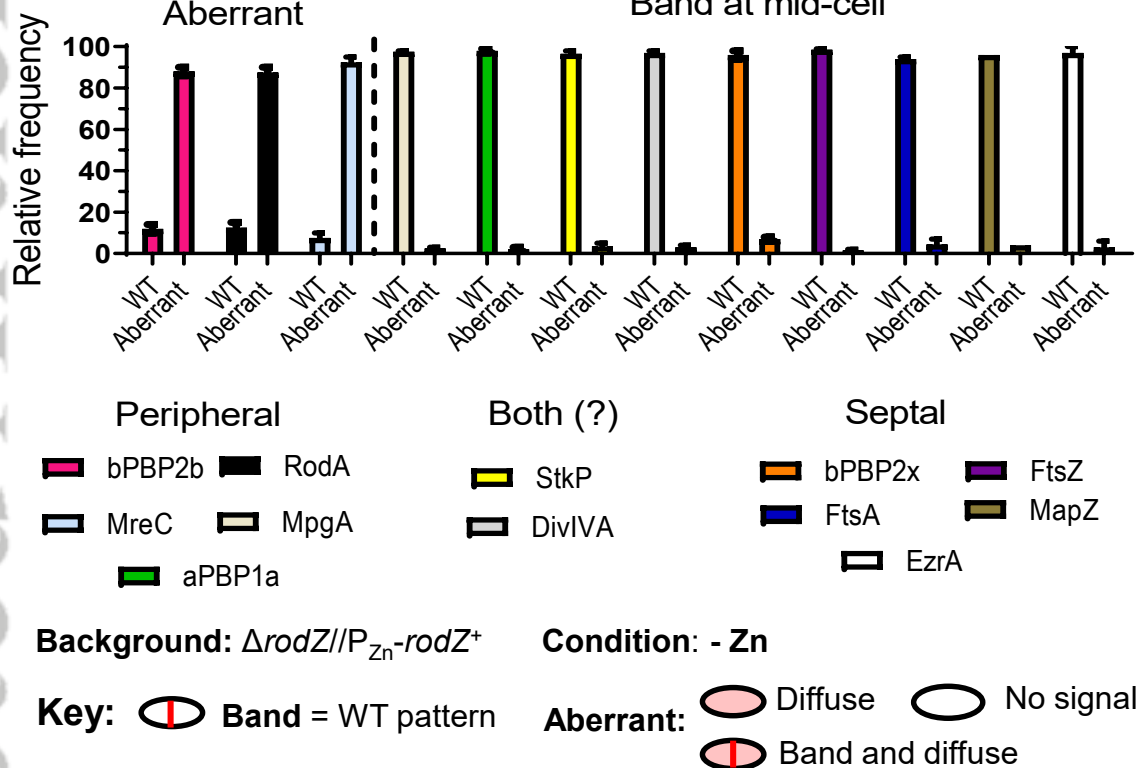
Decreased interaction with:  
 GpsB  
 bPBP2b  
 bPBP2x, FtsW

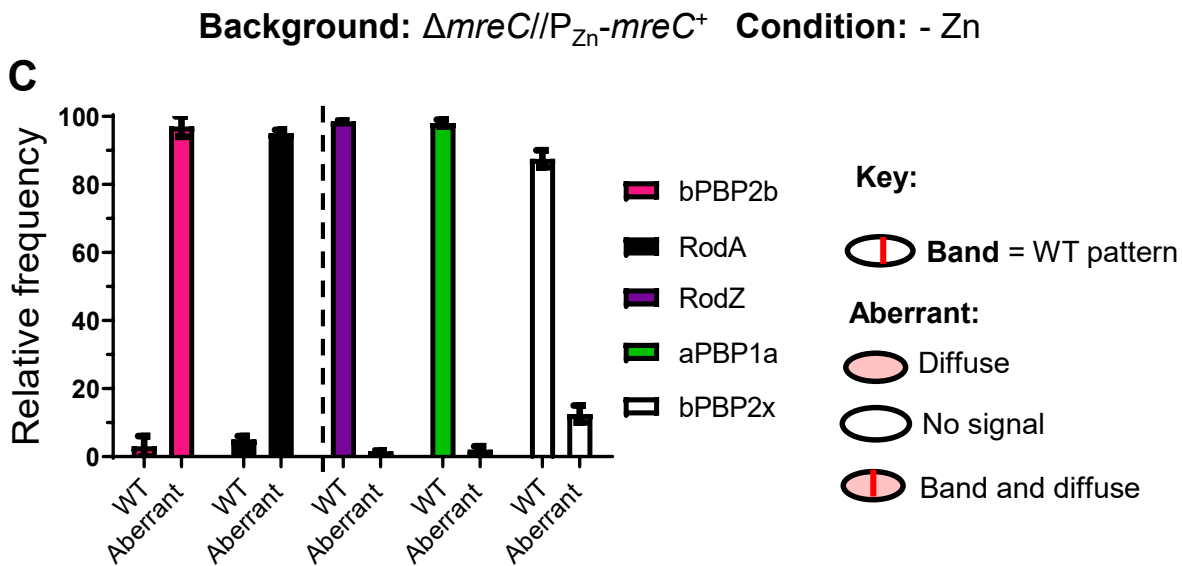
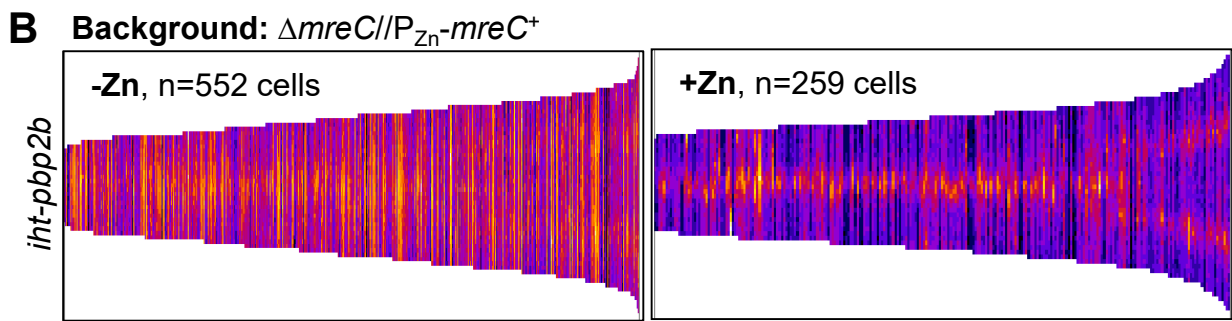
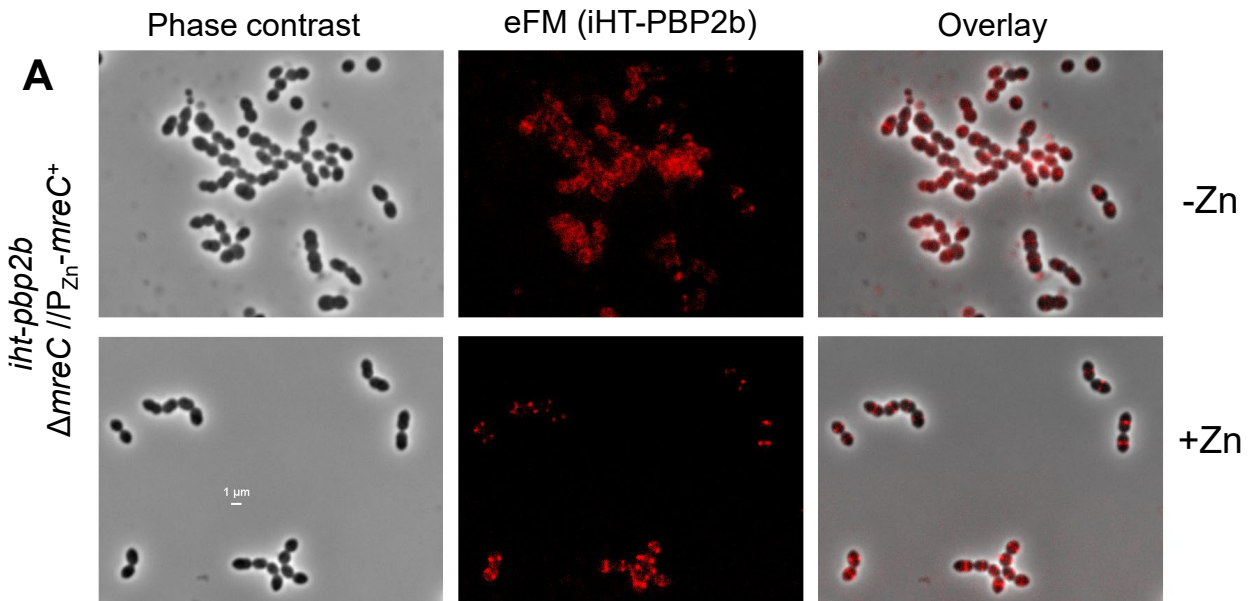


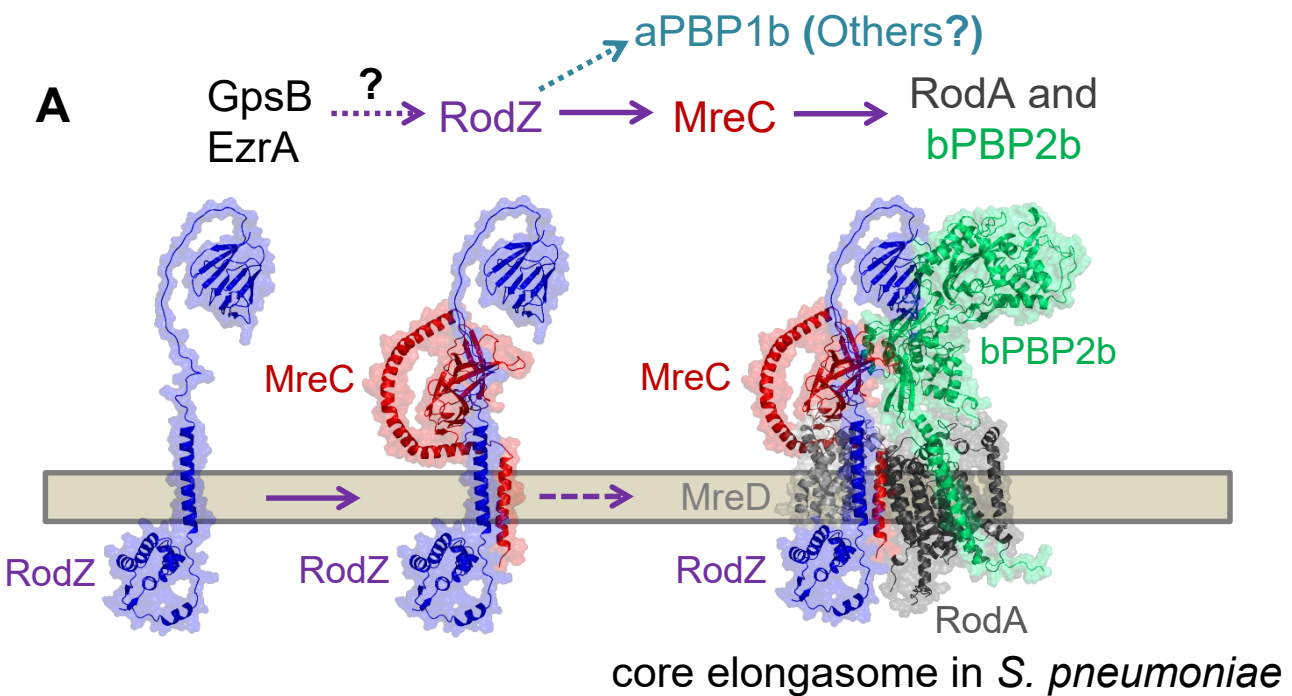
Accepted Article



## Localization patterns of proteins during RodZ depletion







**B** Synthetic-viable relationship specifically between RodZ and aPBP1b

WT RodZ → essential for pPG synthesis by elongasome

ΔRodZ —| blocks pPG elongasome assembly → lethal

ΔPBP1b → enables alternate mechanism that can bypass RodZ function in pPG elongasome

ΔRodZ  
ΔPBP1b → pPG elongasome function restored;  
MreCD, bPBP2b, RodA still required → viable

**C** Synthetic viable relationship between aPBP1a and elongasome components RodZ/MreC/MreD

ΔPBP1a → enables alternate mechanism that can bypass RodZ/MreC/MreD functions in pPG elongasome

ΔMreCD

ΔRodZ  
ΔPBP1a → pPG elongasome function restored; → viable  
bPBP2b, RodA still required

Strain	Genotype	No of colonies	No of transformations	Reads	Bowtie mapped	M1 removed	% mapped	Norm to 12M	Factor	No of TA	reads mapped to TA	TA sites hit by 2 reads	Percent TA 2 hit	Average read count	TA sites hit by 10 reads	Percent TA 10 hit
IU1824	WT parent (D39 <i>rpsL1Δcps</i> )	2.1E+05	11	7.8E+06	7.1E+06	6.1E+05	0.92	1.2E+07	1.7	1.3E+05	1.2E+07	8.0E+04	0.60	87	6.8E+04	0.51
IU14697	<i>Δpbp1b</i>	2.0E+05	2	8.8E+06	4.1E+06	4.4E+06	0.46	1.2E+07	3.0	1.3E+05	1.1E+07	8.2E+04	0.61	82	7.0E+04	0.53
IU10592	<i>ΔkhpB</i>	2.1E+05	5	5.8E+06	5.4E+06	4.5E+05	0.92	1.2E+07	2.2	1.3E+05	1.2E+07	8.4E+04	0.63	87	7.3E+04	0.55
IU18579	<i>Δpbp1a</i>	2.3E+05	3	9.1E+06	8.4E+06	7.0E+05	0.92	1.2E+07	1.4	1.3E+05	1.2E+07	7.6E+04	0.57	88	6.8E+04	0.51
IU13256	<i>Δpbp2a</i>	3.1E+05	4	1.3E+07	5.8E+06	5.3E+05	0.46	1.2E+07	2.1	1.3E+05	1.2E+07	8.4E+04	0.63	88	6.7E+04	0.50

Genome location		Gene	WT		$\Delta pbp1b$		$\Delta khpB$		$\Delta pbp1a$		$\Delta pbp2a$	
			# insertion forward	# insertion reverse								
2021617	2021618	SPD_2044	7	3	9	50	4	18	0	3	0	2
2021619	2021620	SPD_2044	34	32	50	24	311	132	210	315	27	54
2021623	2021624	SPD_2044	151	54	0	0	356	38	0	0	385	185
2021626	2021627	SPD_2044	0	0	124	0	0	0	28	0	25	0
2021639	2021640	SPD_2044	0	0	68	33	49	4	68	55	54	37
2021654	2021655	SPD_2044	0	0	0	0	22	11	51	18	0	0
2021661	2021662	SPD_2044	0	0	0	0	13	81	0	0	0	0
2021670	2021671	SPD_2044	0	0	0	0	0	0	28	45	0	0
2021685	2021686	SPD_2044	0	0	0	0	0	0	0	0	0	0
2021693	2021694	SPD_2044	0	0	0	0	13	108	85	82	0	0
2021695	2021696	SPD_2044	0	0	0	0	228	4	219	109	0	0
2021700	2021701	SPD_2044	0	0	0	0	43	90	87	237	0	0
2021702	2021703	SPD_2044	0	0	0	0	20	69	629	507	0	0
2021717	2021718	SPD_2044	0	0	0	0	56	92	71	50	0	0
2021721	2021722	SPD_2044	0	0	0	0	188	385	114	266	0	0
2021733	2021734	SPD_2044	0	0	0	0	164	40	0	0	0	0
2021738	2021739	SPD_2044	0	0	0	0	0	0	26	27	0	0
2021752	2021753	SPD_2044	0	0	0	0	7	2	9	4	0	0
2021756	2021757	SPD_2044	0	0	0	0	246	47	26	21	0	0
2021789	2021790	SPD_2044	0	0	0	0	7	4	77	67	0	0
2021793	2021794	SPD_2044	0	0	0	0	0	0	0	0	0	0
2021822	2021823	SPD_2044	0	0	0	0	25	36	33	48	0	0
2021828	2021829	SPD_2044	0	0	0	0	9	16	4	7	0	0
2021837	2021838	SPD_2044	0	0	0	0	0	2	13	53	0	0
2021856	2021857	SPD_2044	0	0	0	0	0	0	0	0	0	0
2021861	2021862	SPD_2044	0	0	0	0	190	114	126	106	0	0
2021865	2021866	SPD_2044	0	0	0	0	16	65	166	199	0	0
2021876	2021877	SPD_2044	0	0	0	0	166	49	77	97	0	0
2021883	2021884	SPD_2044	0	0	0	0	0	0	0	0	0	0
2021886	2021887	SPD_2044	0	0	0	0	0	0	82	27	0	0
2021899	2021900	SPD_2044	0	0	0	0	652	193	98	87	0	0
2021908	2021909	SPD_2044	0	0	0	0	2	16	98	222	0	0
2021919	2021920	SPD_2044	0	0	0	0	0	0	94	128	0	0
2021921	2021922	SPD_2044	0	0	0	0	0	0	1	0	0	0
2021932	2021933	SPD_2044	0	0	0	0	134	562	253	168	0	0
2021937	2021938	SPD_2044	0	0	0	0	25	20	226	212	0	0
2021941	2021942	SPD_2044	0	0	0	0	105	455	6	9	0	0
2021947	2021948	SPD_2044	0	0	0	0	251	186	236	101	0	0
2021955	2021956	SPD_2044	0	0	0	0	34	11	172	199	0	0
2021961	2021962	SPD_2044	0	0	0	0	4	2	38	77	0	0
2021973	2021974	SPD_2044	0	0	0	0	34	9	21	11	0	0
2021982	2021983	SPD_2044	0	0	0	0	2	0	57	62	0	0
2021999	2022000	SPD_2044	0	0	0	0	0	0	0	0	0	0
2022009	2022010	SPD_2044	0	0	0	0	3745	2878	706	392	0	0
2022041	2022042	SPD_2044	0	0	0	0	74	43	0	0	0	0
2022044	2022045	SPD_2044	0	0	0	0	148	195	6	6	0	0
2022057	2022058	SPD_2044	0	0	0	0	0	0	36	65	0	0
2022078	2022079	SPD_2044	0	0	0	0	0	0	0	0	0	0
2022084	2022085	SPD_2044	0	0	0	0	692	448	131	148	2	0
2022111	2022112	SPD_2045	0	0	0	0	31	16	21	27	0	0
2022125	2022126	SPD_2045	2	18	0	0	0	0	3	1	0	0
2022131	2022132	SPD_2045	0	0	0	0	0	0	62	24	0	0
2022140	2022141	SPD_2045	0	0	0	0	464	186	1457	1362	0	0
2022145	2022146	SPD_2045	0	0	0	0	488	1239	214	193	0	0
2022151	2022152	SPD_2045	0	0	0	0	280	114	7	13	0	0

2022166	2022167	SPD_2045	0	0	0	0	103	18	1	3	0	0
2022173	2022174	SPD_2045	0	0	0	0	96	116	0	0	0	0
2022189	2022190	SPD_2045	0	0	0	0	58	36	138	68	0	0
2022196	2022197	SPD_2045	0	0	0	0	18	16	131	270	0	0
2022199	2022200	SPD_2045	0	0	0	0	0	9	78	121	0	0
2022232	2022233	SPD_2045	0	0	0	0	36	18	0	3	0	0
2022244	2022245	SPD_2045	0	0	0	0	0	0	0	0	0	0
2022254	2022255	SPD_2045	0	0	0	0	0	0	0	0	0	0
2022265	2022266	SPD_2045	0	0	0	0	38	96	156	226	0	0
2022274	2022275	SPD_2045	0	0	0	0	0	0	31	17	0	0
2022286	2022287	SPD_2045	0	0	0	0	18	4	947	521	0	0
2022289	2022290	SPD_2045	0	0	0	0	11	0	0	0	0	0
2022295	2022296	SPD_2045	0	0	0	0	27	16	264	324	0	0
2022298	2022299	SPD_2045	0	0	0	0	7	22	11	36	0	0
2022301	2022302	SPD_2045	0	0	0	3	20	7	158	60	0	0
2022305	2022306	SPD_2045	0	0	0	0	4	18	4	16	0	0
2022313	2022314	SPD_2045	0	0	0	0	0	0	0	0	0	0
2022319	2022320	SPD_2045	0	0	0	0	0	0	0	0	0	0
2022342	2022343	SPD_2045	0	0	0	0	0	0	0	0	0	0
2022349	2022350	SPD_2045	0	2	0	0	0	0	220	81	0	0
2022352	2022353	SPD_2045	0	0	0	0	25	0	37	17	0	0
2022360	2022361	SPD_2045	0	0	0	0	20	197	1	3	0	0
2022367	2022368	SPD_2045	0	0	0	0	0	0	209	220	0	0
2022370	2022371	SPD_2045	0	0	0	0	0	0	187	81	0	0
2022388	2022389	SPD_2045	0	0	0	0	0	0	0	0	0	0
2022400	2022401	SPD_2045	0	0	0	0	0	0	0	0	0	0
2022415	2022416	SPD_2045	0	0	0	0	108	101	7	1	0	0
2022434	2022435	SPD_2045	0	12	0	0	329	103	476	315	0	0
2022436	2022437	SPD_2045	15	0	154	0	231	502	758	398	10	0
2022439	2022440	SPD_2045	0	0	0	0	464	1328	94	193	0	0
2022452	2022453	SPD_2045	0	0	0	0	40	34	65	122	0	0
2022490	2022491	SPD_2045	0	0	0	0	296	141	62	10	0	0
2022494	2022495	SPD_2045	0	0	0	0	54	67	3	1	0	0
2022523	2022524	SPD_2045	0	0	0	0	20	31	88	160	0	0
2022533	2022534	SPD_2045	0	0	0	0	470	361	33	31	0	0
2022557	2022558	SPD_2045	0	0	0	0	0	0	0	0	0	0
2022571	2022572	SPD_2045	0	0	0	0	4	7	48	165	0	0
2022574	2022575	SPD_2045	0	0	0	0	0	0	0	0	0	0
2022587	2022588	SPD_2045	0	0	0	0	0	0	3	3	0	0
2022610	2022611	SPD_2045	0	0	0	0	36	81	0	0	0	0
2022619	2022620	SPD_2045	0	0	0	0	0	0	78	95	0	0
2022656	2022657	SPD_2045	0	0	0	0	7	4	44	50	0	0
2022679	2022680	SPD_2045	0	0	0	0	0	0	133	71	0	0
2022686	2022687	SPD_2045	0	0	0	0	137	49	14	53	0	0
2022693	2022694	SPD_2045	0	0	0	0	2	4	3	7	0	0
2022724	2022725	SPD_2045	0	0	0	0	90	81	335	325	0	0
2022726	2022727	SPD_2045	0	0	0	0	92	231	650	719	0	0
2022788	2022789	SPD_2045	0	0	0	0	797	748	182	153	0	0
2022796	2022797	SPD_2045	0	0	0	0	7	2	263	217	0	0
2022821	2022822	SPD_2045	0	0	0	0	278	43	284	148	0	0
2022838	2022839	SPD_2045	0	0	0	0	27	9	72	121	0	0
2022846	2022847	SPD_2045	0	0	0	0	0	2	60	143	0	0
2022857	2022858	SPD_2045	0	0	0	0	0	0	0	0	0	0
2022895	2022896	SPD_2045	0	0	0	0	0	0	13	6	0	0
2022903	2022904	SPD_2045	12	3	21	3	249	58	300	95	0	0
2022916	2022917	SPD_2045	0	0	0	0	0	0	0	0	0	0
2022928	2022929	SPD_2045	0	0	0	0	0	2	0	0	0	0
2022934	2022935	IG_SPD_20	0	0	6	0	0	0	0	0	0	0
2022940	2022941	IG_SPD_20	13	3	9	15	78	181	535	233	0	0

2022942	2022943	IG_SPD_2046	0	30	0	0	56	94	3	0	0	0
2022955	2022956	IG_SPD_2046	24	27	216	207	2	0	0	0	2	0
2022960	2022961	IG_SPD_2046	0	0	38	154	36	25	0	0	82	76
2022968	2022969	IG_SPD_2046	0	0	139	89	0	0	0	0	14	16
2022985	2022986	IG_SPD_2046	22	10	9	12	0	0	41	27	0	8
2022988	2022989	SPD_2046	5	12	0	0	0	0	0	0	14	0
2022996	2022997	SPD_2046	29	39	0	0	0	0	0	0	0	0
2023005	2023006	SPD_2046	8	7	0	0	9	9	0	0	0	4
2023020	2023021	SPD_2046	57	25	0	0	11	0	0	0	0	0
2023028	2023029	SPD_2046	0	0	0	0	4	13	1	3	0	0
2023046	2023047	SPD_2046	5	10	9	38	9	45	0	0	0	0
2023053	2023054	SPD_2046	0	0	0	0	31	7	0	0	0	0
2023075	2023076	SPD_2046	0	0	0	0	0	0	0	0	0	0
2023102	2023103	SPD_2046	0	0	0	0	0	0	0	0	0	0
2023118	2023119	SPD_2046	0	0	0	0	0	0	0	0	0	0
2023124	2023125	SPD_2046	0	0	0	0	0	0	0	0	0	0
2023146	2023147	SPD_2046	0	0	3	0	16	0	1	0	8	0
2023191	2023192	SPD_2046	0	0	0	0	0	0	3	1	82	35
2023250	2023251	SPD_2046	0	0	0	0	0	2	0	6	0	0
2023262	2023263	SPD_2046	0	0	0	3	0	0	1	0	0	0
2023298	2023299	SPD_2046	0	0	3	12	2	0	4	7	2	0
2023344	2023345	SPD_2046	2	3	0	0	2	0	0	1	0	0
2023353	2023354	SPD_2046	0	0	0	0	0	0	0	0	0	0
2023356	2023357	SPD_2046	0	0	6	3	0	2	0	0	0	0
2023383	2023384	SPD_2046	3	0	21	18	2	0	0	0	2	0
2023398	2023399	SPD_2046	0	0	0	0	0	0	0	0	0	2
2023404	2023405	SPD_2046	0	0	0	0	0	0	0	0	0	0
2023424	2023425	SPD_2046	3	3	6	3	0	0	0	0	0	0
2023431	2023432	SPD_2046	0	0	0	0	0	0	0	1	2	0
2023448	2023449	SPD_2046	0	0	3	24	0	0	0	0	4	4
2023471	2023472	SPD_2046	2	0	0	0	11	4	0	0	19	21
2023503	2023504	SPD_2046	0	0	0	0	4	2	0	3	4	12
2023517	2023518	SPD_2046	5	2	0	0	0	0	0	0	0	0
2023530	2023531	SPD_2046	2	0	0	0	4	11	0	0	0	0
2023541	2023542	SPD_2046	0	12	6	36	0	0	0	0	0	2
2023568	2023569	SPD_2046	0	0	27	12	0	0	10	1	0	0
2023586	2023587	SPD_2046	0	0	0	0	0	0	0	0	4	0
2023602	2023603	SPD_2046	3	0	3	12	4	0	0	0	0	0
2023619	2023620	SPD_2046	5	10	24	68	2	13	28	10	6	8
2023623	2023624	SPD_2046	3	5	0	6	22	2	9	1	10	4
2023635	2023636	SPD_2046	0	2	3	6	0	0	0	0	0	0
2023637	2023638	SPD_2046	2	0	24	12	0	0	0	0	0	0
2023664	2023665	SPD_2046	0	0	0	0	0	0	0	0	0	2
2023667	2023668	SPD_2046	0	0	0	0	0	0	0	1	6	10
2023692	2023693	SPD_2046	0	0	0	0	7	7	0	0	0	0
2023700	2023701	SPD_2046	0	0	0	0	9	11	9	9	0	0
2023715	2023716	SPD_2046	0	0	3	0	0	0	6	3	2	0
2023754	2023755	SPD_2046	15	2	3	3	4	20	0	0	10	4
2023756	2023757	SPD_2046	121	37	151	24	85	2	283	77	41	6
2023772	2023773	SPD_2046	5	20	71	24	0	0	0	3	43	27
2023775	2023776	SPD_2046	8	12	219	186	45	65	119	45	76	60
2023783	2023784	SPD_2047	0	0	12	53	0	0	0	0	0	0
2023804	2023805	SPD_2047	0	0	12	27	4	4	13	24	0	2
2023809	2023810	SPD_2047	10	0	0	0	31	0	0	0	41	25
2023816	2023817	SPD_2047	0	0	0	0	0	0	0	0	0	0
2023824	2023825	SPD_2047	27	32	47	53	25	11	41	23	0	0
2023839	2023840	SPD_2047	0	0	0	0	0	0	0	0	0	0
2023854	2023855	SPD_2047	2	0	0	0	9	9	0	0	0	0
2023866	2023867	SPD_2047	0	2	30	12	0	0	0	0	0	0

2023872	2023873	SPD_2047	13	7	0	0	16	0	4	3	6	6
2023876	2023877	SPD_2047	7	0	0	0	0	0	0	0	0	0
2023899	2023900	SPD_2047	0	0	0	0	0	0	0	0	0	0
2023942	2023943	SPD_2047	0	0	6	6	0	0	0	0	0	0
2023945	2023946	SPD_2047	2	5	6	71	2	11	4	3	0	0
2023963	2023964	SPD_2047	0	5	3	0	2	0	6	13	4	6
2023967	2023968	SPD_2047	2	2	3	3	0	7	24	4	4	2
2023977	2023978	SPD_2047	0	0	0	0	0	0	1	1	0	8
2023982	2023983	SPD_2047	0	0	6	3	0	0	3	0	2	4
2024011	2024012	SPD_2047	0	0	0	0	0	0	0	0	0	0
2024077	2024078	SPD_2047	0	0	0	0	0	0	1	6	0	0
2024086	2024087	SPD_2047	3	2	18	21	7	2	14	16	0	2
2024107	2024108	SPD_2047	0	0	3	21	0	2	4	11	0	4
2024113	2024114	SPD_2047	0	2	80	47	22	2	17	13	6	10
2024116	2024117	SPD_2047	8	2	50	41	11	4	1	6	37	27
2024118	2024119	SPD_2047	5	22	252	586	67	74	33	132	64	142
2024137	2024138	SPD_2047	3	0	47	12	9	2	40	13	23	12
2024190	2024191	SPD_2047	3	3	0	0	0	0	0	0	0	0
2024344	2024345	SPD_2047	0	0	0	0	0	0	0	0	0	0
2024364	2024365	SPD_2047	2	0	15	18	0	0	0	0	0	0
2024376	2024377	SPD_2047	5	2	0	0	0	0	1	1	0	0
2024382	2024383	SPD_2047	5	2	0	0	0	0	4	3	2	0
2024388	2024389	SPD_2047	0	8	18	12	0	0	0	0	0	0
2024404	2024405	SPD_2047	0	0	0	6	4	7	1	3	10	14
2024409	2024410	SPD_2047	0	0	0	0	0	0	10	0	0	0
2024446	2024447	SPD_2047	0	0	0	0	0	0	0	0	0	0
2024455	2024456	SPD_2047	3	2	3	0	2	0	0	0	0	0
2024464	2024465	SPD_2047	0	0	18	30	0	4	4	4	8	4
2024469	2024470	SPD_2047	0	0	3	9	2	0	3	0	8	2
2024478	2024479	SPD_2047	2	0	21	33	7	7	3	0	4	2
2024484	2024485	SPD_2047	0	0	0	0	7	0	0	0	2	0
2024500	2024501	SPD_2047	0	0	0	0	11	11	1	4	10	14
2024508	2024509	SPD_2047	10	15	0	0	0	0	13	10	21	25
2024510	2024511	SPD_2047	3	8	44	30	4	0	0	0	4	4
2024560	2024561	SPD_2047	0	0	0	0	0	0	0	0	0	0
2024568	2024569	SPD_2047	3	0	0	0	0	0	0	1	0	0
2024579	2024580	SPD_2047	2	2	160	21	20	0	10	0	8	0
2024581	2024582	SPD_2047	7	5	50	30	7	0	20	11	6	0
2024583	2024584	SPD_2047	40	30	9	27	20	54	16	13	8	21
2024599	2024600	SPD_2047	0	0	3	3	0	0	0	0	0	0
2024613	2024614	SPD_2047	0	0	12	33	0	0	9	3	2	4
2024618	2024619	SPD_2048	12	3	0	0	13	0	10	1	0	0
2024625	2024626	SPD_2048	2	13	6	21	2	81	14	13	0	2
2024644	2024645	SPD_2048	0	0	0	21	0	0	14	7	29	16
2024655	2024656	SPD_2048	2	0	21	62	11	13	10	18	12	21
2024662	2024663	SPD_2048	0	0	3	15	0	0	0	0	0	0
2024688	2024689	SPD_2048	0	0	0	0	0	0	26	9	190	134
2024696	2024697	SPD_2048	0	0	0	0	0	0	0	0	0	0
2024712	2024713	SPD_2048	5	10	0	0	9	0	0	0	0	0
2024727	2024728	SPD_2048	18	22	112	136	9	9	0	0	4	8
2024759	2024760	SPD_2048	0	0	0	9	0	0	0	0	0	2
2024762	2024763	SPD_2048	3	8	44	47	16	18	20	13	23	23
2024796	2024797	SPD_2048	0	0	0	0	0	0	0	0	0	0
2024834	2024835	SPD_2048	0	0	0	0	0	0	0	0	0	0
2024837	2024838	SPD_2048	0	0	0	0	0	0	0	0	14	8
2024852	2024853	SPD_2048	0	2	3	0	0	0	0	0	0	0
2024857	2024858	SPD_2048	0	5	3	18	0	0	3	3	0	2
2024877	2024878	SPD_2048	0	0	3	6	0	7	3	3	0	0
2024888	2024889	SPD_2048	0	0	6	24	9	34	3	0	0	0
2024897	2024898	SPD_2048	0	0	0	0	0	0	0	0	0	0
2024918	2024919	SPD_2048	5	8	3	12	7	36	0	0	0	0



2025799	2025800	SPD_2049	0	0	0	0	2	0	0	0	0	0
2025806	2025807	SPD_2049	0	0	0	0	0	0	0	0	0	0
2025810	2025811	SPD_2049	0	0	0	0	0	0	0	0	0	0
2025818	2025819	SPD_2049	0	0	0	0	0	0	0	0	0	0
2025822	2025823	SPD_2049	0	0	0	0	0	0	1	0	0	0
2025829	2025830	SPD_2049	0	0	0	0	0	2	0	0	0	0
2025832	2025833	SPD_2049	0	0	0	0	0	0	0	0	0	0
2025850	2025851	SPD_2049	0	0	0	0	0	0	0	0	0	0
2025853	2025854	SPD_2049	0	0	0	0	0	0	0	0	0	0
2025863	2025864	SPD_2049	0	0	0	0	0	0	0	0	0	0
2025865	2025866	SPD_2049	0	0	0	0	0	0	0	0	0	0
2025875	2025876	SPD_2049	0	0	0	0	0	0	0	0	0	0
2025887	2025888	SPD_2049	0	0	0	0	0	0	0	0	0	0
2025893	2025894	SPD_2049	0	0	0	0	0	0	0	0	0	0
2025898	2025899	SPD_2049	0	0	0	0	0	0	0	0	0	0
2025904	2025905	SPD_2049	0	0	0	0	0	0	0	0	0	0
2025910	2025911	SPD_2049	2	0	0	0	0	0	0	0	0	0
2025914	2025915	SPD_2049	0	0	0	0	0	0	0	0	0	0
2025916	2025917	SPD_2049	0	0	0	0	0	0	0	9	0	0
2025932	2025933	SPD_2049	0	0	0	0	0	0	0	0	0	0
2025938	2025939	SPD_2049	0	0	0	0	0	0	0	0	0	0
2025979	2025980	SPD_2050	0	0	0	0	0	0	0	0	0	0
2025986	2025987	SPD_2050	0	0	0	0	0	0	0	0	0	2
2025989	2025990	SPD_2050	0	0	18	30	0	0	4	0	70	2
2025996	2025997	SPD_2050	0	0	0	0	0	0	14	40	0	0
2026023	2026024	SPD_2050	0	0	27	21	0	0	23	7	0	0
2026032	2026033	SPD_2050	0	0	0	0	0	0	27	18	0	0
2026049	2026050	SPD_2050	35	60	21	9	4	27	14	23	8	25
2026053	2026054	SPD_2050	7	15	36	186	13	20	10	11	0	10
2026074	2026075	SPD_2050	35	13	9	0	4	0	89	33	4	8
2026083	2026084	SPD_2050	0	0	0	0	0	0	0	0	0	0
2026088	2026089	SPD_2050	57	72	258	488	367	562	64	78	64	115
2026095	2026096	SPD_2050	0	0	0	0	52	9	0	1	0	0
2026106	2026107	SPD_2050	0	0	0	6	13	318	0	0	0	2
2026146	2026147	SPD_2050	0	0	0	0	0	0	0	0	0	0
2026152	2026153	SPD_2050	0	0	21	44	0	0	26	13	0	0
2026196	2026197	SPD_2050	2	30	36	127	125	477	50	87	2	2
2026223	2026224	SPD_2050	0	0	36	9	99	31	33	6	39	4
2026235	2026236	SPD_2050	97	116	0	0	31	18	0	0	0	0
2026244	2026245	SPD_2050	50	55	56	118	69	186	6	9	37	66
2026246	2026247	SPD_2050	5	0	0	0	29	13	78	16	49	14
2026257	2026258	SPD_2050	45	74	59	278	67	220	20	41	33	33
2026278	2026279	SPD_2050	10	10	44	3	9	2	3	0	0	0
2026284	2026285	SPD_2050	170	255	77	323	101	477	230	234	181	202
2026286	2026287	SPD_2050	59	39	184	83	172	34	87	28	202	101
2026296	2026297	SPD_2050	72	186	228	702	65	388	58	88	113	206
2026298	2026299	SPD_2050	252	180	9	44	7	16	44	65	0	0
2026301	2026302	SPD_2050	25	17	80	21	25	7	1	0	35	8
2026310	2026311	SPD_2050	0	0	89	148	9	43	0	0	60	99
2026313	2026314	SPD_2050	24	54	6	18	22	25	94	209	146	190
2026337	2026338	SPD_2050	18	15	89	104	25	11	11	21	12	14
2026366	2026367	SPD_2050	0	0	258	225	87	43	7	11	10	4
2026370	2026371	SPD_2050	18	12	0	0	9	11	36	21	29	14
2026403	2026404	SPD_2050	18	10	240	50	0	2	21	6	2	2
2026405	2026406	SPD_2050	62	13	1006	364	629	188	206	81	165	64
2026417	2026418	SPD_2050	3	10	74	30	9	4	124	53	4	4
2026420	2026421	SPD_2050	15	8	255	36	114	31	48	23	0	0
2026434	2026435	SPD_2050	0	0	0	0	0	0	0	0	0	0
2026443	2026444	SPD_2050	0	0	0	0	0	0	0	0	0	0
2026457	2026458	SPD_2050	0	0	0	0	0	0	0	0	0	2
2026462	2026463	SPD_2050	0	0	0	0	181	94	115	50	2	0
2026467	2026468	SPD_2050	0	2	9	12	2	0	33	13	0	0

2026473	2026474	SPD_2050	0	0	0	0	27	60	0	0	0	0
2026502	2026503	SPD_2050	3	0	0	0	0	0	47	58	0	0
2026514	2026515	SPD_2050	0	0	71	80	56	4	0	0	6	2
2026545	2026546	SPD_2050	2	10	287	118	267	90	327	338	0	2
2026555	2026556	SPD_2050	3	3	145	272	20	18	16	30	0	0
2026559	2026560	SPD_2050	7	3	151	59	659	255	408	281	10	2
2026565	2026566	SPD_2050	0	0	0	0	4	4	34	10	0	0
2026579	2026580	SPD_2050	3	0	157	30	125	29	57	20	0	0
2026605	2026606	SPD_2050	0	0	44	95	0	4	28	24	0	0
2026624	2026625	SPD_2050	0	3	27	18	72	54	18	51	0	0
2026648	2026649	SPD_2050	0	0	0	0	0	0	0	0	2	0
2026700	2026701	SPD_2050	0	0	27	263	78	806	354	393	4	0
2026704	2026705	SPD_2050	0	0	21	47	27	36	128	152	0	0
2026737	2026738	SPD_2050	2	0	56	15	92	29	27	24	0	0
2026760	2026761	SPD_2050	0	0	98	252	43	38	152	213	6	19
2026764	2026765	SPD_2050	0	0	56	44	0	0	28	21	0	0
2026770	2026771	SPD_2050	0	0	59	3	251	20	18	6	0	0
2026799	2026800	SPD_2050	0	0	0	50	9	116	14	31	0	0
2026819	2026820	IG_SPD_20	52	30	0	0	233	49	6	6	21	4
2026826	2026827	IG_SPD_20	3	2	9	41	2	25	0	0	16	25
2026829	2026830	IG_SPD_20	0	0	3	6	60	49	23	17	4	4
2026834	2026835	IG_SPD_20	37	39	18	24	9	18	7	28	8	12
2026839	2026840	IG_SPD_20	2	2	0	0	0	7	0	0	0	0
2026842	2026843	SPD_2051	0	0	6	12	0	0	0	0	0	6
2026853	2026854	SPD_2051	29	25	36	30	4	0	9	4	0	0
2026858	2026859	SPD_2051	15	17	9	163	0	31	0	11	31	107
2026868	2026869	SPD_2051	82	139	101	266	29	83	17	51	45	140
2026883	2026884	SPD_2051	17	37	12	56	20	81	1	4	70	78
2026886	2026887	SPD_2051	86	15	260	24	18	0	62	7	0	0
2026916	2026917	SPD_2051	8	3	0	0	9	0	0	0	0	0
2026921	2026922	SPD_2051	12	2	89	9	9	0	67	11	6	4
2026931	2026932	SPD_2051	12	22	12	9	0	0	0	0	0	2
2026980	2026981	SPD_2051	0	0	12	24	0	0	10	0	31	56
2026993	2026994	SPD_2051	8	22	0	6	0	0	0	0	0	12
2027014	2027015	SPD_2051	0	0	0	0	0	0	0	7	0	0
2027047	2027048	SPD_2051	0	0	0	0	0	0	0	0	0	0
2027050	2027051	SPD_2051	18	8	27	12	13	4	6	1	4	2
2027054	2027055	SPD_2051	32	13	12	33	4	65	28	28	33	29
2027068	2027069	SPD_2051	5	7	41	24	7	0	0	0	19	4
2027071	2027072	SPD_2051	74	92	6	6	0	0	0	0	4	8
2027075	2027076	SPD_2051	52	27	21	27	9	13	26	4	70	70
2027086	2027087	SPD_2051	0	0	0	6	0	0	0	0	0	0
2027092	2027093	SPD_2051	3	0	36	38	0	0	0	0	0	0
2027098	2027099	SPD_2051	0	0	0	0	0	0	0	0	0	0
2027107	2027108	SPD_2051	0	0	12	6	4	0	0	0	8	6
2027140	2027141	SPD_2051	86	34	9	0	4	0	0	0	0	0
2027144	2027145	SPD_2051	30	17	44	0	29	2	44	16	82	52
2027177	2027178	SPD_2051	0	0	3	3	9	9	0	0	19	29
2027195	2027196	SPD_2051	0	0	0	0	0	0	27	6	119	31
2027212	2027213	SPD_2051	7	3	0	0	0	2	0	0	0	2
2027223	2027224	SPD_2051	0	0	0	15	0	0	1	1	0	0
2027273	2027274	SPD_2051	0	0	0	0	11	11	3	0	0	2
2027279	2027280	SPD_2051	0	0	9	21	9	18	0	0	2	2
2027282	2027283	SPD_2051	0	0	6	12	0	0	0	0	0	0
2027287	2027288	SPD_2051	13	27	24	38	18	52	3	9	19	45
2027298	2027299	SPD_2051	0	0	0	0	0	0	0	0	0	0
2027326	2027327	SPD_2051	0	0	0	0	0	0	0	0	2	0
2027332	2027333	SPD_2051	0	0	0	0	0	0	0	0	25	19
2027345	2027346	SPD_2051	0	0	0	0	0	0	0	0	0	0
2027360	2027361	SPD_2051	3	0	53	323	0	11	4	10	21	31

2027374	2027375	SPD_2051	15	3	6	3	20	7	0	1	4	2
2027377	2027378	SPD_2051	20	24	15	86	13	7	18	34	2	6
2027390	2027391	SPD_2051	0	0	0	0	4	9	0	0	0	2
2027399	2027400	SPD_2051	0	0	18	3	0	0	0	0	39	25
2027420	2027421	SPD_2051	8	2	47	18	34	4	26	17	0	10
2027463	2027464	SPD_2051	7	2	0	0	13	4	6	6	0	0
2027471	2027472	SPD_2051	0	0	0	0	0	2	3	0	0	0
2027491	2027492	SPD_2051	0	0	0	0	0	0	0	0	0	0
2027498	2027499	SPD_2051	2	7	0	9	0	2	4	6	37	47
2027516	2027517	SPD_2051	34	89	0	0	0	0	0	0	2	0
2027526	2027527	SPD_2051	52	66	0	18	7	11	0	0	0	0
2027536	2027537	SPD_2051	7	7	0	0	0	4	0	0	0	2
2027554	2027555	SPD_2051	0	0	6	0	0	2	7	24	49	64
2027558	2027559	SPD_2051	0	0	15	53	2	2	0	0	21	27
2027594	2027595	SPD_2051	62	40	47	44	81	25	85	45	111	78
2027596	2027597	SPD_2051	12	17	36	18	18	16	9	10	6	2
2027606	2027607	SPD_2051	0	0	0	6	0	0	0	1	2	4
2027614	2027615	SPD_2051	0	0	30	95	4	13	0	0	0	0
2027622	2027623	SPD_2051	0	0	0	0	0	0	0	7	0	0
2027633	2027634	SPD_2051	0	0	0	0	0	0	0	0	0	0
2027648	2027649	SPD_2051	0	0	0	9	0	0	1	3	4	10
2027673	2027674	SPD_2051	54	34	24	9	11	2	1	0	60	31
2027695	2027696	SPD_2051	5	3	6	24	0	4	0	0	8	12
2027698	2027699	SPD_2051	84	12	89	0	4	0	20	0	227	0
2027728	2027729	SPD_2051	52	29	53	9	2	0	0	0	0	0
2027744	2027745	SPD_2051	0	0	0	0	0	0	0	0	4	33
2027759	2027760	SPD_2051	25	17	21	12	2	2	3	0	39	19
2027765	2027766	SPD_2051	20	15	0	0	0	0	0	0	0	0
2027774	2027775	SPD_2051	0	0	0	0	18	7	16	18	0	0
2027781	2027782	SPD_2051	0	0	0	3	2	0	1	1	29	19
2027802	2027803	SPD_2051	5	10	0	0	0	0	0	6	6	0
2027815	2027816	SPD_2051	2	5	6	15	0	0	0	1	0	0
2027824	2027825	SPD_2051	7	12	6	38	0	0	4	10	0	0
2027833	2027834	SPD_2051	0	0	33	18	4	4	20	9	8	4
2027836	2027837	SPD_2051	0	0	0	27	2	16	16	30	37	33
2027846	2027847	SPD_2051	0	0	0	6	9	22	0	0	2	4
2027854	2027855	SPD_2051	0	0	38	0	7	0	0	0	0	0
2027875	2027876	SPD_2051	67	57	0	0	13	11	24	21	14	16
2027894	2027895	SPD_2051	57	27	36	18	0	0	0	0	0	4
2027899	2027900	SPD_2051	32	45	21	0	16	7	0	1	0	4
2027931	2027932	SPD_2051	0	0	3	0	0	0	0	3	25	12
2027939	2027940	SPD_2051	76	37	21	9	2	2	33	3	68	25
2027943	2027944	SPD_2051	0	0	0	0	45	0	0	0	31	16
2027968	2027969	SPD_2051	0	0	18	53	13	16	6	1	33	33
2027972	2027973	SPD_2051	0	0	0	0	0	0	0	0	4	2
2027987	2027988	SPD_2051	29	10	30	9	36	25	13	7	2	6
2028003	2028004	SPD_2051	0	2	0	0	0	0	0	0	2	0
2028013	2028014	SPD_2051	8	15	0	0	11	36	13	14	2	2
2028025	2028026	SPD_2051	0	0	0	0	4	18	4	0	0	0
2028069	2028070	SPD_2051	0	0	3	0	7	2	0	0	0	0
2028083	2028084	SPD_2051	0	0	21	24	20	0	0	0	21	10
2028093	2028094	SPD_2051	2	7	0	0	0	2	0	0	4	8
2028096	2028097	SPD_2051	59	67	0	0	0	9	7	4	6	10

Locus	Gene name	# TA	Count Ratio (mut/WT)			
			$\Delta pbp1b$	$\Delta khpB$	$\Delta pbp1a$	$\Delta pbp2a$
SPD_2044	<i>mreD</i>	49	1.3	52***	31***	2.7
SPD_2045	<i>mreC</i>	63	2.8	181***	245***	0.2*
SPD_2046	<i>cbiQ</i>	46	2.2	1.0	1.3	1.1
SPD_2047	<i>cbiO1</i>	49	6.6**	1.5	1.9	1.9
SPD_2048	<i>cbiO2</i>	46	6.3***	2.1	1.5	3.3
SPD_2049	<i>pgsA</i>	55	0.8	2.0	0.8	0.8
SPD_2050	<i>rodZ</i>	59	3.9***	3.8***	2.6***	1.1
SPD_2051	<i>spd_2051</i>	90	1.3	0.5	0.4**	1.1

\*, P<0.05

\*\*, P<0.01

\*\*\*, P<0.005

Mann-Whitney test (see *Experimental Procedures* )